Transition from ultrapotassic kamafugitic to sub-alkaline magmas: Sr, Nd, and Pb isotope, trace element and 40Ar-39Ar age data from

JOURNAL OF PETROLOGY | VOLUME 50 | NUMBER 7 | PAGES 1327–1357 | 2009 | doi:10.1093/petrology/egp003

Transition from Ultrapotassic Kamafugitic to Sub-alkaline Magmas: Sr, Nd, and Pb Isotope, Trace Element and ^{40}Ar–^{39}Ar Age Data from the Middle Latin Valley Volcanic Field, Roman Magmatic Province, Central Italy

ELENA BOARI[1], SIMONE TOMMASINI[1], MARINELLA A. LAURENZI[2] AND SANDRO CONTICELLI[1,3]*

[1]DIPARTIMENTO DI SCIENZE DELLA TERRA, UNIVERSITÀ DEGLI STUDI DI FIRENZE, VIA GIORGIO LA PIRA, 4, I-50121, FIRENZE, ITALY

[2]ISTITUTO DI GEOSCIENZE E GEORISORSE, CONSIGLIO NAZIONALE DELLE RICERCHE, VIA MORUZZI, 1, I-56124, PISA, ITALY

[3]ISTITUTO DI GEOSCIENZE E GEORISORSE, CONSIGLIO NAZIONALE DELLE RICERCHE, VIA GIORGIO LA PIRA, 4, I-50121, FIRENZE, ITALY

RECEIVED MARCH 16, 2008; ACCEPTED JANUARY 1, 2009
ADVANCE ACCESS PUBLICATION FEBRUARY 19, 2009

The Middle Latin Valley volcanic field forms part of the Roman Magmatic Province and includes Pleistocene monogenetic volcanism characterized by the emplacement of small lava flows and minor pyroclastic ejecta and flows. The absence of a main volcanic edifice and of a large, shallow-level magma reservoir allows the eruption of primitive magmas. Geochemical and petrological data suggest that at least four types of mafic parental magmas are present within the volcanic field: (1) melilite-bearing ultrapotassic (kamafugitic); (2) plagioclase-bearing and -free leucititic (HKS); (3) shoshonitic; (4) sub-alkaline. ^{40}Ar–^{39}Ar dating reveals diachronous emplacement of mafic magmas with different levels of K enrichment; the kamafugitic lavas are the oldest and the sub-alkaline lavas the youngest. Incompatible trace element contents strictly follow K_2O, but overall the groups of rocks show similar trace element fractionation, with high field strength elements less enriched than large ion lithophile elements. Despite a restricted range in MgO and SiO_2 contents, the Middle Latin Valley volcanic rocks have highly variable Sr, Nd and Pb isotopic compositions. The sub-alkaline rocks have the lowest $^{87}Sr/^{86}Sr$ and the highest $^{143}Nd/^{144}Nd$, whereas the kamafugitic rocks have the highest $^{87}Sr/^{86}Sr$ and the lowest $^{143}Nd/^{144}Nd$. Intermediate isotopic compositions between these two end-members are shown by leucitites–plagio-leucitites and shoshonites. A clear, time-dependent trend of isotopic variation is observed. This also holds true for Pb isotope compositions, with shoshonitic and sub-alkaline rocks showing the most radiogenic signatures and the kamafugitic rocks the least radiogenic signatures. The overall geochemical characteristics of the magmas can be reconciled in terms of a model involving recycling of marly shales within the upper mantle; this overprinted earlier pervasive metasomatism related to melts (supercritical fluids) derived from altered oceanic basalts. The crustal derived (marl) end-member is considered to have been concentrated within a metasomatic vein network within the lithosphere, whereas the supercritical fluid-metasomatized end-member occurs within the surrounding mantle. Early partial melting of veins produced strongly undersaturated melilite-bearing ultrapotassic magma (kamafugitic). The progressive exhaustion of the veined mantle increased the

*Corresponding author. E-mail: sandro.conticelli@unifi.it

contribution of the surrounding mantle to magma production, explaining the decrease of K_2O with time in the mafic magmas and the geochemical and isotopic transition from leucititic–plagio-leucititic to shoshonitic and sub-alkaline magmas, the latter being the youngest products erupted.

KEY WORDS: *melilite- and leucite-bearing ultrapotassic rocks; shoshonite; calc-alkaline; trace elements; Sr–Nd–Pb isotopes; ^{40}Ar–^{39}Ar ages; Roman Magmatic Province; Middle Latin Valley*

INTRODUCTION

Potassic and ultrapotassic magmatism at destructive plate boundaries is commonly associated with calc-alkaline magmatism (e.g. Barberi *et al.*, 1973; van Bergen *et al.*, 1992; Francalanci *et al.*, 1993, 2004, 2007; Carmichael *et al.*, 1996; Hoogewerff *et al.* 1997; Peccerillo, 2005; Tommasini *et al.*, 2007). Potassic and ultrapotassic igneous rocks from within-plate and plate-margin tectonic settings are clearly distinguished based on their trace element and isotopic characteristics, but there remains some debate concerning the origin of the isotopic signatures (e.g. Rogers *et al.*, 1985, 1992, 1998; Conticelli & Peccerillo, 1992; Altherr *et al.*, 2004, 2008; Davies *et al.*, 2006; Mirnejad & Bell, 2006). In Central Italy all of the types of ultrapotassic rock recognized by Foley *et al.* (1987) are found; lamproites, kamafugites, leucitites and plagio-leucitites occur intimately associated in time and space with shoshonitic, high-K calc-alkalic and calc-alkalic rocks (Conticelli *et al.*, 1992, 2001, 2009*a*; Peccerillo, 2005). Despite their petrological and mineralogical differences, these rock types display similar incompatible trace element patterns, albeit different isotopic signatures (Conticelli *et al.*, 2002).

A further debate concerns the time-dependent transition from ultrapotassic to shoshonitic and sub-alkaline magmas that is observed in the Quaternary Italian volcanic provinces. This has been attributed either to a diminishing contribution to melt production from net-veined metasomatized lithospheric mantle with respect to the surrounding mantle (e.g. Perini *et al.*, 2004; Conticelli *et al.*, 2007; Avanzinelli *et al.*, 2009), or to different depths of mantle partial melting (e.g. Peccerillo & Panza, 1999; Peccerillo, 2005; Frezzotti *et al.*, 2007). Investigating this issue in large composite volcanoes is complicated by shallow-level differentiation processes, which can dramatically change the geochemical characteristics of the volcanic rocks (e.g. Barbieri *et al.*, 1988; Conticelli *et al.*, 1991, 1997; Ferrari *et al.*, 1996; Pappalardo *et al.*, 1999; Perini *et al.*, 2000, 2003, 2004; Beccaluva *et al.*, 2002; Conte & Dolfi, 2002).

The Middle Latin Valley is a small volcanic field in which potassic and ultrapotassic magmas were erupted from small, monogenetic, centres within a restricted area (Fig. 1), during the middle Pleistocene (Civetta *et al.*, 1979, 1981; Pasquarè *et al.*, 1985). Recently, sub-alkaline magmatic rocks with possible calc-alkaline affinity and ultrapotassic rocks with kamafugitic affinity have been recognized (Boari & Conticelli, 2007). The eruption sequence of the magma types is obscured by both the paucity of age determinations (Basilone & Civetta, 1975; Fornaseri, 1985) and the lack of clear volcano-stratigraphic relationships between the centres (Angelucci *et al.*, 1974; Acocella *et al.*, 1996; Sani *et al.*, 2004). In this study we have complemented existing age determinations with new $^{40}Ar/^{39}Ar$ dating to clarify the temporal transition between the magma types. As a consequence of the limited differentiation of these magmas en route to the surface, the Middle Latin Valley volcanic field offers a unique opportunity, by means of a detailed petrological, geochemical and Sr–Nd–Pb isotopic study, to unravel the genetic relationships between strongly alkaline and sub-alkaline magmatism at destructive plate boundaries.

GEOLOGICAL BACKGROUND AND VOLCANOLOGY

The Middle Latin Valley volcanic field is located in the Southern Latium area (Fig. 1), some hundred kilometres south of Rome, and developed during the Pleistocene between 0·7 and 0·1 Ma (e.g. Basilone & Civetta, 1975; Fornaseri, 1985). It is the only area of the Roman Magmatic Province that lacks a large volcanic edifice; only small volumes of primitive magmas have erupted from scattered monogenetic volcanic centres (Civetta *et al.*, 1979, 1981; Boari, 2005; Boari & Conticelli, 2007; Frezzotti *et al.*, 2007). The total volume of erupted magma is significantly lower than in all the other volcanic districts of the Roman Magmatic Province, probably as a result of the distinctive geological and geodynamic evolution of the Apennine chain and Adriatic foreland in this area (D'Agostino *et al.*, 2005). Monogenetic volcanoes are spread over a restricted area between the Apennine chain and the Monti Lepini well within the valley of the Sacco River (Fig. 1), the median sector of the Latin Valley, which is a NNW–SSE depression between the Apennine chain and the 'Monti Lepini–Monti Ausoni' peri-Tyrrhenian ridge. The volcanic field is made up of cinder cones, small lava fields with plateau-like structures, short lava tongues and tuff rings with associated small-volume hydromagmatic pyroclastic flows. The vents are arranged along two main tectonic trends. The main tectonic structure is represented by the NNW–SSE border fault at the foot of Monti Lepini, developed during post-orogenic extension following the eastward movement of the Apennine compression front. This tectonic lineament is cut by younger tectonic

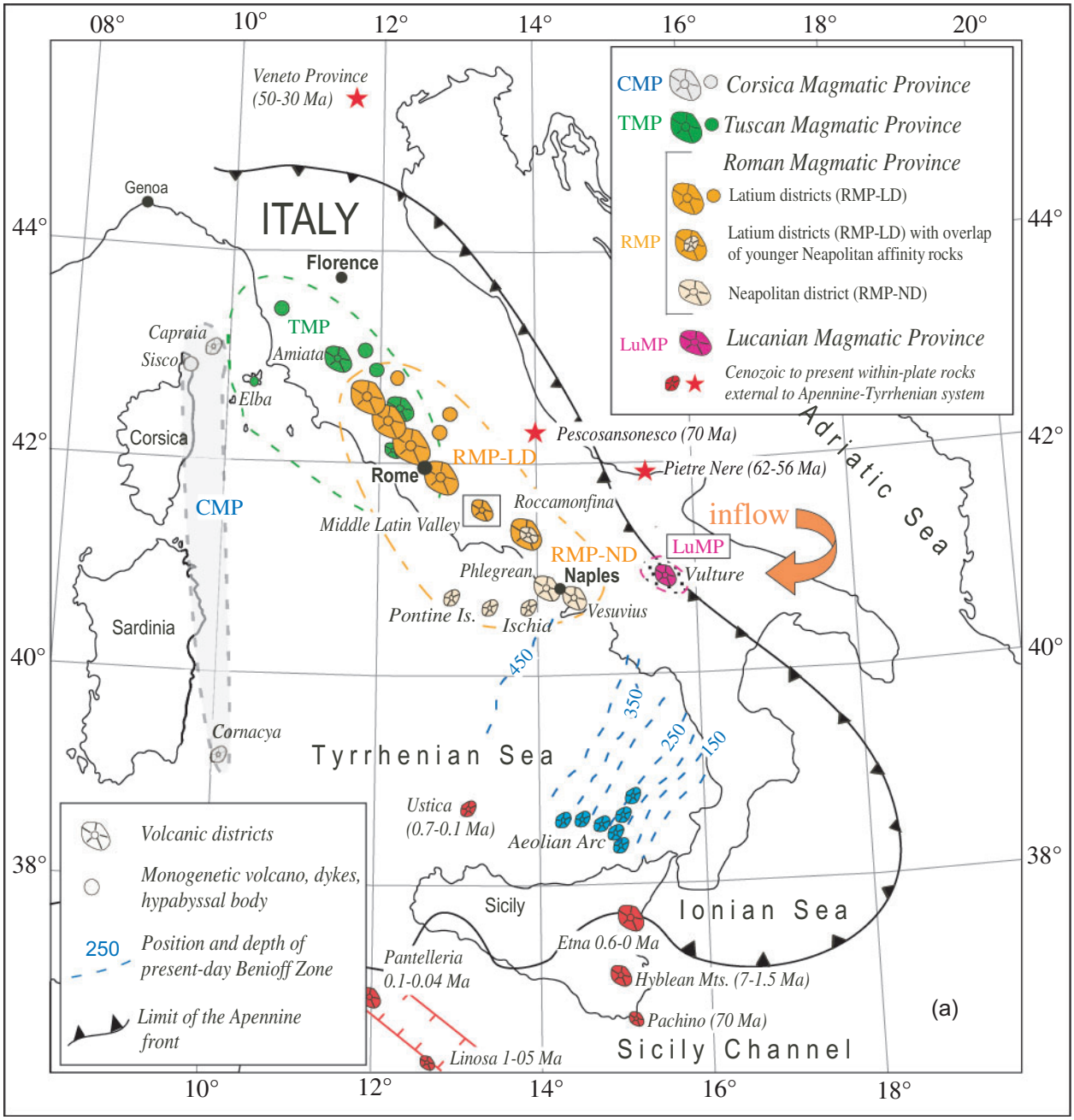

Fig. 1. Distribution of the Plio-Pleistocene volcanic rocks in the Italian peninsula (a), and a geological sketch map of the Sacco River Valley (b) (i.e. Middle Latin Valley volcanic field). Drawn after Pasquaré *et al.* (1985), Conticelli *et al.* (2004, 2007), Sani *et al.* (2004) and Boari & Conticelli (2007). Main monogenetic volcanoes are represented by cinder cones, tuff rings and small plateau-like lava flows.

structures made up of north–south- and NNE–SSW-trending dextral strike-slip faults (Sani *et al.*, 2004; Fig. 1). Volcanic activity was subsequently controlled by these tectonic structures, which provided preferential pathways for the mafic low-viscosity magmas to reach the surface (Acocella *et al.*, 1996).

SAMPLING AND ANALYTICAL METHODS

Eighty samples representing the entire spectrum of volcanic products of the Middle Latin Valley volcanic field were collected and processed. The degree of weathering was

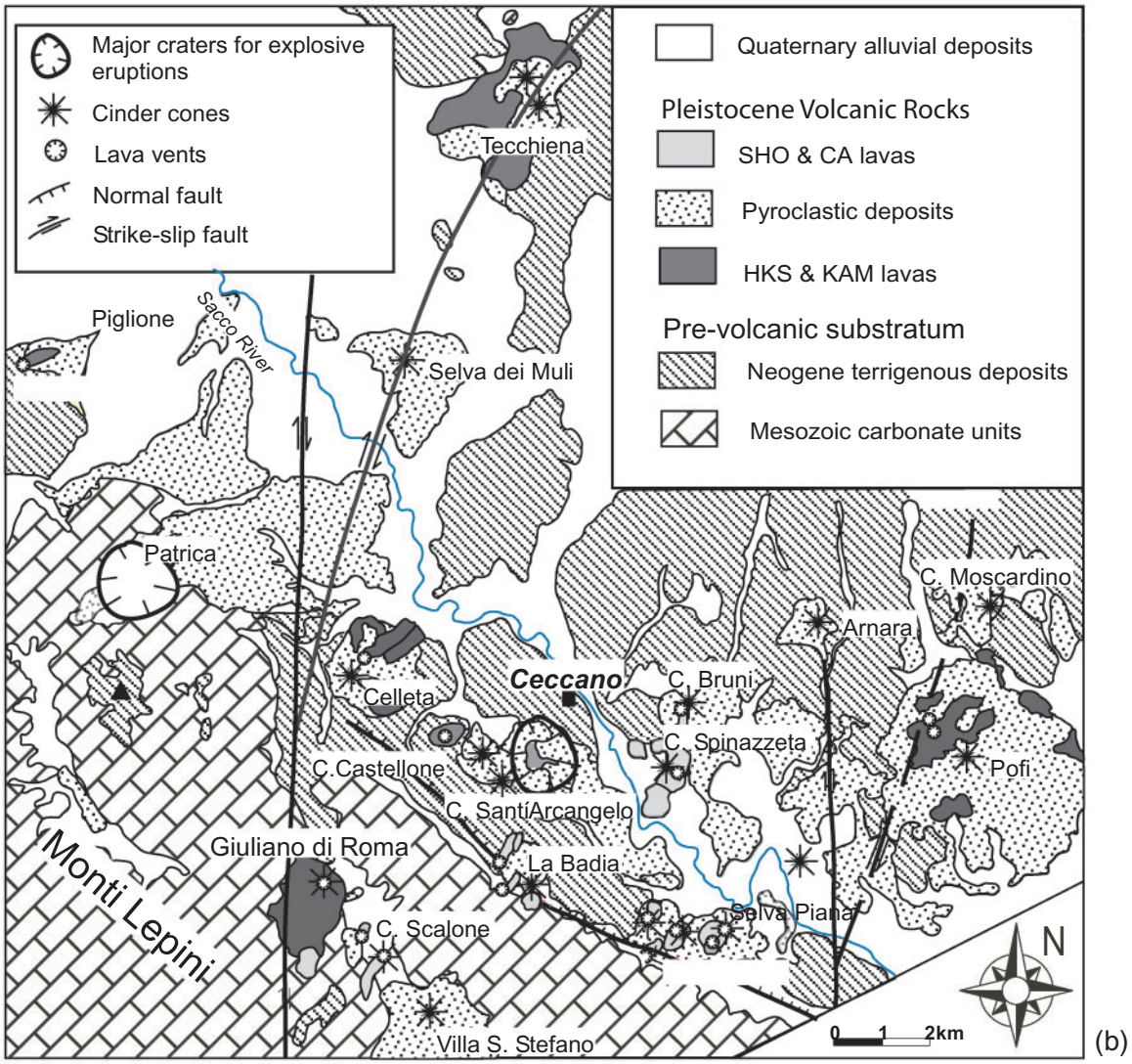

Fig. 1. Continued.

evaluated by preliminary petrographic study using both optical and X-ray diffraction (XRD) methods (Boari & Conticelli, 2007); only unaltered samples were selected for detailed study. Selected samples were ground in agate mills for bulk-rock analysis. Table 1 lists the locations of all samples, their geographical coordinates, rock type and mineralogy.

Thirteen samples, representative of the entire period of volcanic activity, were selected for ^{40}Ar–^{39}Ar dating, on the basis of the degree of freshness and K content (Table 2; the complete dataset is provided as Electronic Appendix 1 at http://petrology.oxfordjournals.org). Samples were crushed and sieved, and suitable phases for dating were separated using conventional magnetic and gravimetric methods, followed by hand-picking. In general, we used the groundmasses (from 160 to 250 μm) from most of the samples, with the exception of a few samples that had sufficient phenocrysts to allow separation of microcrystals of leucite (ERN 56 and 86) and of centimetre-sized phlogopite phenocrysts (ERN 101 and 102). The selected phases were washed with methanol and rinsed many times in deionized water in an ultrasonic bath. Samples were wrapped in aluminium foil and packed in a quartz tube together with aliquots of the age monitor Fish Canyon Tuff (FCT) biotite (Baksi *et al.*, 1996) and were irradiated for 2 h in the core of the 250 kW TRIGA reactor, Pavia University. The updated age calibration of FCT biotite against FCT sanidine 28·26 ± 0·18 Ma (2σ) (Di Vincenzo & Skàla, 2009) has been used to calculate the irradiation factor J. A second set of samples was irradiated following the same procedure and neutron flux, using FCT

Table 1: Sample list, localities, coordinates, and petrography of samples from the Middle Latin Valley volcanic field

Type	Sample	Locality	Latitude	Longitude	Volcanic centre	Volcanic type	Rock type	Texture	Mineralogy
sed	ERN57	Colle Morrone	41°33′28″N	13°18′11″E	—	—	limestone	—	—
KAM	ERN55	Colle Castellone	41°34′08″N	13°18′01″E	Castellone	cinder cone	lava flow	sub-porphyritic	**lct** + **cpx** + **olv** + lct + mel + cpx + opq + phl + ne + *cal*
KAM	ERN56	Colle Castellone	41°34′02″N	13°18′07″E	Castellone	cinder cone	lava flow	sub-porphyritic	**lct** + **cpx** + lct + cpx + mel + opq + phl + ne + apa + *cal*
KAM	ERN84s	Colle Castellone	40°33′49″N	12°18′08″E	Castellone	cinder cone	lava flow	sub-porphyritic	**cpx** + lct + cpx + mel + phl + ne + apa + *cal*
KAM	ERN84t	Colle Castellone	40°33′49″N	12°18′08″E	Castellone	cinder cone	lava flow	sub-porphyritic	**lct** + **cpx** + **olv** + lct + cpx + mel + opq + phl + ne + *cal*
KAM	ERN84	Colle Castellone	40°33′49″N	12°18′08″E	Castellone	cinder cone	lava flow	sub-porphyritic	**lct** + **cpx** + **olv** + lct + cpx + mel + opq + phl + ne + *cal*
KAM	ERN42	Patrica, village	41°35′23″N	13°14′29″E	Patrica	tuff ring	pyrocl. flow	vitroclastic	**cpx** + mel + olv + glass + *cal*
KAM	PAT	Patrica, village	41°35′23″N	13°14′29″E	Patrica	tuff ring	pyrocl. flow	vitroclastic	**olv(chr)** + **cpx** + **mel** + **hya** + **mtc** + lct + opq + spn + apa + gl
KAM	ERN31	Frosinone, Selva dei Muli	41°37′43″N	13°17′39″E	Patrica	tuff ring	pyrocl. flow	vitroclastic	**lct** + **cpx** + mel + phl + gl
KAM	ERN63	Celleta, Fornelli	41°37′43″N	13°17′39″E	Patrica	tuff ring	pyrocl. flow	vitroclastic	**olv(chr)** + **cpx** + phl + gl + *cal*
KAM	ERN101	Tomacella	—	—	Patrica	tuff ring	pyrocl. flow	vitroclastic	cpx + mel + lct + phl + gl
KAM	ERN102	Tomacella	—	—	Patrica	tuff ring	pyrocl. flow	vitroclastic	cpx + mel + lct + phl + gl
KAM	ERN103	Tomacella	—	—	Patrica	tuff ring	xenolith	porphyritic	—
HKS	ERN39	Morolo, il Piglione	41°37′31″N	13°12′39″E	Piglione	lava vent	lava flow	aphyric	cpx + olv + lct + mel + opq
HKS	ERN41	Morolo, il Piglione	41°37′38″N	13°12′37″E	Piglione	lava vent	lava flow	aphyric	cpx + olv + lct + mel + opq
HKS	ERN40	Morolo, il Piglione	41°37′34″N	13°12′38″E	Piglione	lava vent	lava flow	aphyric	cpx + olv + lct + mel + opq
HKS	ERN86	Colle Sant'Arcangelo	41°33′42″N	13°18′29″E	Arcangelo	cinder cone	lava flow	aphyric	cpx + lct + opq + phl + ne
HKS	ERN85	Colle Sant'Arcangelo	41°33′42″N	13°18′29″E	Arcangelo	cinder cone	lava flow	aphyric	cpx + lct + opq + phl + ne
HKS	ERN61	Celleta, Case Folgara	41°34′17″N	13°17′34″E	Celleta	plateau-like field	lava flow	porphyritic	**cpx** + **olv(chr)** + lct + opq + ne + gl
HKS	ERN64	Celleta, Fornelli	41°34′47″N	13°16′59″E	Celleta	plateau-like field	lava flow	sub-porphyritic	**olv(chr)** + **cpx** + lct + crypto gdm
HKS	ERN58	Celleta, Case Schiappa	41°34′00″N	13°17′23″E	Celleta	plateau-like field	lava flow	sub-porphyritic	**cpx** + **olv(chr)** + lct + cpx + opq + gl
HKS	ERN62	Celleta, Case Folgara	41°34′17″N	13°17′33″E	Celleta	plateau-like field	lava flow	porphyritic	**cpx** + **olv(chr)** + **lct** + lct + crypto gdm
HKS	ERN65	Celleta, Pescara	41°34′47″N	13°16′59″E	Celleta	plateau-like field	lava flow	sub-porphyritic	**olv(chr)** + **cpx** + lct + crypto gdm
HKS	ERN60	Celleta, Case Folgara	41°34′17″N	13°17′34″E	Celleta	plateau-like field	lava flow	sub-porphyritic	**cpx** + **olv(chr)** + lct + opq + ne + gl
HKS	ERN67	Celleta, Quattrini quarry	41°34′59″N	13°17′24″E	Celleta	plateau-like field	lava flow	porphyritic	**olv(chr)** + **cpx** + **lct** + lct + cpx + opq + gl
HKS	ERN59	Celleta, 2nd traversa di Celleta	41°33′51″N	13°17′20″E	Celleta	plateau-like field	lava flow	sub-porphyritic	**cpx** + **olv(chr)** + lct + cpx + opq + glass
HKS	ERN66	Celleta, railway tunnel	41°34′55″N	13°17′19″E	Celleta	plateau-like field	lava flow	sub-porphyritic	**cpx** + **olv(chr)** + cpx + lct + opq + phl + apa
HKS	ERN50	Giuliano di Roma, Costa Mastrogiacomo	41°21′03″N	13°16′42″E	Giuliano	lava field	lava flow	porphyritic	**cpx** + **olv(chr)** + cpx + lct + opq + hbl + ne + apa + *anc*
HKS	ERN46	Giuliano di Roma, soccer field	41°32′28″N	13°16′24″E	Giuliano	lava field	lava flow	aphyric	lct + cpx + olv + gl
HKS	ERN44	Giuliano di Roma, village	41°32′22″N	13°16′41″E	Giuliano	lava field	neck	porphyritic	**cpx** + **olv(chr)** + **lct** + cpx + lct + opq + gl
HKS	ERN48	Giuliano di Roma, Madonna Pietromaggio	41°32′20″N	13°16′24″E	Giuliano	lava field	lava flow	sub-porphyritic	**cpx** + **olv(chr)** + cpx + lct + opq + gl
HKS	ERN87	Giuliano di Roma, Valcatora	41°31′22″N	13°17′03″E	Giuliano	lava field	neck	porphyritic	**cpx** + **olv(chr)** + lct + cpx + opq

(continued)

Table 1: Continued

Type	Sample	Locality	Latitude	Longitude	Volcanic centre	Volcanic type	Rock type	Texture	Mineralogy
HKS	ERN52	Giuliano di Roma–Villa S. Stefano road	41°31′58″N	13°17′15″E	Giuliano	lava field	lava flow	sub-porphyritic	**olv(chr)** + **cpx** + lct + cpx + opq + apa
HKS	ERN53	Giuliano di Roma–Villa S. Stefano road	41°31′58″N	13°17′15″E	Giuliano	lava field	lava flow	sub-porphyritic	**olv(chr)** + **cpx** + lc + cpx + opq
HKS	ERN47	Giuliano di Roma, Pietromaggio	41°32′14″N	13°16′27″E	Giuliano	lava field	lava flow	sub-porphyritic	**cpx** + **olv** + lct + cpx + opq + gl
HKS	ERN24	Giuliano di Roma, Case Ledanno	—	—	Giuliano	lava field	lava flow	sub-porphyritic	**cpx** + **olv(chr)** + lct + cpx + opq + gl
HKS	ERN45	Giuliano di Roma, Costa Mastrogiacomo	41°32′27″N	13°16′30″E	Giuliano	lava field	lava flow	aphyric	lct + cpx + olv + gl
HKS	ERN49	Giuliano di Roma, Costa Mastrogiacomo	41°31′60″N	13°16′26″E	Giuliano	lava field	lava flow	porphyritic	**cpx** + **olv(chr)** + **hbl** + lct + cpx + opq + apa
HKS	ERN22	Giuliano di Roma, village	—	—	Giuliano	lava field	lava flow	sub-porphyritic	**cpx** + **olv** + plg + cpx + opq + olv + gl
HKS	ERN54	Giuliano di Roma, village	41°32′11″N	13°16′44″E	Giuliano	lava field	lava flow	sub-porphyritic	**cpx** + **olv** + lct + cpx + opq + gl
HKS	ERN30	Frosinone, Selva dei Muli	41°37′43″N	13°17′39″E	Selva Muli	cinder cone	bomb	aphyric	cpx + gl
HKS	ERN29	Frosinone, Selva dei Muli	41°37′43″N	13°17′39″E	Selva Muli	cinder cone	bomb	sub-porphyritic	cpx + ant + gl
HKS	ERN32	Frosinone, Selva dei Muli	41°37′43″N	13°17′39″E	Selva Muli	cinder cone	lapilli	hyaline	gl
HKS	ERN36	Tecchiena, Quarticciolo	41°40′33″N	13°19′16″E	Tecchiena	plateau-like field	lava flow	sub-porphyritic	**cpx** + **olv** + cpx + lct + olv + plg + gl
HKS	ERN33	Tecchiena, Monastery	41°41′09″N	13°19′20″E	Tecchiena	plateau-like field	lava flow	porphyritic	**cpx** + **olv** + **plg** + cpx + lct + olv
HKS	ERN34	Tecchiena, Monastery	41°41′09″N	13°19′20″E	Tecchiena	plateau-like field	lava flow	porphyritic	**cpx** + **lct** + **olv** + **plg** + lct + cpx + plg + opq + apa + *anc*
HKS	ERN28	Tecchiena, Monastery	41°41′09″N	13°19′20″E	Tecchiena	plateau-like field	lava flow	sub-porphyritic	**cpx** + **olv** + cpx + lct + apa + plg
HKS	ERN26	Tecchiena–Alatri road	41°41′49″N	13°20′16″E	Tecchiena	plateau-like field	lava flow	sub-porphyritic	**cpx** + **olv** + cpx + lct + plg + opq + apa
HKS	ERN38	Tecchiena Fosso San Pietro	41°39′54″N	13°19′01″E	Tecchiena	plateau-like field	lava flow	porphyritic	**cpx** + **olv** + **lct** + cpx + lct + plg + opq + gl
HKS	ERN27	Tecchiena, Monastery	41°41′09″N	13°19′20″N	Tecchiena	plateau-like field	lava flow	sub-porphyritic	**cpx** + **olv** + lct + crtpto gdm
HKS	ERN37	Tecchiena, Campone	41°39′58″N	13°19′32″E	Tecchiena	plateau-like field	lava flow	sub-porphyritic	**cpx** + **olv** + cpx + lct + plg + opq + apa
HKS	ERN70	Pofi, Colle Santa Lucia	41°34′08″N	13°26′13″E	Pofi	lava field	lava flow	sub-porphyritic	**cpx** + **olv(chr)** + lct + plg + cpx + olv + opq + apa
HKS	ERN72	Pofi, Fontana dell'Ocaro	41°33′08″N	13°25′15″E	Pofi	lava field	lava flow	sub-porphyritic	**cpx** + **olv(chr)** + lct + cpx + plg + opq + bio + apa
HKS	ERN69	Pofi, Molino dei Ripi	41°33′41″N	13°26′02″E	Pofi	lava field	lava flow	sub-porphyritic	**cpx** + **olv(chr)** + lct + cpx + plg + opq + apa
HKS	ERN99	Santa Croce di Pofi	41°33′54″N	13°24′30″E	Pofi	lava field	lava flow	sub-aphyric	**cpx** + **olv(chr)** + lct + crypto gdm
HKS	ERN73	Pofi, Colle Bove	41°33′18″N	13°24′50″E	Pofi	lava field	lava flow	sub-porphyritic	**olv(chr)** + **cpx** + cpx + lct + opq + plg + apa

HKS	ERN75	Pofi, Frantoio	41°34′41″N	13°25′35″E	Pofi	lava field	lava flow	sub-porphyritic	**cpx** + **olv(chr)** + lct + cpx + olv + plg + opq
HKS	ERN68	Pofi, Case Recino	41°33′58″N	13°26′41″E	Pofi	lava field	lava flow	sub-porphyritic	**cpx** + **olv** + lct + plg + cpx + olv + opq
HKS	ERN98	Pofi, Poggio Cisterna	41°34′40″N	13°24′48″E	Pofi	lava field	lava flow	sub-aphyric	**cpx** + **olv(chr)** + lct + crypto gdm
HKS	ERN74	Pofi, Case Costantini	41°33′32″N	13°24′48″E	Pofi	lava field	lava flow	sub-porphyritic	**cpx** + **olv(chr)** + lct + cpx + plg + opq
HKS	ERN71	Pofi, Colle Marte	41°34′01″N	13°25′40″E	Pofi	lava field	lava flow	sub-porphyritic	**cpx** + **olv(chr)** + lct + plg + cpx + hbl + opq
TRS	ERN23	Valcatora, Case Scalone	—	—	Valcatora	dyke	neck	porphyritic	**cpx** + **olv** + plg + cpx + lct + olv + opq
SHO	ERN92	Selva Piana, Colle Egidi	41°31′41″N	13°21′46″E	Selva Piana	cinder cone	lapilli	hypohyaline	**cpx** + **olv** + cpx + plg + gl
SHO	ERN89	Selva Piana, Colle Vento	41°31′45″N	13°21′58″E	Selva Piana	cinder cone	lava flow	sub-porphyritic	**cpx** + **olv** + cpx + plg + gl
SHO	ERN20	Colle Spinazzeta, railway	41°33′13″N	13°21′00″E	Spinazzeta	cinder cone	neck	porphyritic	**olv(chr)** + **cpx** + plg + cpx + olv + opq
SHO	ERN77	Colle Spinazzeta, railway	41°33′13″N	13°21′00″E	Spinazzeta	cinder cone	neck	porphyritic	**cpx** + **olv(chr)** + plg + olv + cpx + opq + lct
SHO	ERN21	Colle Spinazzeta, railway	41°33′07″N	13°21′08″E	Spinazzeta	cinder cone	lava flow	porphyritic	**cpx** + **olv(chr)** + plg + olv + cpx + opq
SHO	ERN78	Colle Spinazzeta, railway	41°33′07″N	13°21′08″E	Spinazzeta	cinder cone	lava flow	porphyritic	**cpx** + **olv(chr)** + plg + cpx + opq
SHO	ERN91	Selva Piana, Villa Sant'Ermete	41°31′35″N	13°21′21″E	Selva Piana	cinder cone	lava flow	porphyritic	**cpx** + **olv(chr)** + plg + cpx + opq + olv + lct
SHO	ERN97	Selva Piana, Colle Vescovo	41°32′02″N	13°21′28″E	Selva Piana	cinder cone	lava flow	porphyritic	**olv(chr)** + **cpx** + plg + cpx + opq
SHO	ERN96	Selva Piana, Fontanile Colle Vescovo	41°32′02″N	13°21′28″E	Selva Piana	cinder cone	lava flow	porphyritic	**olv(chr)** + **cpx** + plg + cpx + opq
CA	ERN80	La Badia, Case Piedimonte	41°32′23″N	13°19′12″E	La Badia	lava vent	lava flow	sub-porphyritic	**cpx** + **olv(chr)** + plg + cpx + olv + gl
CA	ERN100	Pofi, village	41°33′50″N	13°24′50″E	Pofi	cinder cone	scoria	sub-aphyric	**cpx** + gl
CA	ERN76	Colle Spinazzeta, top	41°33′37″N	13°21′30″E	Spinazzeta	cinder cone	lava flow	sub-porphyritic	**cpx** + **olv** + opq + crypto gdm
CA	ERN25	Fosso Valera, hill at 134 m a.s.l.	41°32′41″N	13°22′57″E	Colle 134	cinder cone	lava flow	porphyritic	**cpx** + **olv** + plg + opq + cpx + gl
CA	ERN83	La Badia, Case Piedimonte	41°32′35″N	13°19′19″E	La Badia	lava vent	bomb	porphyritic	**cpx** + **olv** + crypto gdm
CA	ERN82	La Badia, Case Masi	41°32′41″N	13°19′06″E	La Badia	lava vent	lava flow	porphyritic	**cpx** + **olv** + gl
CA	ERN81	La Badia, Case Masi	41°32′41″N	13°19′06″E	La Badia	lava vent	lava flow	porphyritic	**olv** + **cpx** + plg + cpx + opq
CA	ERN95	Selva Piana, Colle degli Scolopi	41°32′09″N	13°21′20″E	Selva Piana	cinder cone	lava flow	porphyritic	**cpx** + **olv** + **plg** + cpx + plg + opq + olv
CA	ERN94	Selva Piana, Colle degli Scolopi	41°32′09″N	13°21′20″E	Selva Piana	cinder cone	lava flow	porphyritic	**cpx** + **olv** + **plg** + cpx + plg + opq + olv
CA	ERN93	Selva Piana, Colle degli Scolopi	41°32′09″N	13°21′20″E	Selva Piana	cinder cone	lava flow	porphyritic	**olv** + cpx + plg + opq + olv

KAM, kamafugitic; HKS, high-potassium series (Appleton, 1972), made up of leucitites and plagioclase-leucitites; TRS, transitional between HKS and SHO; SHO, shoshonites (Conticelli *et al.*, 2004; former KS of Civetta *et al.*, 1981); CA, calc-alkaline type sub-alkaline basalts; pyrocl. flow, pyroclastic flow; olv, olivine; chr, chromite; mtc, monticellite; cpx, clinopyroxene; mel, melilite; hbl, hornblende; phl, phlogopite; bio, biotite; plg, plagioclase; ant, anorthoclase; kf, sanidine; hya, hyalophane; lct, leucite; an, analcime; ne, nepheline; apa, apatite; spn, spinel; opq, opaques; gl, glass; cal, calcite; gdm, groundmass; crypto, cryptocrystalline. Phases in bold are phenocrysts; phases in parentheses are enclosed in the preceding host; phases in italics are secondary minerals.

Table 2: Summary of the $^{40}Ar/^{39}Ar$ data for the Middle Latin Valley volcanic field

Series	Locality	Sample	Phase	*n*	^{39}Ar (%)	Plateau age (ka)	2σ	MSWD	Isochron age (ka)	2σ	MSWD	$^{40}Ar/^{36}Ar$ (initial)	2σ	Total age (ka)	2σ
KAM	Colle Castellone	ERN 56	leucite	6	91	600	±4	0·5	599	±5	0·6	299	±11	602	±4
KAM	La Tomacella, lower	ERN 102	phlogopite	8		421*	±13	0·8	419	±23	0·9	297	±7		
KAM	La Tomacella, upper	ERN 101	phlogopite	6		407*	±10	0·8	415	±27	1·0	294	±6		
HKS	Piglione	ERN 40	groundmass	6	80	610	±10	1·6	573	±61	1·4	312	±27	633	±14
HKS	Tecchierna	ERN 34	groundmass			n.d.			n.d.					412	±11
HKS	Celleta	ERN 60	groundmass	10	98	413	±6	0·9	412	±7	1·0	297	±6	410	±7
HKS	Giuliano di Roma	ERN 50	groundmass	10	100	391	±6	0·7	396	±11	0·6	291	±10	387	±9
HKS	Colle Sant'Arcangelo	ERN 86	leucite	4	73	252	±4	0·6	252	±34	1·0	295	±33	260	±4
TRS	Valcatora	ERN 23	groundmass	12	100	376	±8	0·6	371	±15	0·6	298	±6	379	±10
SHO	Selva Piana	ERN 91	groundmass	10	100	359	±11	1·0	405	±60	0·9	288	±9	357	±13
SHO	Spinazzeta	ERN 20	groundmass	10	100	345	±7	1·7	352	±23	1·7	292	±23	345	±9
CA	Colle Vescovo	ERN 94	groundmass	4	66	300	±28	0·9	n.d.					269	±37
CA	Pofi, village	ERN 100	groundmass	8	97	289	±32	0·4	282	±78	0·5	298	±20	298	±43

n, number of steps used in the plateau calculation; ^{39}Ar (%), percentage of ^{39}Ar degassed used in the plateau calculation; KAM, kamafugitic; HKS, plagio-leucitites and leucitites, former High Potassium Series of Appleton (1972); TRS: transitional between HKS and shoshonitic rocks; SHO, shoshonitic rocks (Conticelli *et al.*, 2004), former KS (Potassium Series) of Civetta *et al*. (1981); CA, calc-alkaline type basalts. Errors on ages include the uncertainty on the irradiation J factor.
*Weighted average of single crystal dating.

sanidine as the age monitor (28·03 Ma, Jourdan & Renne, 2007).

The samples were loaded into 9 mm diameter wells machined in a copper disc. The section of the ultra-high vacuum extraction line that was opened to air to load the samples was heated to about 180°C for 8 h to outgas all the air adsorbed on the exposed surfaces. The samples were then step-heated using the defocused beam of a diode-pumped Nd–YAG laser in continuous mode. The laser beam passes through a faceted lens that produces an even spatial distribution of the beam power and, as the laser beam surface is smaller than the area analysed, the beam was slowly rastered over the entire sample. The evolved gas was cleaned for 15 min with two SAES AP10 getters held at ~400°C and one SAES GP50 getter held at room temperature. Some samples of the second set were also cleaned with hot titanium (800°C). ERN 101 and ERN 102 phlogopite crystals were analysed as single crystals: some crystals were fused in two steps, a low laser power (i.e. temperature) cleaning step, followed by the fusion step; other crystals were fused in a single step. Ar isotopes were measured with a MAP 215–50 mass spectrometer at the IGG-CNR, Pisa, in peak jumping mode, using a Balzers electron multiplier. Raw mass spectrometer data were corrected for blanks (measured every 2–3 steps), mass discrimination, ^{37}Ar and ^{39}Ar decay, and nuclear interferences from Ca and K using the ArArCALC software (Koppers, 2002). Errors on the ages of each step include uncertainties related to the regression of the intensities of each isotope, procedural blanks, nuclear interferences and mass discrimination corrections. Uncertainties on each step age do not include the uncertainty on the J factor, whereas the errors on total fusion ages in the Supplementary Data table (Electronic Appendix 1) and all the errors in Table 2 do include that error.

The criteria used for the age results summarized in Table 2 are the following: a plateau needs at least 70% of ^{39}Ar release and three consecutive steps agreeing at the 2σ level. Plateau ages were calculated assuming an atmospheric $^{40}Ar/^{36}Ar$ initial ratio (i.e. 295·5), and weighing each step by the inverse variance of its analytical error. Inverse isochron calculations were performed on the same steps used to calculate the plateau age, to check the consistency of the assumption about the Ar isotopic initial ratio. Ages of samples ERN 101 and ERN 102 are expressed as the weighted average of single crystal ages and isochron ages (Table 2).

Major and some trace elements on whole-rock samples were determined at the Dipartimento di Scienze della Terra (DST) of the Università degli Studi di Firenze using an integrated X-ray fluorescence (XRF) and wet chemical method. XRF analysis was carried out on pressed powder pellets with a boric acid support using a Philips spectrometer. Matrix correction effects were performed according

to Franzini *et al.* (1972) and de Vries & Jenkins (1971) for major and trace elements, respectively. Na_2O and MgO contents were determined by atomic absorption spectrometry (AAS), FeO by titration (Shapiro & Brannock, 1962), and loss on ignition (LOI) by gravimetry. To tackle the problem of evaluating the accuracy of analyses, K_2O and CaO contents were checked randomly by AAS; the bias within the XRF data is within the estimated error levels (Table 3; the complete dataset is provided as Electronic Appendix 2). Other trace elements, marked with an asterisk in Table 3, were determined by inductively coupled plasma mass spectrometry (ICP-MS) at the Geowissenschaftliches Zentrum der Universität Göttingen (GZG) on a VG PQ2 system. Analytical accuracies are synonymous with the significant digits of concentrations reported in Table 3. One sample (ERN 20es) had its trace element characteristics determined by instrumental neutron activation analysis (INAA) at the DST of the Università degli Studi di Firenze following the procedure described by Poli *et al.* (1977).

Sr, Nd, and Pb isotope compositions (Table 4) were determined at the DST of the Università degli Studi di Firenze following the procedures outlined by Avanzinelli *et al.* (2005). Additional detailed set-up and calibration procedures for Pb purification and isotopic measurements were reported by Boari (2005). Although weathering was carefully checked for before sample selection, to avoid possible Pb, Sr, and Nd contamination, rock powders were leached before digestion. Leaching was performed with 2N HCl on a hot plate (60°C). Sample powders were digested in a HNO_3–HF–HCl mixture and Sr and Nd fractions were collected using standard liquid chromatographic techniques. Sr and Nd isotopic compositions were measured by positive thermal ionization mass spectrometry using a ThermoFinnigan Triton TI© in multi-dynamic mode (Thirlwall, 1991). Sr and Nd isotopic compositions are exponentially corrected for fractionation to $^{86}Sr/^{88}Sr = 0{\cdot}1194$ and $^{146}Nd/^{144}Nd = 0{\cdot}7219$. The $^{87}Sr/^{86}Sr$ average value for the NBS 987 reference sample was $0{\cdot}710251 \pm 12$ (2σ, $n = 120$) and the $^{143}Nd/^{144}Nd$ average value for the La Jolla reference sample was $0{\cdot}511845 \pm 7$ (2σ, $n = 55$). Pb was purified following the method described by Deniel & Pin (2001) using 100–150 μm Sr-spec resins in quartz micro-columns. The Pb yield was evaluated to be about 90%. Pb samples were loaded onto zone-refined Re filaments, with addition of 1 μl of silica gel and 1 μl of high-purity H_3PO_4 and measured in static mode with a ThermoFinnigan Triton TI© at ~1400°C. Mass bias was monitored with repeated measurements of the SRM 981 reference standard and we obtained a mass discrimination factor (ε) of 0·15% per a.m.u. The external reproducibility of the international reference standard SRM 981 was: $^{208}Pb/^{204}Pb = 36{\cdot}495 \pm 23$; $^{207}Pb/^{204}Pb = 15{\cdot}423 \pm 7$; $^{206}Pb/^{204}Pb = 16{\cdot}888 \pm 6$; $^{207}Pb/^{206}Pb = 0{\cdot}91328 \pm 15$; $^{208}Pb/^{207}Pb = 2{\cdot}3662 \pm 4$; $^{208}Pb/^{206}Pb = 2{\cdot}1610 \pm 7$ (2σ, $n = 45$). Total procedure blanks for Sr, Nd and Pb were <200, <150 and <300 pg, respectively, requiring no blank correction to the samples.

PETROGRAPHY AND CLASSIFICATION

The majority of the rocks have aphyric to sub-aphyric textures, although phenocryst proportions greater than 10 vol. % are occasionally found in some of the less alkaline rocks with a rather variable mineralogy, as discussed by Boari & Conticelli (2007). Mafic minerals are the predominant microphenocrysts, with olivine and clinopyroxene ubiquitously present (Table 1). Four groups of rocks have been recognized, with variable alkali contents and petrographic characteristics.

Kamafugitic rocks (KAM) are characterized by the presence of abundant clinopyroxene, leucite, and melilite, and minor olivine, monticellite, apatite, nepheline, Ba-rich phlogopite and Ba-rich sanidine. Kamafugitic rocks have the highest contents of K_2O (9·3–9·9 wt %) and the lowest contents of SiO_2 (45·5–46·5 wt %), and Al_2O_3 (16·2–16·6 wt %), although they are not as low as the Al_2O_3 contents of Umbrian kamafugites (i.e. San Venanzo and Cuppaello; Conticelli *et al.*, 2007, and references therein). On the total alkalis vs silica (TAS) diagram (Le Bas *et al.*, 1986) they plot well within the field of foidites (Fig. 2), close to the Colle Sant'Arcangelo foidites belonging to the leucititic and plagio-leucititic group of rocks.

Plagioclase leucititic (Foley, 1992*a*) and leucititic rocks (HKS; High Potassium Series; Appleton, 1972) are characterized by the presence of abundant clinopyroxene, leucite and, in many cases, plagioclase phenocrysts in addition to olivine, opaque phases, nepheline, amphibole, phlogopite, and apatite. Secondary analcime occurs in weathered samples, which were not analysed in this study. HKS rocks have variable but high K_2O contents (5·7–9·1 wt %), and plot in the TAS diagram within the fields of basanite and phonolitic tephrite, with the exception of the Colle Sant'Arcangelo lavas, which plot within the foidite field (Fig. 2). Within this group of rocks, the highest SiO_2 range (47·4–49·7 wt %) is shown by the lavas and scoriae of the Tecchiena plateau-like field (Fig. 2).

Shoshonitic rocks (SHO) are characterized by the occurrence of abundant clinopyroxene and plagioclase with euhedral olivine and opaque phases. The groundmass has a microcrystalline intersertal texture with fresh interstitial brown glass. Rare leucite crystals occur within the groundmass of some shoshonitic rocks. Shoshonites are characterized by fairly low K_2O contents (2·7–3·4 wt %) and plot within the field of potassic trachybasalts in the TAS diagram (Fig. 2).

Table 3: Major (wt %) and trace (ppm) element compositions of representative samples from the Middle Latin Valley

Group:	limestone	KAM	KAM	HKS	HKS	HKS	HKS	HKS	HKS	HKS	HKS	HKS
Sample:	ERN57	ERN56	ERN84	ERN86	ERN40	ERN58	ERN60	ERN66	ERN50	ERN44	ERN48	ERN29
Note:	limestone	lava	lava	lava	lava	lava	lava	lava	lava	lava	lava	bomb
SiO_2	7·66	46·0	46·5	46·8	46·7	46·8	46·9	47·3	46·5	46·6	46·8	46·8
TiO_2	0·07	1·06	1·10	0·83	0·98	0·84	0·84	0·80	0·84	0·85	0·85	1·04
Al_2O_3	2·09	16·5	16·6	18·2	16·8	17·5	17·5	17·8	17·2	16·5	17·2	18·0
Fe_2O_3	0·62	4·59	5·33	4·93	4·06	4·31	4·85	3·56	4·48	5·49	4·05	7·89
FeO	0·13	3·18	2·83	3·24	2·92	3·05	2·65	3·70	3·42	2·49	3·67	1·02
MnO	0·03	0·14	0·15	0·16	0·13	0·14	0·15	0·14	0·15	0·16	0·15	0·16
MgO	1·05	4·61	4·07	3·63	6·27	5·49	5·19	5·20	6·25	6·55	6·05	5·02
CaO	47·6	10·6	10·3	9·64	10·3	11·3	11·2	10·6	11·1	11·4	11·4	11·0
Na_2O	0·55	2·17	1·56	2·17	2·59	1·97	2·07	2·11	2·18	1·92	1·94	1·48
K_2O	0·28	9·77	9·53	9·14	7·99	7·62	7·49	7·60	6·65	7·23	6·98	5·31
P_2O_5	0·08	0·97	0·92	0·50	0·42	0·41	0·37	0·36	0·36	0·37	0·39	0·37
LOI	39·9	0·47	1·07	0·70	0·80	0·67	0·88	0·85	0·84	0·47	0·61	1·80
Sum	100·0	100·0	100·0	100·0	100·0	100·0	100·0	100·0	100·0	100·0	100·0	100·0
Mg-no.	—	56·82	52·68	49·66	66·58	62·33	60·68	61·11	63·64	64·80	63·32	56·33
Li*	4·3	32·4	31·8	26·7	26·2	28·8	33·8	34·9	30·1	29·5	25·7	20·2
Be*	0·22	8·25	8·41	9·76	6·94	5·92	5·81	6·37	6·03	6·35	5·69	4·35
Sc*	1·2	20·1	20·4	11·0	20·1	18·7	18·3	18·4	22·4	23·6	21·0	20·9
V*	17	223	228	275	198	236	229	230	240	n.a.	240	205
Cr	b.d.l.	13	13	26	205	124	106	98	182	175	173	34
Co	1·90	28·5	29·0	26·7	25·5	26·1	25·6	25·3	27·7	30·0	27·2	28·3
Ni	b.d.l.	34·0	30·9	27·0	95·0	47·0	47·0	45·0	73·0	71·0	61·0	40·2
Cu*	3·10	93·6	87·8	71·8	46·8	70·7	70·0	51·8	74·4	n.a.	54·8	90·4
Zn*	14·7	71·2	73·4	74·2	57·7	66·1	68·1	69·4	60·4	n.a.	61·7	66·2
As*	5·04	17·5	12·3	8·74	15·7	13·2	8·14	10·8	9·23	7·60	7·24	9·55
Rb*	15	491	504	447	391	377	388	429	446	456	395	952
Sr*	386	2500	1870	2260	2140	2130	2190	2260	1790	1870	1900	1860
Y*	4·5	43·2	42·8	40·0	33·2	35·0	34·6	35·1	32·0	33·6	32·6	32·0
Zr*	10	547	512	417	344	293	294	298	280	290	271	266
Nb*	1·62	35·2	35·2	20·9	24·5	13·7	14·4	14·8	13·5	13·9	12·3	12·4
Mo*	1·44	1·21	1·75	2·71	1·69	3·75	3·67	4·31	2·27	1·73	2·67	1·38
Sn*	0·29	6·79	4·83	5·51	5·19	3·99	3·87	3·87	3·65	3·70	3·78	3·93
Sb*	0·16	1·41	1·18	0·74	1·56	0·97	0·99	0·88	0·77	0·70	0·64	0·66
Cs*	0·59	53·9	60·8	41·0	38·6	36·1	36·6	40·6	31·0	31·4	28·8	57·6
Ba*	56	4010	3930	1470	1980	1630	1660	1720	1150	1250	1230	1660
La*	4·30	241	226	129	146	108	109	111	93·0	94·4	93·3	95·1
Ce*	7·14	478	452	279	283	227	229	231	205	206	206	205
Pr*	0·97	52·7	50·8	32·5	30·9	26·5	26·6	26·6	23·7	24·2	24·1	23·4
Nd*	3·84	196	189	125	113	101	101	101	92·2	94·5	93·9	91·0
Sm*	0·78	33·7	32·4	22·6	19·7	18·9	18·8	18·5	17·3	17·6	17·8	17·3
Eu*	0·19	7·03	6·76	4·63	4·17	4·01	3·98	3·98	3·66	3·69	3·76	3·86
Gd*	0·84	28·8	27·8	19·6	17·3	16·6	16·6	16·5	15·2	15·5	15·6	15·4
Tb*	0·13	3·02	2·92	2·23	1·91	1·92	1·90	1·90	1·78	1·81	1·84	1·81
Dy*	0·72	11·9	11·5	9·66	8·28	8·53	8·41	8·39	7·99	8·18	8·19	8·15
Ho*	0·15	1·84	1·79	1·62	1·40	1·44	1·44	1·43	1·37	1·39	1·42	1·39
Er*	0·42	4·81	4·62	4·33	3·79	3·81	3·80	3·84	3·62	3·68	3·72	3·65
Tm*	0·06	0·50	0·49	0·51	0·45	0·46	0·45	0·46	0·43	0·45	0·45	0·44
Yb*	0·36	3·01	2·91	3·12	2·71	2·79	2·79	2·82	2·65	2·68	2·73	2·69
Lu*	0·06	0·42	0·42	0·45	0·40	0·41	0·41	0·42	0·39	0·40	0·41	0·39
Hf*	0·34	14·9	12·3	10·5	9·17	7·60	7·67	7·60	7·76	7·94	7·60	7·59
Ta*	0·10	1·07	0·84	0·99	1·46	0·59	0·71	0·69	0·61	0·58	0·47	0·62
W*	0·24	6·68	9·62	10·2	6·75	7·09	5·38	6·25	5·64	4·84	5·35	4·11
Tl*	0·08	1·99	1·92	3·04	2·02	1·62	1·86	2·34	1·62	0·76	1·80	0·70
Pb*	0·20	133	134	79·4	81·3	61·6	68·1	58·7	48·2	37·9	43·7	37·2
Bi*	0·02	0·32	0·18	0·51	0·09	0·36	0·17	0·37	0·24	0·07	0·17	0·06
Th*	1·00	93·5	90·5	53·5	61·6	41·0	41·8	43·1	32·0	32·4	30·9	32·3
U*	2·26	7·57	6·07	11·2	13·1	9·91	10·1	10·0	7·45	8·31	7·62	7·16

(continued)

Table 3: Continued

Group:	HKS	HKS	HKS	HKS	SHO	SHO	SHO	SHO	SHO	CA	CA	CA
Sample:	ERN34	ERN37	ERN73	ERN68	ERN23	ERN 20es	ERN77	ERN91	ERN97	ERN76	ERN83	ERN94
Note:	lava	lava	lava	lava	lava	lava	lava	lava	lava	lava	lava	lava
SiO_2	48·5	49·7	47·5	47·6	48·0	48·5	48·7	49·6	49·6	48·6	48·7	50·3
TiO_2	0·82	0·71	0·76	0·78	0·94	0·75	0·74	0·81	0·75	0·76	0·82	0·77
Al_2O_3	18·1	19·0	18·0	17·8	18·7	17·4	17·0	17·8	18·1	16·2	17·4	18·5
Fe_2O_3	4·37	3·56	3·56	3·02	2·08	2·45	2·40	3·50	3·92	3·10	3·91	3·45
FeO	2·86	2·79	3·80	4·23	5·80	4·92	4·99	4·28	3·66	4·72	4·57	4·19
MnO	0·14	0·14	0·15	0·15	0·15	0·15	0·15	0·15	0·15	0·15	0·16	0·15
MgO	4·46	3·91	6·04	5·72	6·21	8·33	8·47	6·55	6·56	9·33	8·08	7·00
CaO	10·1	8·82	9·97	10·6	11·2	11·6	11·9	11·0	10·9	12·1	12·1	10·4
Na_2O	2·85	2·68	2·28	2·03	2·27	2·37	2·19	2·48	2·44	2·59	2·98	3·37
K_2O	6·90	7·82	6·70	7·08	4·05	3·08	2·76	3·39	3·18	0·73	0·54	0·74
P_2O_5	0·31	0·30	0·41	0·43	0·28	0·26	0·24	0·22	0·22	0·21	0·22	0·24
LOI	0·69	0·61	0·82	0·59	0·37	0·23	0·49	0·20	0·49	1·40	0·89	0·93
Sum	100·0	100·0	100·0	100·0	100·0	100·0	100·0	100·0	100·0	100·0	100·3	100·0
Mg-no.	57·81	57·65	64·27	63·21	62·82	70·93	71·20	64·79	65·58	72·17	67·57	66·70
Li*	40·8	48·0	33·6	28·8	20·8	n.a.	19·9	25·3	24·8	16·3	17·6	19·1
Be*	6·14	6·71	6·37	6·22	3·37	n.a.	2·10	2·27	2·25	1·47	1·63	1·70
Sc*	17·4	11·9	19·0	20·5	18·7	30·1	27·5	25·7	24·8	33·0	32·3	27·6
V*	211	202	227	224	224	n.a.	209	226	220	209	221	215
Cr	71	28	118	129	117	372	408	167	166	563	319	217
Co	23·2	20·3	25·7	25·9	28·9	36·0	32·6	31·9	31·4	35·8	34·3	32·8
Ni	42·0	31·0	55·0	55·0	35·0	60	69·0	41·0	40·0	97·0	58·0	47·0
Cu*	64·6	49·0	72·5	66·6	44·2	n.a.	74·7	84·1	78·2	68·4	63·6	44·5
Zn*	64·9	68·7	65·4	63·3	72·1	n.a.	60·2	66·3	63·6	58·2	60·0	61·5
As*	11·6	9·84	8·67	7·93	4·88	n.a.	3·66	3·90	3·71	2·96	3·63	3·00
Rb*	395	560	476	403	246	n.a.	173	160	190	181	130	134
Sr*	1920	2080	1800	1730	1310	n.a.	913	n.a.	n.a.	1030	n.a.	1080
Y*	29·8	31·7	34·4	33·6	28·6	n.a.	20·6	n.a.	n.a.	21·6	n.a.	23·3
Zr*	269	293	298	289	193	n.a.	105	n.a.	n.a.	116	n.a.	131
Nb*	15·2	17·4	13·9	12·9	12·4	n.a.	9·10	9·45	9·34	6·76	6·88	7·87
Mo*	3·98	4·07	2·07	1·95	2·73	n.a.	2·17	2·39	2·07	1·43	1·87	1·41
Sn*	3·47	3·50	3·88	3·97	3·38	n.a.	1·90	2·24	2·27	1·74	1·91	2·03
Sb*	0·93	1·07	3·80	0·74	0·25	n.a.	0·14	0·28	0·26	0·09	0·17	0·16
Cs*	33·6	46·1	32·3	29·8	13·6	n.a.	9·11	10·6	10·6	6·99	7·40	8·11
Ba*	1320	1370	892	859	699	n.a.	533	566	556	461	454	520
La*	96·4	104	96·3	93·2	58·4	n.a.	39·1	42·1	42·2	31·0	30·8	37·1
Ce*	205	219	213	209	131	n.a.	82·2	88·7	90·9	66·5	66·8	78·8
Pr*	23·0	24·4	24·7	24·5	15·9	n.a.	9·81	10·5	10·7	8·07	8·21	9·43
Nd*	86·0	90·4	95·8	94·8	63·5	n.a.	38·8	41·2	42·1	32·8	33·4	37·7
Sm*	15·8	16·2	17·9	17·9	12·5	7·3	7·71	8·17	8·44	6·82	7·08	7·60
Eu*	3·38	3·49	3·67	3·71	2·79	1·50	1·94	2·02	2·06	1·72	1·77	1·91
Gd*	14·0	14·6	15·8	15·7	11·2	n.a.	7·45	7·79	7·90	6·45	6·69	7·29
Tb*	1·62	1·68	1·85	1·86	1·42	0·88	0·99	1·03	1·05	0·88	0·91	0·96
Dy*	7·23	7·55	8·40	8·43	6·90	n.a.	5·13	5·36	5·42	4·55	4·82	5·06
Ho*	1·24	1·31	1·45	1·45	1·26	n.a.	0·96	1·00	1·02	0·86	0·91	0·95
Er*	3·37	3·54	3·84	3·84	3·44	n.a.	2·63	2·77	2·78	2·34	2·47	2·63
Tm*	0·41	0·45	0·47	0·47	0·43	n.a.	0·35	0·37	0·37	0·31	0·33	0·35
Yb*	2·54	2·72	2·88	2·86	2·70	2·00	2·15	2·27	2·31	1·91	2·02	2·15
Lu*	0·38	0·41	0·43	0·43	0·41	0·27	0·33	0·35	0·35	0·29	0·31	0·33
Hf*	7·08	7·49	8·13	8·18	5·77	2·9	3·68	3·79	3·80	3·17	3·17	3·50
Ta*	0·76	0·88	0·66	0·62	0·82	0·53	0·53	0·62	0·62	0·33	0·45	0·51
W*	5·48	7·15	4·91	4·50	2·31	n.a.	1·41	2·17	1·88	0·85	1·74	0·97
Tl*	1·87	2·42	2·32	2·21	1·01	n.a.	0·55	0·54	0·52	0·38	0·31	0·32
Pb*	69·1	74·4	41·2	40·3	18·9	n.a.	17·1	21·2	21·3	12·4	13·0	16·1
Bi*	0·51	0·43	0·22	0·17	0·06	n.a.	0·10	0·03	0·05	0·14	0·08	0·03
Th*	37·5	41·7	32·2	30·5	38·0	13·1	13·1	13·7	13·7	8·51	8·72	10·7
U*	8·88	10·3	7·26	6·88	3·94	n.a.	3·49	4·34	4·51	2·45	2·69	2·94

*Data obtained by ICP-MS at Göttingen Universität, except for ERN 22, determined by INAA at Università degli Studi di Firenze.

KAM, melilite-bearing kamafugitic rocks; HKS, plagioclase leucitites and leucitites, former High Potassium Series by Appleton (1972); SHO, shoshonitic rocks (Conticelli *et al.*, 2004), former Potassium Series (KS) of Civetta *et al.* (1981); CA, calc-alkaline like rocks (Boari & Conticelli, 2007). bd.l., below detection limit; n.a., not analysed. Mg-number = MgO/(MgO + 0·85 FeO_{tot}). The entire dataset is available as Electronic Appendix 2 at http://petrology.oxfordjournals.org.

Table 4: Isotopic compositions of Sr, Nd and Pb in selected bulk-rock samples from the Middle Latin Valley

Group	Volcanic centre	Sample	Age (ka)	$^{87}Sr/^{86}Sr$	2σ	$(^{87}Sr/^{86}Sr)_i$	$^{143}Nd/^{144}Nd$	2σ	$^{206}Pb/^{204}Pb$	$^{207}Pb/^{204}Pb$	$^{208}Pb/^{204}Pb$
limestone		ERN57	600	0·708841	±7	0·708840	0·512151	±4	n.a.	n.a.	n.a.
KAM	Colle Castellone	ERN56	600	0·711176	±6	0·711171	0·512120	±5	18·726	15·670	38·969
KAM	Colle Castellone	ERN84	600	0·711156	±7	0·711149	0·512119	±4	18·736	15·682	39·009
HKS	Piglione	ERN40	610	0·710238	±7	0·710233	0·512132	±5	18·771	15·680	39·010
HKS	Tecchiena	ERN34	412	0·709421	±6	0·709418	0·512142	±5	18·815	15·688	39·048
HKS	Tecchiena	ERN37	412	0·709419	±7	0·709414	0·512145	±5	18·846	15·726	39·175
HKS	Selva dei Muli	ERN29	412 (i)	0·709229	±6	0·709221	0·512150	±4	18·799	15·698	39·080
HKS	Celleta	ERN58	413	0·709815	±6	0·709812	0·512121	±5	18·802	15·688	39·046
HKS	Celleta	ERN60	413	0·709805	±8	0·709802	0·512121	±6	18·805	15·689	39·041
HKS	Celleta	ERN66	413	0·709810	±8	0·709807	0·512121	±4	18·792	15·678	38·998
HKS	Giuliano di Roma	ERN44	391	0·709731	±7	0·709727	0·512141	±5	18·812	15·686	39·042
HKS	Giuliano di Roma	ERN48	391	0·709655	±6	0·709652	0·512147	±4	18·823	15·694	39·065
HKS	Giuliano di Roma	ERN50	391	0·709742	±6	0·709738	0·512139	±4	18·810	15·686	39·036
HKS	Pofi (old)	ERN73	390	0·709718	±7	0·709714	0·512136	±4	18·846	15·696	39·074
HKS	Pofi (old)	ERN68	390	0·709724	±7	0·709720	0·512144	±4	18·847	15·707	39·115
HKS	Colle Sant'Arcangelo	ERN86	252	0·710071	±7	0·710069	0·512127	±6	18·780	15·681	39·017
SHO	Valcatora	ERN23	376	0·708419	±7	0·708416	0·512246	±4	18·891	15·682	39·038
SHO	Selva Piana	ERN91	359	0·706973	±6	0·706971	0·512341	±5	18·899	15·681	39·025
SHO	Selva Piana	ERN97	359	0·706979	±6	0·706976	0·512348	±5	18·910	15·692	39·064
SHO	Colle Spinazzeta	ERN 20es	345	0·706967	±7	0·706965	0·512347	±5	18·949	15·700	39·111
SHO	Colle Spinazzeta	ERN77	345	0·706981	±6	0·706978	0·512361	±4	18·934	15·677	39·036
CA	Colle Spinazzeta	ERN76	269	0·706534	±6	0·706532	0·512373	±6	18·940	15·675	39·030
CA	La Badia	ERN83	269	0·706604	±7	0·706602	0·512374	±5	18·922	15·688	39·053
CA	Selva Piana	ERN94	269	0·706779	±7	0·706778	0·512360	±4	18·917	15·695	39·090

Samples were analysed at the Dipartimento di Scienze della Terra of the Università degli Studi di Firenze following the procedure described by Avanzinelli *et al*. (2005). n.a., not analysed; KAM, melilite-bearing kamafugitic rocks; HKS, plagioclase leucitites and leucitites, former High Potassium Series of Appleton (1972); SHO, shoshonitic rocks (Conticelli *et al*., 2004), former Potassium Series (KS) of Civetta *et al*. (1981); CA, calc-alkaline like rocks (Boari & Conticelli, 2007). Initial values are age corrected using the ages reported in this study. Italicized ages are K/Ar determinations from Basilone & Civetta (1975), and (i) inferred from similar stratigraphic position (average value from Tecchiena and Celleta, and stratigraphic relationship with Patrica hydromagmatic pyroclastic flow).

Sub-alkaline rocks with calc-alkaline (CA) affinity are characterized by the occurrence of abundant clinopyroxene and plagioclase with minor euhedral olivine, opaque phases, and phlogopite. They have the lowest K_2O contents (0·21–0·84 wt %), associated with the highest Na_2O contents (3·1–3·6 wt %). In the TAS diagram the CA rocks plot within the field of basalts, and straddle the alkaline–sub-alkaline divide of Kuno (1968).

Ar–Ar DATING

The Middle Latin Valley volcanic field has neither a large central volcanic edifice nor a large area covered by pyroclastic deposits that might be used as stratigraphic markers. Age determinations are thus necessary to constrain the volcanic succession and to unravel any time-dependent compositional variations. Twelve out of 13 samples gave statistically robust ages (Table 2; Electronic Appendix 3). Ten step-heating analyses of groundmasses and leucite phenocrysts show plateaux, which often comprise all steps. In almost all the groundmass samples the plateau steps encompass wide variations in K/Ca ratios (Electronic Appendices 1 and 3). The K/Ca values on average decrease with increasing temperature in all the groundmass samples, according to their paragenesis (Table 1). The main K-bearing phase is leucite in the HKS samples and sometimes in the SHO samples (ERN 91). In the other samples potassium is mainly hosted in

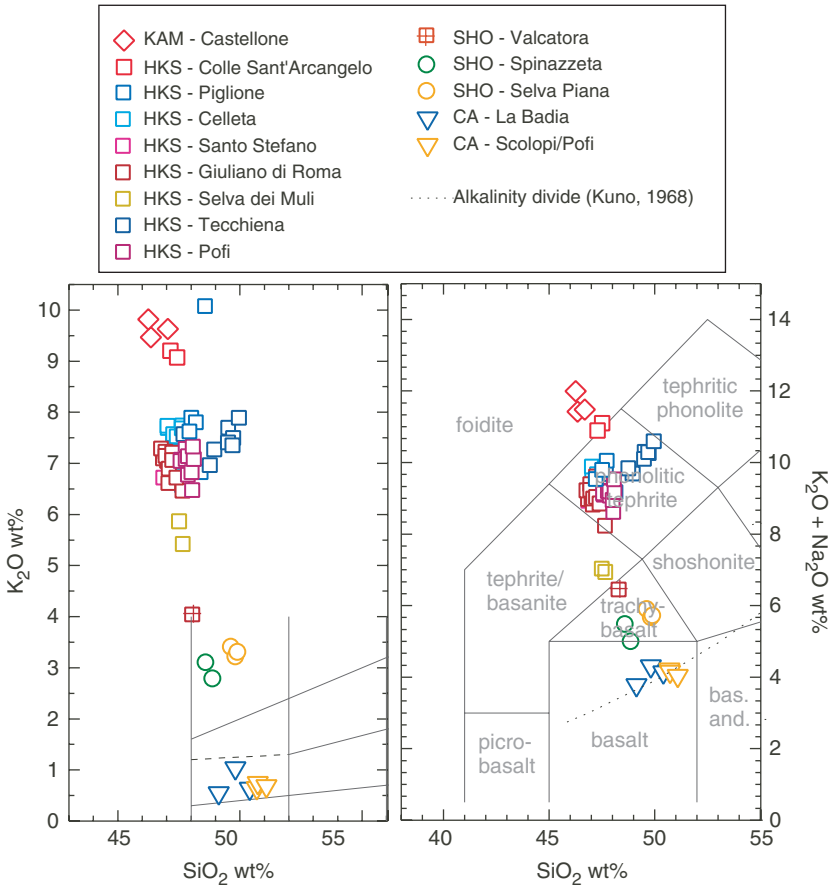

Fig. 2. $K_2O + Na_2O$ vs SiO_2 (Le Bas *et al.*, 1986) and K_2O vs SiO_2 (Peccerillo & Taylor, 1976) classification diagrams for volcanic rocks of the Middle Latin Valley volcanic field. Data are plotted on a volatile-free basis. Weathered samples are not included.

plagioclase and glass (where present). All K-bearing phases dominate the low- and intermediate-temperature steps, whereas the Ca-bearing phases, mainly clinopyroxene, outgas at higher temperatures.

Isochron ages are identical within 2σ error to the plateau ages, with intercepts on the $^{36}Ar/^{40}Ar$ axis corresponding to the atmospheric value (i.e. $^{40}Ar/^{36}Ar = 295{\cdot}5$). Uncertainties are high for those samples that show low dispersion of data points and hence a poorly defined least-square fit line. The total ages, calculated from the sum of radiogenic ^{40}Ar and equivalent to a K/Ar age, do not differ substantially from the plateau ages, indicating that the samples are sufficiently undisturbed (Table 2). Only two samples (ERN 40 and ERN 86) clearly show older ages at high-temperature steps, coupled with low K/Ca ratios, but the step extents are so narrow that the total ages are almost unaffected. In the leucite crystals of sample ERN 86 high-temperature older ages might be due to a small amount of excess ^{40}Ar linked to apatite found as minute inclusions. The groundmass of sample ERN 40 has a $^{40}Ar/^{36}Ar = 312 \pm 27$, which although within error of the atmospheric value, could cause a slight overestimation of its plateau age (Electronic Appendix 3).

The two samples of Patrica hydromagmatic pyroclastic flows, ERN 101 and ERN 102, contain centimetre-sized phlogopite crystals that might represent either phenocrysts or xenocrysts. Single crystal dating was performed on both samples, and whereas ERN 102 shows a unique population, the ERN 101 data are much more scattered. The majority of the crystals display the same isochron age as ERN 102, although three crystals peak at about 750 ka. The concordance of a subordinate number of crystals to a specific age is probably indicative of their xenocrystic nature rather than the presence of excess Ar.

The new age determinations, covering the entire range of activity of the Middle Latin Valley volcanism, range between 600 and 250 ka. Literature K/Ar ages of the Middle Latin Valley rocks indicate a wider period of activity, ranging between 690 and 80 ka, as published by Basilone & Civetta (1975) and Fornaseri (1985). The compositional characteristics of the rocks that those workers dated were not provided, making it difficult to compare

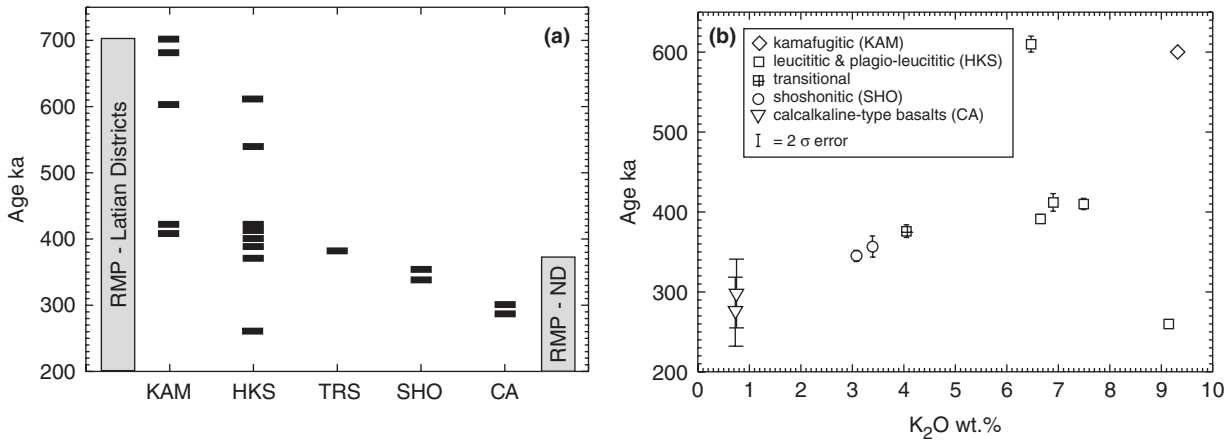

Fig. 3. Age distribution of volcanism in the Middle Latin Valley area (a) with data from the present study and the literature (Basilone & Civetta, 1975; Marra *et al.*, 2004, and references therein); (b) age (ka) vs K_2O (wt %) for the new $^{40}Ar/^{39}Ar$ measurements performed in this study; 2σ error bars are indicated. When not shown the 2σ error is smaller than the symbol size.

the two datasets. The data reported by Fornaseri (1985) are sourced by a personal communication, and are also characterized by extremely low percentages of radiogenic ^{40}Ar, even for relatively old and/or K-rich samples, when compared with the data from Basilone & Civetta (1975) and from this study, and therefore they have not been used. The geographical pairing with samples from Basilone & Civetta (1975) is limited to three; one sample is concordant and two disagree. None of them probably derive from the same lava flows because the paragenesis of one (discordant) sample and the grain sizes of the other two, where leucite was too small to be separated, do not agree with the literature data. The remaining two samples are stratigraphically below and older than the newly dated overlying samples. The use of the Basilone & Civetta (1975) data does not change substantially the reconstruction of the Middle Latin Valley volcanic activity; it only pushes back the first recorded activity at the surface by some 90 kyr. The presence of products younger than 250 ka, not found in the present study, remains, however, an open question. The initial activity at ~600 ka involves kamafugitic and HKS magmas. The bulk of magmas were erupted between 420 and 250 ka; again, the first products of this second period were kamafugitic and HKS, followed by shoshonitic and calc-alkaline types (Fig. 3). An HKS lava flow from Colle Sant'Arcangelo has the youngest age (~250 ka).

TRACE ELEMENTS AND Sr–Nd–Pb ISOTOPES

The Middle Latin Valley volcanic rocks are predominantly mafic and weakly porphyritic. Olivine phenocryst cores are always in equilibrium with the whole-rock composition, consistent with the primitive nature of the magmas. The four magma types have different degrees of incompatible trace element enrichment: the highest abundances are shown by the leucite-bearing melilitites (KAM) and the lowest by the CA-type sub-alkaline basalts (Table 3). Chondrite-normalized rare earth element (REE) patterns (Fig. 4), are light REE (LREE) enriched with leucite-bearing melilitites (KAM) having the highest abundances (i.e. La ~ 1000 × chondrite) and the CA-type sub-alkaline basalts the lowest abundances (i.e. La ~ 100 × chondrite). Leucitites, plagioclase-leucitites and shoshonites plot between these two end-members (Fig. 4). Chondrite-normalized $(Tb/Yb)_N$ values are greater than unity in all rock types, although this ratio progressively decreases from leucite-bearing melilitites [KAM = $(Tb/Yb)_N = 4{\cdot}3$], to leucitites–plagioclase leucitites [HKS: $2{\cdot}6 < (Tb/Yb)_N < 3$], shoshonites [SHO: $2{\cdot}0 < (Tb/Yb)_N < 2{\cdot}2$], and CA-type sub-alkaline basalts [CA: $(Tb/Yb)_N = 1{\cdot}9$].

All four groups of rocks have fairly similar incompatible trace element patterns normalized to primordial mantle (Fig. 5), although a number of differences are observed. Leucite-bearing melilitites (KAM) have the largest positive anomaly in Cs and Pb, and a small Th peak; large troughs are shown at Ba, Ta, Nb, and Ti, and minor ones at P, and Hf (Fig. 5). Similar patterns are shown by the mafic leucitites and mafic plagioclase leucitites (HKS) but the small positive Th anomaly disappears, and a small positive Sr anomaly is observed. Leucite-free rocks, shoshonitic (SHO) and calc-alkaline-type sub-alkaline basalts (CA) are characterized by smaller fractionation between large ion lithophile elements (LILE) and high field strength elements (HFSE) with respect to leucite-bearing rocks (Fig. 5). Shoshonites still have positive anomalies in Cs and Pb, but these are smaller than those shown by the leucite-bearing rocks (Fig. 5), with increasing magnitude of the positive anomaly in Sr and U.

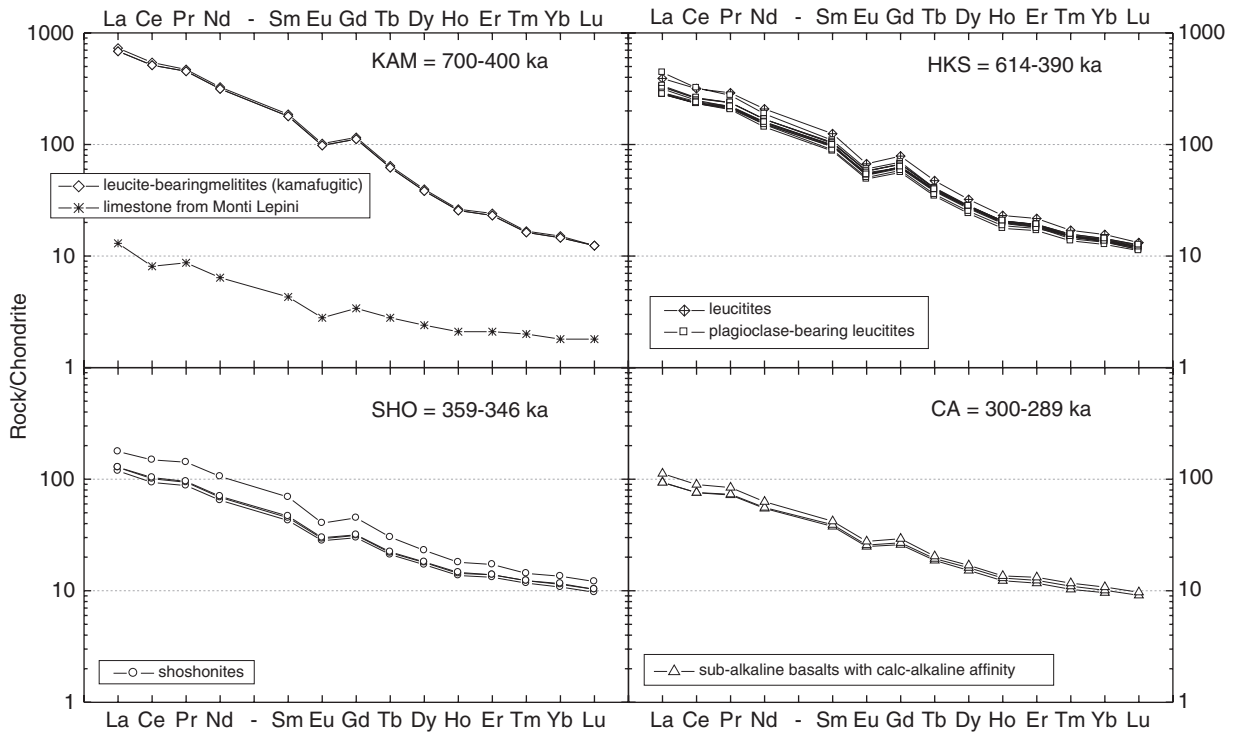

Fig. 4. Chondrite-normalized (Sun & McDonough, 1989) rare earth element patterns for the Middle Latin Valley volcanic rocks. Each group is reported separately. Limestone (ERN 57) is also reported for comparison.

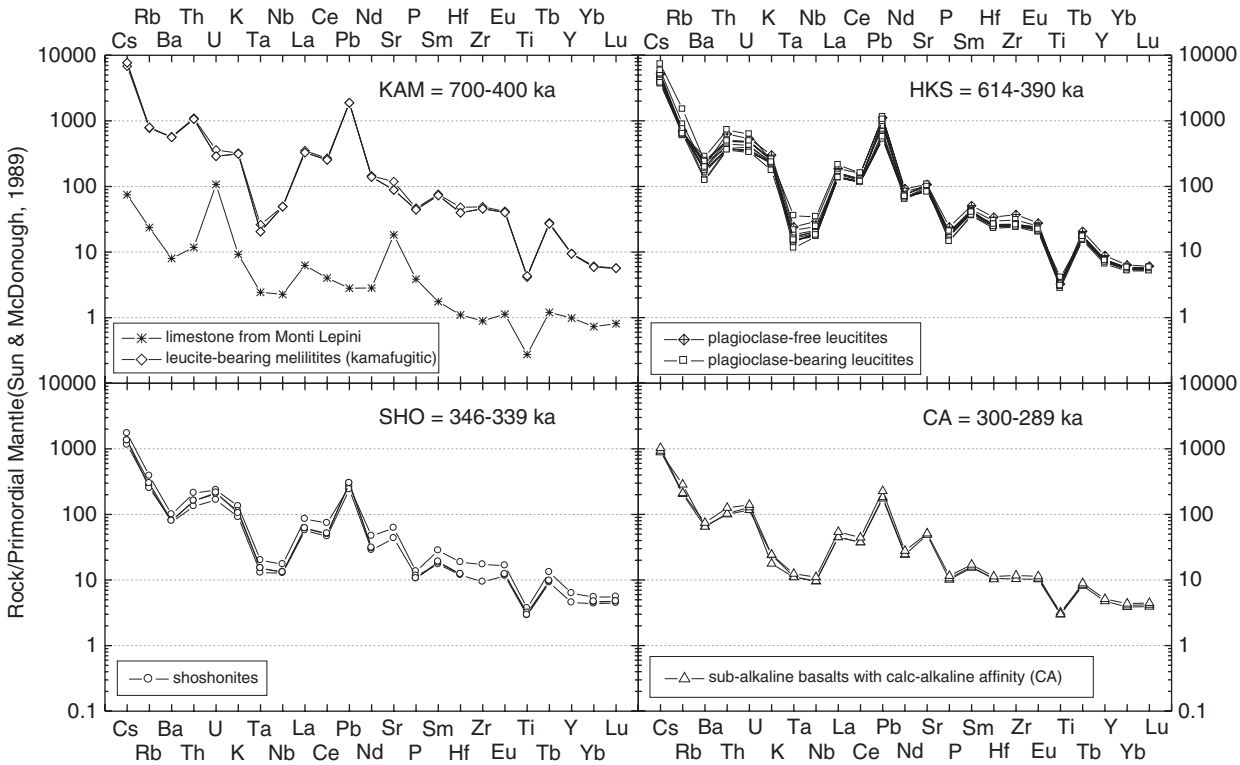

Fig. 5. Incompatible trace element patterns normalized to primordial mantle values (Sun & McDonough, 1989) for the Middle Latin Valley volcanic rocks.

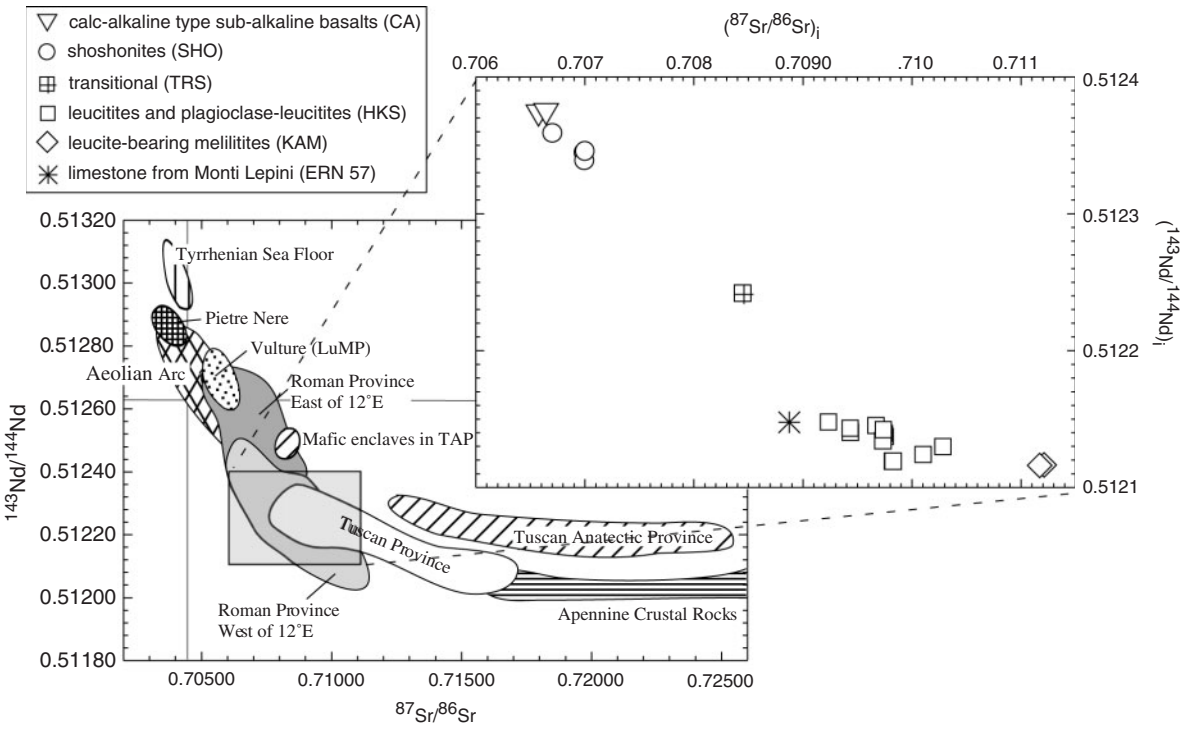

Fig. 6. Initial $^{143}Nd/^{144}Nd$ vs initial $^{87}Sr/^{86}Sr$ isotopic compositions for Italian potassic and ultrapotassic rocks. Fields have been drawn on the basis of data from Conticelli *et al.*, (1992, 1997, 2001, 2002, 2004, 2007, 2009*a*, 2009*b*), Conticelli (1998), Pappalardo *et al.* (1999), Perini *et al.* (2004), Avanzinelli *et al.* (2008) and Boari *et al.* (2009), and the authors' unpublished data (e.g. Vulture, Vesuvius). The inset shows an enlargement of the data for the Middle Latin Valley volcanic field. Symbol size is larger than analytical error (2σ).

The calc-alkaline-type sub-alkaline basalts are characterized by the smallest positive anomalies in Cs and Pb, the smallest troughs in Nb, Ta, and Ti, and the largest positive anomaly in Sr. The normalized Ta/Nb value is less than unity in the KAM and HKS rocks, around unity in SHO rocks, and greater than unity in CA rocks (Fig. 5).

A large range in Sr–Nd isotope composition is observed (Table 4) covering almost the entire range of the Roman Magmatic Province from the northernmost sectors (RMP-LD) to the southernmost ones (RMP-ND; Fig. 6). Mafic leucite-bearing melilitites (KAM), representing the oldest volcanic activity, have the most extreme compositions ($^{87}Sr/^{86}Sr = 0{\cdot}711156 \pm 7$ to $0{\cdot}711176 \pm 6$; $^{143}Nd/^{144}Nd = 0{\cdot}512119 \pm 4$ to $0{\cdot}512120 \pm 5$). Leucitites and plagioclase leucitites (HKS) show little variation in $^{143}Nd/^{144}Nd$ but consistent $^{87}Sr/^{86}Sr_i$ variations. On the other hand, the CA-type sub-alkaline basalts have the lowest $^{87}Sr/^{86}Sr_i$ coupled with the highest $^{143}Nd/^{144}Nd$. Shoshonites (SHO), with the exception of one sample, have Sr and Nd isotope compositions similar to the CA-type sub-alkaline basalts (CA). The outlier sample has transitional geochemical and isotopic characteristics between SHO and HKS rocks, along with the occurrence of leucite in the groundmass (Fig. 7). No significant Sr isotope variations, however, are observed within each group of rocks despite their significant variations in MgO content (Fig. 7).

In a $^{208}Pb/^{204}Pb$ vs $^{206}Pb/^{204}Pb$ diagram (Fig. 8), the leucite-bearing rocks (i.e. KAM and HKS) plot within the field of mafic leucite-bearing rocks from the Latian districts of the Roman Magmatic Province (RMP-LD), whereas leucite-free rocks overlap the field of volcanic rocks from the Neapolitan District (RMP-ND). A small gap between these two fields is also observed. The Pb isotope compositions of the Middle Latin Valley mafic rocks cover almost the entire spectrum of values of the entire Roman Magmatic Province (Fig. 8), filling the intermediate portion of the diagram, with the rocks of the Tuscan and the Lucanian (e.g. Vulture volcano) magmatic provinces at the low and high $^{206}Pb/^{204}Pb$ ends, respectively. The $^{208}Pb/^{204}Pb$ vs $^{206}Pb/^{204}Pb$ data define an apparent trend pointing to the Adriatic foreland values represented by the Cretaceous volcanic rocks of La Queglia–Pescosansonesco (PS) and Punta delle Pietre Nere (PN) alkaline within-plate oceanic basalts.

DISCUSSION

The magmatic rocks of the Middle Latin Valley volcanic district have distinctive geochemical and isotopic characteristics that span almost the entire range of the Roman Magmatic Province. The Valley lies in an area of the Italian peninsula where the underlying Adriatic slab

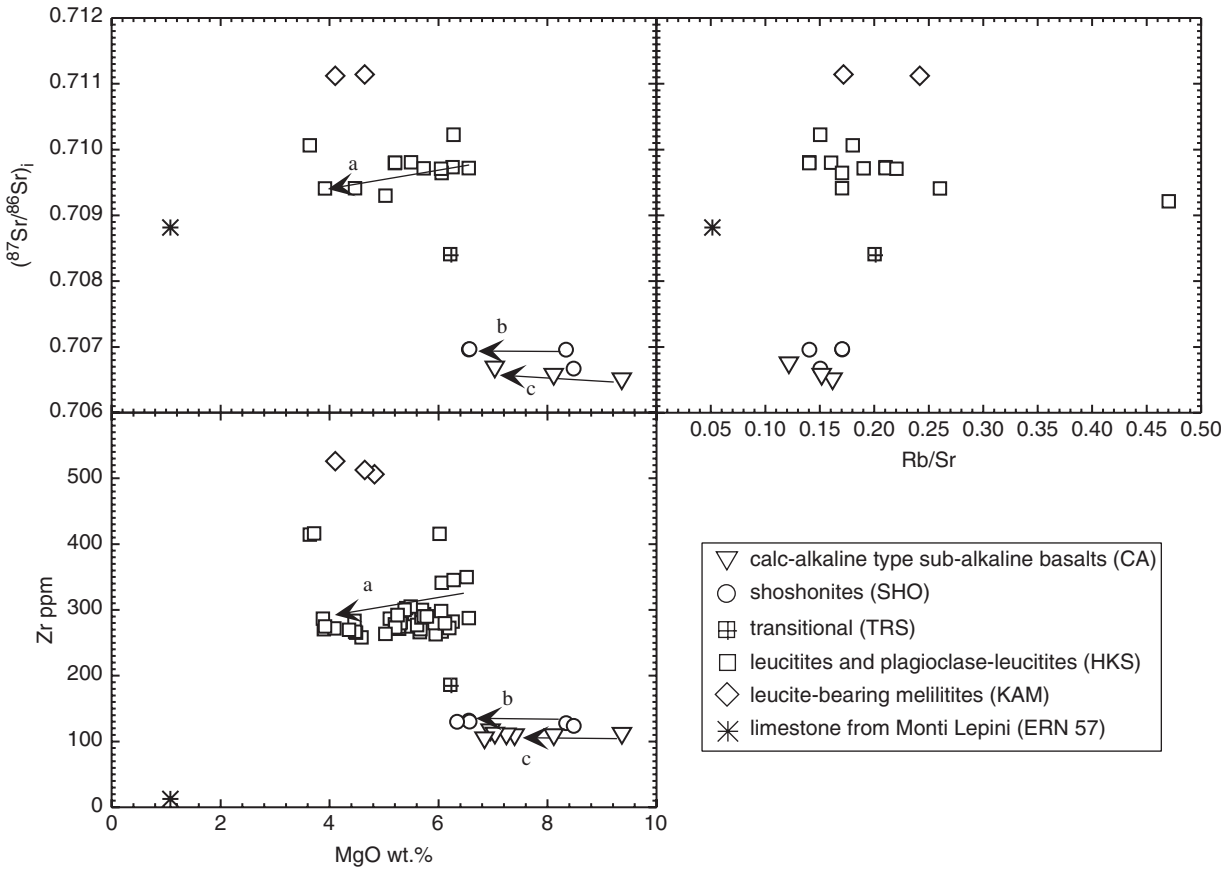

Fig. 7. Variation diagrams for initial $^{87}Sr/^{86}Sr$ and Zr vs MgO, taken as a differentiation index, and of initial $^{87}Sr/^{86}Sr$ vs Rb/Sr for rocks of the Middle Latin Valley volcanic field. Symbol size is larger than analytical error for Sr isotope (2σ). Arrows indicate possible liquid lines of descent; a, leucitites and plagioclase leucitites; b, shoshonites; c, calc-alkaline type sub-alkaline basalts. Variations in the higher MgO compositions are thought to be a primary characteristic of magmas.

displays tears and ruptures (Lucente *et al.*, 1999; Faccenna *et al.*, 2001; Rosenbaum *et al.*, 2008, and references therein). The sequence of arrival at the surface of mafic magmas with different chemical and isotopic characteristics, and the origin of the variation observed, may shed further light on the unusual geodynamic setting of the Italian peninsula, on the nature of the mantle source(s) and on the magma generation processes involved in the transition from ultrapotassic to sub-alkaline magmas in a very short time.

Volcanic succession and geochronology

The Middle Latin Valley volcanic activity was contemporaneous with that of the northernmost sector of the Roman Magmatic Province (RMP-LD: Roman Magmatic Province—Latian Districts; Fig. 3a; see also Marra *et al.*, 2004, for a review). The end of the volcanic activity in this region overlaps partially with the onset of volcanic activity in the southernmost sector of the Roman Magmatic Province (RMP-ND: Roman Magmatic Province—Neapolitan District), which includes the volcanoes south of Roccamonfina (Fig. 1), clustering around the Neapolitan urban area (i.e. Somma–Vesuvius, Ischia, Phlegrean Fields, and Procida volcanoes). Similar to most of the RMP-LD volcanoes, the magmas of the Middle Latin Valley exhibit a progressive decrease in alkalinity with time (Fig. 3b). Leucite-bearing melilitites (KAM) range from about 600 ka (upper lava flows from the top of Colle Castellone, Fig. 1) to about 415 ka (Patrica hydromagmatic pyroclastic flows). Three phlogopite xenocrysts from the Patrica pyroclastic flows yield older ages (~750 ka), possibly recording the incipient onset of volcanism in the area. In other Roman province volcanoes (RMP-LD) shoshonites were erupted after episodes of caldera collapse (e.g. Marra *et al.*, 2004). In the Middle Latin Valley volcanic field shoshonitic rocks were erupted at ~350 ka, similar to the Roccamonfina volcano (e.g. Conticelli *et al.*, 2009a, and references therein), between most of the HKS and CA-type volcanic rocks (Fig. 3b).

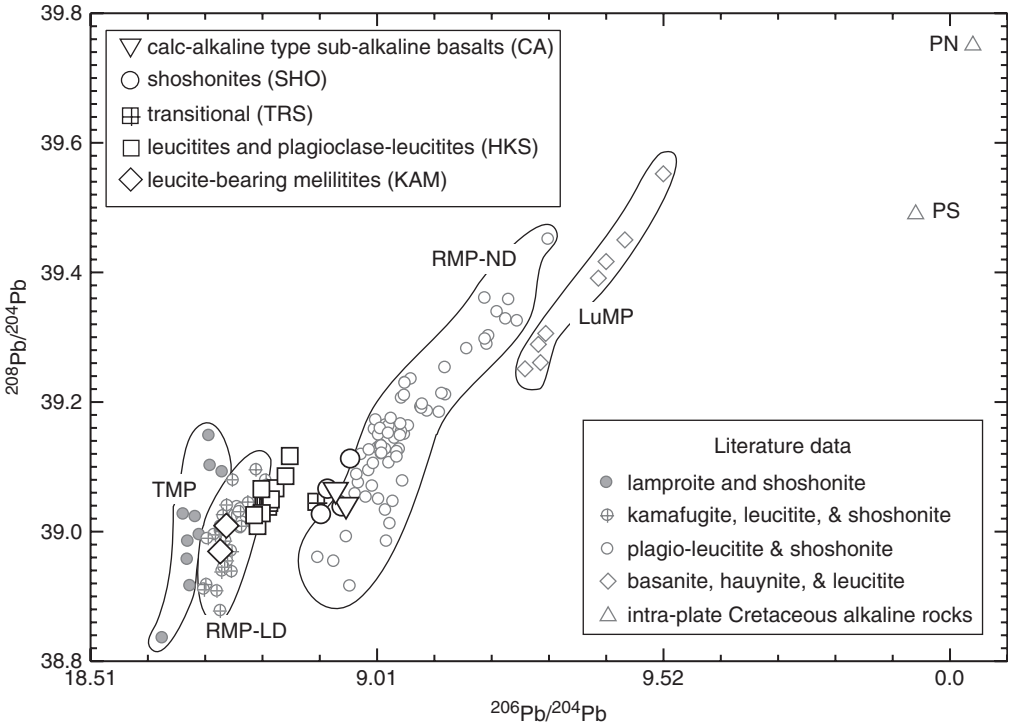

Fig. 8. $^{208}Pb/^{204}Pb$ vs $^{206}Pb/^{204}Pb$ for the Middle Latin Valley volcanic rocks. Isotopic compositions of the Italian potassic and ultrapotassic rocks are also reported. Data sources are Conticelli *et al.* (1992, 1997, 2002, 2004, 2007, 2009*a*, 2009*b*), Conticelli (1998), Pappalardo *et al.* (1999), Perini *et al.* (2004), Avanzinelli *et al.* (2008), Boari *et al.* (2009) and author's unpublished data (e.g. Vulture, Vesuvius). It should be noted that rocks from the Tuscan Magmatic Province (TMP), Latian Districts of the Roman Magmatic Province (RMP-LD), Neapolitan District of the Roman Magmatic Province (RMP-ND) and Lucanian Magmatic Province (LuMP) plot along parallel variation trends with increasingly radiogenic Pb southward. Leucite-bearing Middle Latin Valley rocks plot within the field of the RMP-LD, whereas leucite-free rocks plot at the boundary of the field for the RMP-ND. Compositions for Punta delle Pietre Nere (PN) and La Queglia–Pescosansonesco (PS) intraplate alkaline rocks from the foreland are also reported for comparison (Conticelli *et al.* 2007).

This is also shown by field relationships: CA-type lavas in the Pofi area are separated from the underlying HKS rocks by a paleosoil, whereas shoshonitic lavas at Colle Spinazzeta occur at the bottom of the local volcanic succession, which consists only of SHO- and CA-type products. In summary, the clear correlation between ages and composition of the primitive magmas is a striking feature and testifies to the occurrence of a time-related variation in the magma generation process.

Magma differentiation and crustal contamination

The large geochemical and isotopic variations in the volcanic products can be either generated by combined shallow-level differentiation and crustal contamination processes or inherited from the mantle source(s). In Fig. 7, $^{87}Sr/^{86}Sr_i$ exhibits a broad negative correlation with MgO, although several gaps are evident between the various groups of rocks. Second-order liquid lines of descent are observable within each group of rocks (Fig. 7). For example, the leucititic and plagio-leucititic rocks (HKS) have a range of MgO contents (6·5–3·6 wt %), and MgO correlates with small but significant variations in trace element contents and radiogenic isotope composition (e.g. $^{87}Sr/^{86}Sr_i$ varies from 0·70922 to 0·71023) independent of the main trend (Fig. 7). The same holds true for the shoshonitic and CA-type rocks, which display a slightly smaller range of MgO variation, but at higher MgO contents (Fig. 7), with negligible radiogenic isotope variation (Table 4). These second-order trends may reflect differentiation processes from a parent magma belonging to the same group.

Differentiation from the most mafic (ERN 76) to the most evolved CA-type magma (ERN 95) can be quantitatively modelled, considering both major and trace elements, by a crystal fractionation process involving removal of olivine (3%) + clinopyroxene (11%) ± magnetite (1·1%) ± apatite (0·5%). Similarly, the evolution within the shoshonite group of rocks (SHO) can be modelled by crystal fractionation of olivine (2·7%) + clinopyroxene (6·8%) ± magnetite (0·4%) ± apatite (0·5%). Reflecting the significant variation in Sr isotope composition (Fig. 7), the evolution of the leucititic and plagio-leucititic rocks (HKS) demands an open-system model; that is, crystal fractionation plus crustal

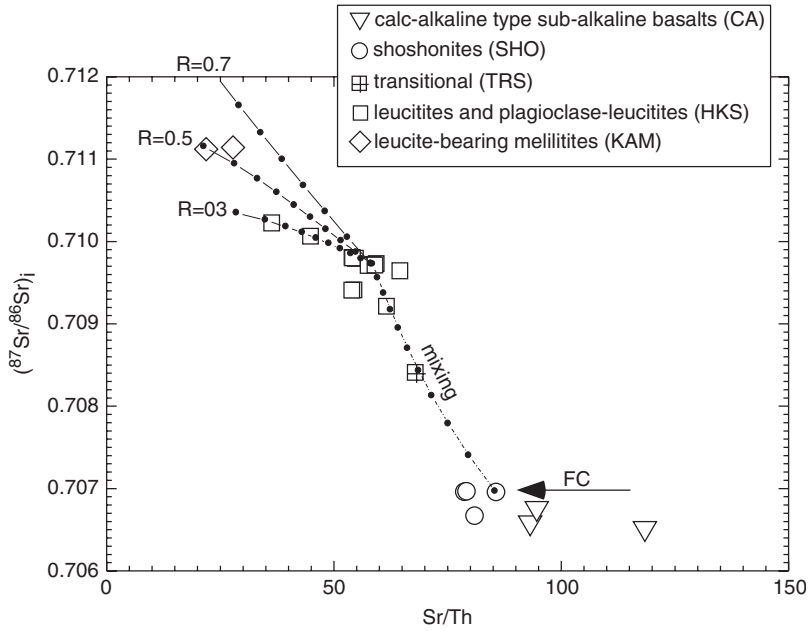

Fig. 9. $^{87}Sr/^{86}Sr_i$ vs Sr/Th for the Middle Latin Valley volcanic rocks with simulated AFC pathways within the leucititic and plagio-leucititic (HKS) group. A marlstone from the Apennines (Sr 327 ppm, Th 10·9 ppm, $^{87}Sr/^{86}Sr = 0{\cdot}7173$) has been taken as the contaminant (e.g. Melluso *et al.*, 2003; Conticelli *et al.*, 2009*a*). Dots on the lines represent the amount of residual magma F, from 1·0 to 0·1 in 0·1 steps; R, ratio of assimilation/fractional crystallization; $D^{Sr}{}_{s/l} = 0{\cdot}212$, $D^{Th}{}_{s/l} = 0{\cdot}005$; partition coefficients after Francalanci *et al.* (1987), Francalanci (1989) and Foley & Jenner (2004). Mixing line (dotted) represents the modelled process to obtain the composition of the transitional sample from Valcatora ERN 23. Dots on mixing line represent 10% increments between the two end-members (HKS, ERN 44 from Giuliano di Roma; SHO, ERN 20 from Colle Spinazzeta).

assimilation (AFC, DePaolo, 1981). The evolution of the HKS rocks can be modelled starting from the most mafic sample (ERN 44) and using a marlstone from the Apennines as the crustal contaminant with a low rate of assimilation vs crystallization ($R = 0{\cdot}3$, Fig. 9).

It is tempting to suppose that the melilite-bearing kamafugite (KAM) from Colle Castellone can also be modelled by an open-system process. The model results (Fig. 9) indicate, however, that relating the kamafugites to the HKS rocks would require a relatively high rate of assimilation vs crystallization ($R = 0{\cdot}5$) and a small amount of residual liquid ($F = 0{\cdot}1$), inconsistent with their strong silica undersaturation (Table 3). Indeed, marlstone assimilation at $R = 0{\cdot}5$ would increase the activity of silica in the residual magma ($F = 0{\cdot}1$) beyond the stability of melilite, leucite and olivine.

The transitional (TRS) sample ERN 23, which has an intermediate chemical and isotopic composition between the HKS and SHO rocks, could be the result of a mixing process between leucititic (40 vol.%) and shoshonitic (60 vol.%) magmas (Fig. 9).

Origin of the crustal signature and nature of the metasomatized agent

The most mafic rocks within the Middle Latin Valley exhibit a negative correlation between MgO and K_2O, incompatible trace elements and Sr isotopes (Fig. 7). Moreover, the extreme enrichment in incompatible trace elements of the leucite-bearing melilititic rocks (KAM) is coupled with the strongest LILE/HFSE fractionation. Incompatible trace element patterns (Fig. 5) closely resemble those of upper crustal sedimentary rocks, albeit with higher normalized abundances (Rudnick & Fountain, 1995; Plank & Langmuir, 1998). To explain the strong crustal signature shown by the Italian ultrapotassic rocks several researchers have invoked low-pressure crustal contamination processes involving either terrigeneous sediments (Gasperini *et al.*, 2002) or limestones (Iacono Marziano *et al.*, 2008) during magma ascent to the surface. The derivation of ultrapotassic silica-undersaturated rocks (i.e. leucite-bearing) through assimilation of pure limestone plus fractionation of clinopyroxene has also been claimed to explain the increase in silica undersaturation correlated with the K_2O increase (Iacono Marziano *et al.*, 2008). In theory, both hypotheses might be applied to the Middle Latin Valley rocks. In Fig. 10, an AFC model has been investigated taking as crustal contaminant both a marly slate and a pure limestone. The limestone is from Colle Morrone (ERN 57), a hill nearby Colle Castellone belonging to the Monti Lepini ridge; the marly slate is from the sedimentary rocks cropping out in the Northern Apennine (Melluso *et al.*, 2003; Conticelli *et al.*, 2009*b*).

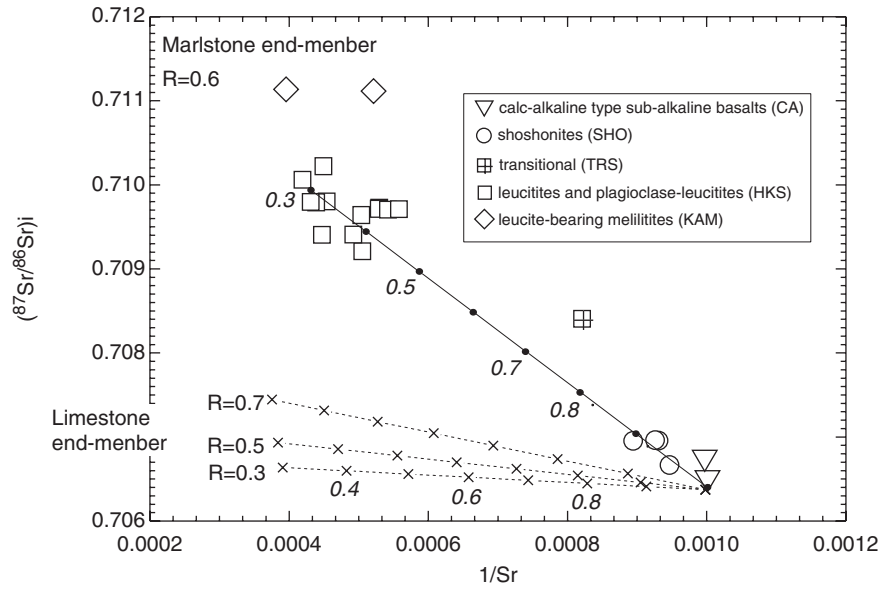

Fig. 10. $^{87}Sr/^{86}Sr_i$ vs 1/Sr for the Middle Latin Valley volcanic rocks with simulated pathways of AFC differentiation using either a limestone (crosses and dashed lines) or a carbonate-rich silicoclastic sediment (marlstone) (filled dots and line). Numbers in italics represent the fraction of residual magma F. The AFC process using the limestone ERN 57, with $D^{Sr}_{s/l} = 0{\cdot}2$ and different assimilation rates ($R = 0{\cdot}3$, 0·5 and 0·7) is unable to fit the compositional variations of the volcanic rocks. On the other hand, the best AFC fit for the studied rocks is obtained using a marlstone from the Apennines with 327 ppm Sr and $^{87}Sr/^{86}Sr = 0{\cdot}7173$, with $D^{Sr}_{s/l} = 0{\cdot}25$ and $R = 0{\cdot}6$. Partition coefficients used are after Francalanci *et al.* (1987), Francalanci (1989) and Foley & Jenner (2004).

Shoshonites and calc-alkaline type basalts are taken as the parental magmas for the AFC process to produce ultrapotassic silica-undersaturated magmas (HKS or KAM). In the case of limestone as crustal contaminant, none of the modelled pathways at different R values (0·3, 0·5, and 0·7) match the trend exhibited by the most primitive volcanic rocks of each group (Fig. 10). On the other hand, considering the marly slate as contaminant, it is possible to model the observed trend in the data with $R = 0{\cdot}6$ and $F = 0{\cdot}3$, using $D^{Sr}_{s/l} = 2{\cdot}5$. Such a high R value, however, is not consistent with: (1) olivine on the liquidus of the HKS and KAM magmas, as shown by Boari & Conticelli (2007); (2) the thermodynamic characteristics of silicate magmas (Spera & Bohrson, 2001). In addition, Fig. 10 shows that melilite-bearing kamafugitic rocks do not fit the modelled liquid line of descent.

Considering that shallow-level crustal contamination did not change substantially the chemical and isotopic composition of the mafic magmas, we can assume that their high and fractionated incompatible trace element patterns are a primary source-related characteristic (Fig. 5), as originally argued by several workers for the Roman Magmatic Province *sensu lato* (e.g. Cox *et al.*, 1976; Peccerillo, 1985; Rogers *et al.*, 1985). The same conclusion has been reached by other workers for lamproitic ultrapotassic rocks (e.g. Conticelli, 1998; Turner *et al.*, 1999; Murphy *et al.*, 2002). LILE/HFSE fractionation is the typical characteristic of magmas generated at destructive plate boundaries (see, e.g. Wilson, 1989, for a comprehensive overview). Its origin has long been discussed and the contribution of recycled sediments via subduction—through slab dehydration and melting—is the most feasible process (e.g. Kay, 1980; Arculus & Johnson, 1981; White & Dupré, 1986; Ben Othman *et al.*, 1989; Tatsumi, 1989; Saunders *et al.*, 1991; Schmidt & Poli, 1998; Kessel *et al.*, 2005; Klimm *et al.*, 2008). In the case of sediment recycling, the depletion of HFSE, with the exception of Th, is thought to be due to either the original trace element signature of the sedimentary recycled component (Plank & Langmuir, 1998) or possible retention of HFSE by residual phases during partial melting of the sediment (Elliott *et al.*, 1997). In Fig. 11, Th/Nb is plotted vs La/Nb and shows that the studied rocks have a large range of values, with leucite-bearing rocks (KAM and HKS) displaying very high La/Nb and Th/La > 0·3, which is incompatible with bulk-sediment recycling within the mantle (Plank, 2005). In addition, the Middle Latin Valley leucite-bearing rocks overlap the fields of Plio-Pleistocenic ultrapotassic rocks from the northernmost regions of the Italian Peninsula (i.e. Tuscan Magmatic Province and Roman Magmatic Province—Latian Districts; Fig. 11). A smaller involvement of a recycled sedimentary component is shown by the leucite-free rocks (SHO and CA) from the Middle Latin Valley, with shoshonites straddling the Th/La = 0·3 line (Fig. 11). On the other hand, ultrapotassic and shoshonitic rocks from the RMP-ND and post-caldera Roccamonfina

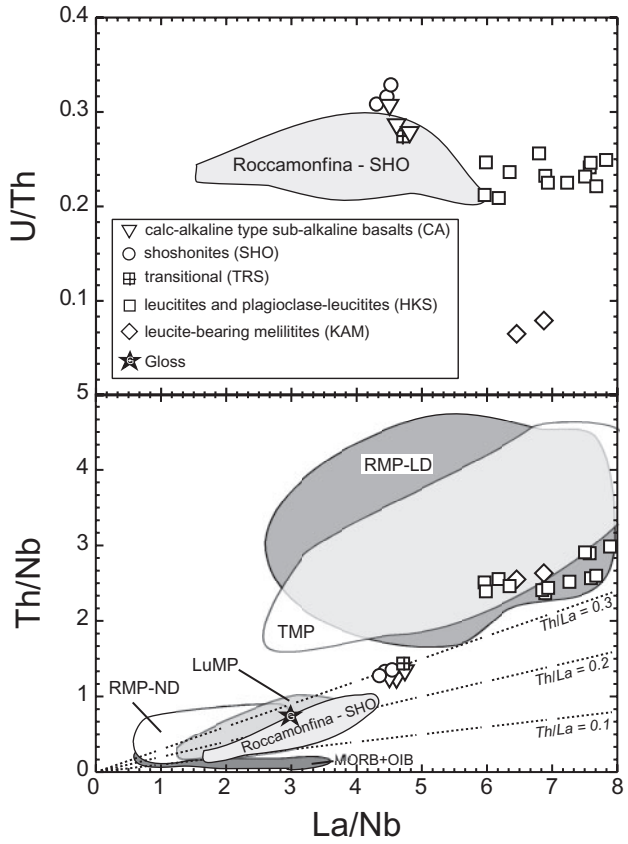

Fig. 11. Th/Nb and U/Th vs La/Nb variations for the for the Middle Latin Valley rocks compared with volcanic rocks from Tuscan magmatic Province (TMP), Latian Districts of the Roman Magmatic Province (RMP-LD), Neapolitan District of the Roman Magmatic Province (RMP-ND), and Lucanian Magmatic Province (LuMP; Vulture volcano). Fields have been drawn on the basis of data from Conticelli *et al.* (1992, 1997, 2001, 2002, 2004, 2007, 2009*a*, 2009*b*), Conticelli (1998), Pappalardo *et al.* (1999), Perini *et al.* (2004), Avanzinelli *et al.* (2008) and Boari *et al.* (2009), and author's unpublished data (e.g. Vulture, Vesuvius). Th/La lines and fields for MORB and OIB are from Plank (2005). It should be noted that arc basalts plot within the 0·1 and 0·3 Th/La lines, and continental upper crustal rocks plot within the 0·2 and 0·3 Th/La lines (see Plank, 2005, fig. 1). GLOSS, global subducted sediment (Plank & Langmuir, 1998).

lavas have significantly lower Th/Nb and La/Nb values, as a result of their higher Nb contents with respect to the mafic volcanic rocks of the RMP-LD (Figs 11 and 12). In summary, the high Th/Nb (Fig. 11) of the Middle Latin Valley magmatic rocks is clearly suggestive of their derivation from a source metasomatized by a melt originating from a recycled sedimentary component (Elliott *et al.*, 1997; Plank, 2005). The low U/Th values of the most mafic rocks of the Middle Latin Valley are also strongly suggestive of a metasomatizing agent dominated by a melt rather than a hydrous fluid component (Fig. 11). The extremely high Th/La values can be tentatively explained by the presence of residual garnet during melting of the subducted sediments, although it is perhaps necessary to consider also the role of LREE-bearing accessory phases in producing melts with Th/La > 1 (e.g. Klimm *et al.*, 2008).

Variation in the degree of melting of recycled sediment is able to produce metasomatizing melts that are strongly enriched in highly incompatible trace elements (Johnson & Plank, 1999), although the presence of residual rutile can buffer the enrichment in HFSE and control Nb/Ta fractionation (Stoltz *et al.*, 1996). In detail, Nb/Ta, evaluated on the basis of ICP-MS data, varies from slightly sub-chondritic to strongly supra-chondritic in a systematic way from the CA-type rocks to the ultrapotassic leucite–melilitites (KAM) (Fig. 13). Island arc volcanic rocks are generally characterized by chondritic to supra-chondritic Nb/Ta values in response to different degrees of partial melting of the asthenospheric mantle wedge: the higher the degree of partial melting the lower the Nb/Ta (Stolz *et al.*, 1996). As a corollary, melt extraction can result in a peridotitic mantle source with sub-chondritic values (Pfänder *et al.*, 2007). In the Middle Latin Valley mafic rocks, Nb/Ta increases systematically with an increase in the crustal component (Figs 12 and 13). Thus, we can envisage a mixed mantle source consisting of residual and enriched mantle domains, the latter formed by interaction with partial melts originating from subducted sediments. These high-silica melts, as a result of the low solubility of Ti in highly silicic melts (Ryerson & Watson, 1987), can have supra-chondritic Nb/Ta ratios because of the presence of rutile in the residue.

A strongly residual nature for the pre-metasomatic mantle wedge has been proposed by Boari & Conticelli (2007) on the basis of the composition of olivine–spinel (chromite) pairs in equilibrium with the mineralogy and bulk composition of the magmas from which they crystallized. No differences have been observed in the chemical composition of olivine–chromite pairs from the various groups of Middle Latin Valley rocks, arguing for a similar pre-metasomatic peridotitic source component for the parental magmas of all four groups of rocks. A residual peridotitic component has also been proposed in the mantle source of most of the parental magmas of the Tuscan, Roman and Lucanian magmatic provinces (e.g. Conticelli & Peccerillo, 1992; Conticelli *et al.*, 1992, 2007; Downes *et al.*, 2002; Perini & Conticelli, 2002). This is supported by the few mantle xenoliths found within the Tuscan and Lucanian magmatic provinces (i.e. Conticelli & Peccerillo, 1990; Downes *et al.*, 2002). Such depleted mantle sources are characteristic of old subcontinental lithospheric mantle (e.g. Hawkesworth *et al.*, 1990).

The strong heavy REE (HREE) fractionation in the leucite-bearing melilititic rocks along with its systematic decrease towards the sub-alkaline magmas (Fig. 4) might be indicative of residual garnet in the mantle source.

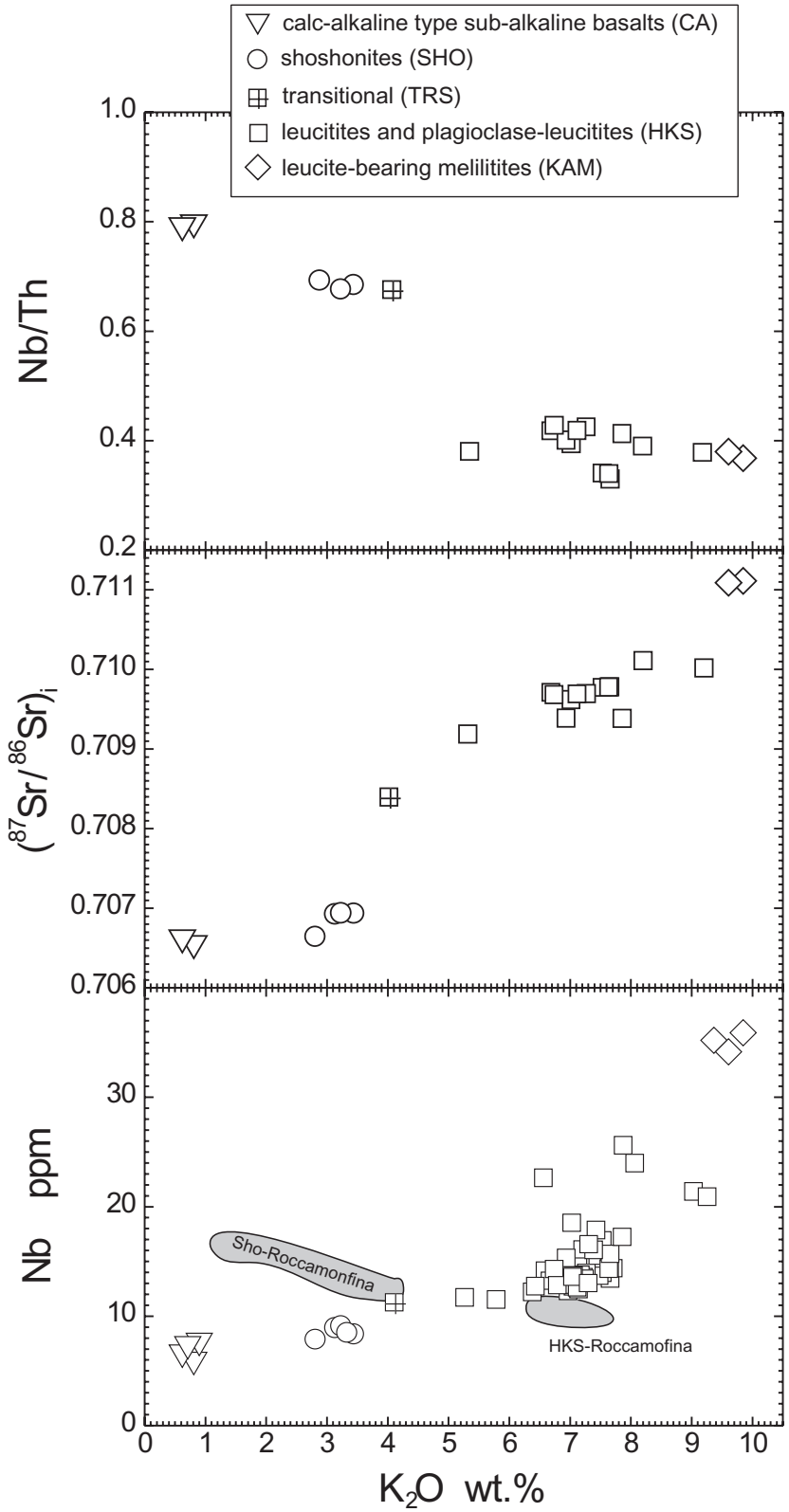

Fig. 12. Nb, $^{87}Sr/^{86}Sr_i$ and Nb/Th vs K_2O for the Middle Latin Valley rocks. The field for Roccamonfina rocks is shown in the Nb diagram (Conticelli *et al.*, 2009*a*).

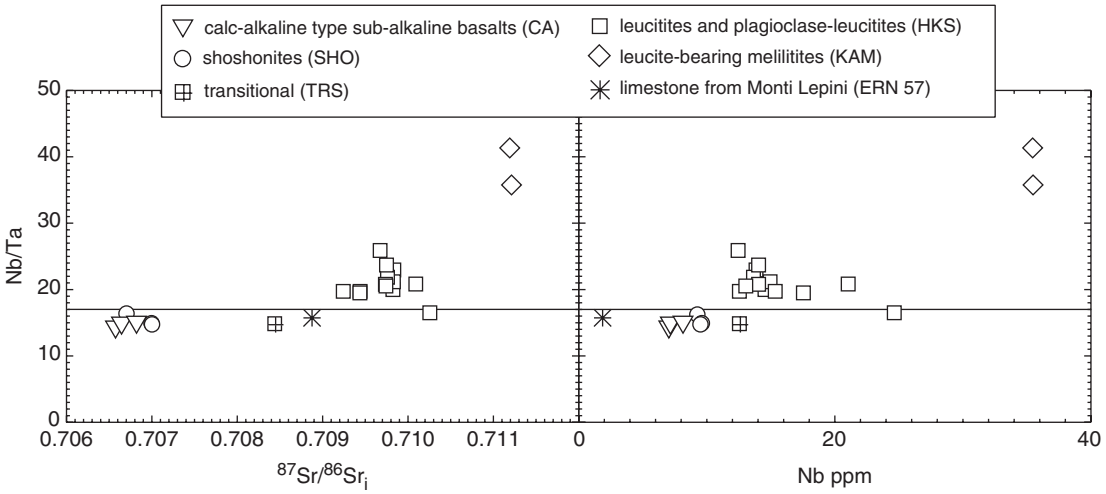

Fig. 13. Nb/Ta vs Nb and $^{87}Sr/^{86}Sr_i$ for the Middle Latin Valley rocks. Horizontal line refers to the chondritic value calculated from Sun & McDonough (1989). Nb/Ta correlates positively with $^{87}Sr/^{86}Sr_i$ (i.e. with the amount of crustal component in the mantle source of the samples).

Similar to Nb/Ta (Fig. 13), however, HREE fractionation is also correlated with an increasing contribution of the crustal component, arguing for a characteristic of the metasomatizing agent (i.e. residual garnet after sediment melting) rather than a characteristic acquired during mantle melting (Avanzinelli *et al.*, 2008).

Questions remain about the clear negative anomaly in Ba with respect to adjacent elements (Rb, Th). Avanzinelli *et al.* (2008) demonstrated that such a Ba anomaly is a common feature of all Roman Province and Tuscan magmas and is exhibited by a number of potential sedimentary end-members within the Mediterranean region in contrast to other sediments worldwide (e.g. GLOSS; Plank & Langmuir, 1998; Conticelli *et al.*, 2009*b*).

Genesis of leucite-bearing rocks and transition to sub-alkaline leucite-free magmas

The genesis of leucite-bearing ultrapotassic rocks and the transition from kamafugitic to leucititic and plagioleucititic magmas appears to be broadly time related, although there are some overlaps (Fig. 3b). Neither AFC nor shallow-level limestone contamination is able to explain the geochemical and isotopic variations observed in the KAM and HKS mafic rocks in a conceivable petrological framework (Figs 9 and 10).

A likely scenario for the genesis of the source of the ultrapotassic magmas is that silicic melts derived from subducted pelagic or terrigeneous sediments were channelled in the overlying lithospheric mantle, forming a zone of hybrid veined mantle. Metasomatic reactions between the recycled crust-derived melts and the refractory lithospheric peridotite wall-rocks produced veins of either phlogopite-bearing harzburgite or phlogopite-bearing orthopyroxenite on the basis of (1) clinopyroxene depletion of the pre-metasomatic peridotitic component, and (2) the amount of metasomatic silicic melt involved in the process (i.e. Edgar, 1987; Kushiro, 1990; Foley, 1994, and references therein).

Incongruent melting of a phlogopite-bearing harzburgite would, however, produce Al- and Ca-poor ultrapotassic magmas (i.e. lamproites; Foley, 1994, and references therein). On the other hand, primary melilititic magmas can be formed by small melting degrees, under high X_{CO2} conditions, of clinopyroxene-rich peridotitic sources (Brey & Green, 1975; Brey, 1978). Kamafugitic magmas are an ultrapotassic variant of melilititic magmas in equilibrium with a phlogopite-bearing lherzolite or phlogopite-bearing wehrlite, and are considered to be generated by mantle melting under extremely high X_{CO2} conditions, even at low pressure (e.g. Edgar *et al.*, 1976, 1980; Arima & Edgar, 1983; Wendlandt & Eggler, 1980*a*, 1980*b*; Lloyd *et al.*, 1985; Edgar, 1987). Conticelli (1989) provided arguments for the genesis of Italian kamafugites, and ultrapotassic olivine- and clinopyroxene-melilitites, through melting of re-fertilized subcontinental lithospheric mantle under high X_{CO2} conditions at low pressure. Such conditions are confirmed by the high flux of deep CO_2 recorded in the Italian peninsula (Gambardella *et al.*, 2004), which has a carbon and oxygen isotope signature typical of sedimentary rocks (e.g. Minissale, 2004, and references therein). A potential CO_2 source could be sedimentary carbonates recycled within the mantle via subduction. Pure sedimentary carbonates are thought to behave as refractory phases at sub-arc depths (e.g. Yaxley & Green, 1994; Molina & Poli, 2000;

Schmidt *et al.*, 2004). Recently, Thomsen & Schmidt (2008) showed that carbonated pelites are capable of producing K-rich granitic or phonolitic melts at temperatures from 900°C (2·4 GPa) to 1070°C and high *P*. When these metasomatic melt compositions are mixed with depleted mantle wedge a potential source for kamafugitic magmatism is achieved (Avanzinelli *et al.*, 2009, and references therein). An alternative scenario is provided when the CO_2-rich volatile component is released during partial melting of subducted marly sediments as consequence of devolatilization of the $CaCO_3$ component. Melting of the siliceous portion of the sediment causes the potassium and the incompatible trace element enrichment, whereas devolatilization of the $CaCO_3$ component supplies CO_2 to the system. Avanzinelli *et al.* (2008) have provided arguments based on trace element characteristics, Sr–Nd isotopes, and U–Th disequilibria for recycling of marly sediments to explain the observed variations in mafic Roman Province ultrapotassic magmas.

On the basis of the above considerations, we have modelled the mantle source of the Middle Latin Valley magmas, based on mixing between melts of recycled marly sediments and depleted subcontinental lithospheric mantle. The composition of the depleted mid-ocean ridge basalt (MORB) mantle (DMM, Workman & Hart, 2005) has been taken as a proxy for the subcontinental lithospheric mantle beneath the Middle Latin Valley. The composition of an Apennine marlstone (Melluso *et al.*, 2003, 2005*a*, 2005*b*; Conticelli *et al.*, 2009*b*) has been used as the crustal end-member. In addition, a second metasomatic component has been introduced, derived from the melting of basalts forming the subducted oceanic crust (Becker *et al.*, 2000) to form a supercritical liquid, and taking into account the trace element mobility factors given by Kessel *et al.* (2005). The mantle source of the leucite–melilititic rocks (KAM) falls on a mixing line between the DMM and ~7% of the recycled carbonate-rich sedimentary component, whereas the mantle source of the leucititic and plagioclase leucititic (HKS) and leucite-free (SHO and CA) rocks reveals a significant contribution from the basaltic component of the subducted oceanic crust (Figs 14 and 15). This points to a decrease in the amount of the sedimentary component from the ultrapotassic to the sub-alkaline mafic rocks, as also corroborated by the positive correlation of Sr isotope composition with K_2O (Fig. 12).

Taking into consideration the U/Th ratio as a tracer of fluid or melt signatures (e.g. Hawkesworth *et al.*, 1997), the low values in the Middle Latin Valley magmatic rocks are suggestive of a metasomatizing agent dominated by a melt component rather than a hydrous fluid (Fig. 11). The slight increase from the leucite-bearing melilitites (KAM) to the leucitites and plagioclase leucitites and then to leucite-free rocks (SHO and CA) (Fig. 11) argues, however, for a minor contribution of hydrous fluids, released perhaps by dehydration of the subducted basaltic component. Avanzinelli *et al.* (2008) supported this hypothesis on the basis of a lack of ^{238}U excess in the recent mafic volcanic rocks from the Latian Districts of the Roman Magmatic Province (RMP-LD), including some of the Middle Latin Valley mafic samples.

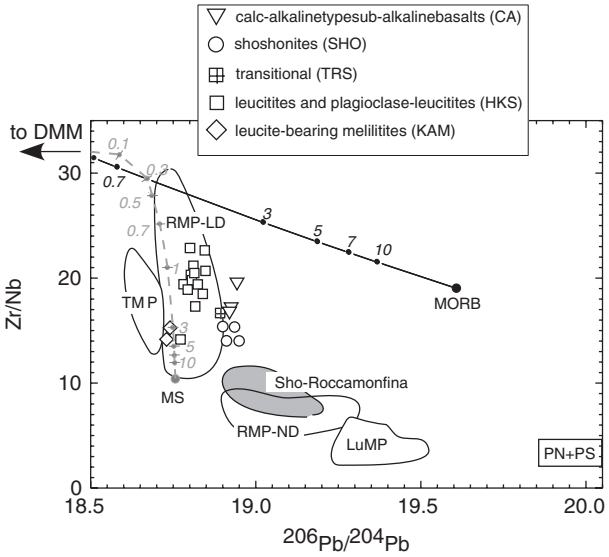

Fig. 14. Zr/Nb vs $^{206}Pb/^{204}Pb$ for the Middle Latin Valley rocks compared with volcanic rocks from Tuscan magmatic Province (TMP), Latian Districts of the Roman Magmatic Province (RMP-LD), Neapolitan District of the Roman Magmatic Province (RMP-ND), and Lucanian Magmatic Province (LuMP; Mount Vulture). PS, Pescosansonesco dykes; PN, Punta delle Pietre Nere dykes. Fields have been drawn on the basis of data from Conticelli *et al.* (1992, 1997, 2002, 2004, 2007, 2009*a*), Conticelli (1998), Pappalardo *et al.* (1999), Perini *et al.* (2004), Avanzinelli *et al.* (2008) and Boari *et al.* (2009). Leucite-free rocks (SHO and CA) have more radiogenic $^{206}Pb/^{204}Pb$, but the values are not as high as those for Roccamonfina volcano and RMP-ND. Metasomatism of the mantle source has been modelled using the composition of DMM, as the pre-enrichment mantle end-member (Workman & Hart, 2005), and mixing it with supercritical liquids (Kessel *et al.*, 2005) from (1) a marlstone (MS) from the Apennines (Conticelli *et al.*, 2009*b*) (grey dashed line), and (2) altered MORB (Becker *et al.*, 2000) (continuous line). The trace element mobility factors used are from Kessel *et al.* (2005) and refer to supercritical liquids formed at 900°C and 6 GPa (available at www.nature.com/nature/journal/v437/n7059/extref/nature03971-61.xls). The Middle Latin Valley samples plot between the two model curves, with kamafugites and leucitites from the RMP-LD falling close to the DMM–sediment mixing line. Dots on the mixing lines represent the percentages of the marlstone- and basalt-derived supercritical liquids mixed with the DMM source to form the metasomatized vein component and the metasomatized surrounding mantle component, respectively.

Network veined mantle and genesis of leucite-free rocks

The genesis of the leucite-free rocks is still matter of debate. The occurrence of leucite-free rocks in the late stages of magmatism is a general characteristic of the Tuscan and Roman magmatic provinces (Peccerillo, 2005, for a

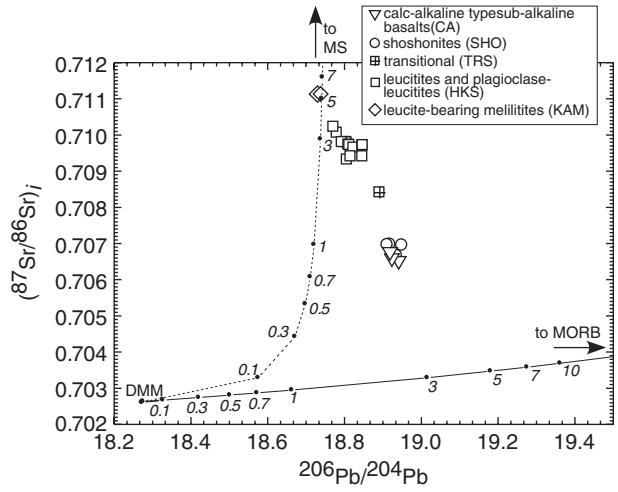

Fig. 15. $^{87}Sr/^{86}Sr_i$ vs $^{206}Pb/^{204}Pb$ for the Middle Latin Valley volcanic rocks. As in Fig. 14, metasomatism of the mantle source has been modelled using the composition of DMM, as the pre-enrichment mantle end-member (Workman & Hart, 2005), and mixing it with supercritical liquids (Kessel *et al.*, 2005) from (1) a marlstone (MS) from the Apennines (Conticelli *et al.*, 2009*b*) (dashed line), and (2) altered MORB (Becker *et al.*, 2000) (continuous line). The trace element mobility factors used are from Kessel *et al.* (2005) and refer to supercritical liquids formed at 900°C and 6 GPa (available at www.nature.com/nature/journal/v437/n7059/extref/nature03971-6l.xls). Dots on the mixing lines represent the percentages of the marlstone- and basalt-derived supercritical liquids mixed with the DMM source to form the metasomatized vein component and the metasomatized surrounding mantle component, respectively.

review; Conticelli *et al.*, 2007). An exception to this general rule is represented by the Somma–Vesuvius magmas, in the Neapolitan District of the Roman Province (RMP-ND), which can be distinguished from the other Roman Province magmatic rocks based on their geochemical, isotopic, and chronological characteristics (Beccaluva *et al.*, 1991; Peccerillo, 2005, for a review).

The Middle Latin Valley volcanic field occurs on the boundary between the Latian (RMP-LD) and Neapolitan (RMP-ND) sectors. Three hypotheses have been proposed for the origin of the leucite-free rocks: (1) partial melting of different zones within the metasomatized mantle lithosphere enriched by a similar crustal-derived component (Peccerillo & Panza, 1999; Frezzotti *et al.*, 2007); (2) the arrival of a within-plate mantle component from the Adriatic foreland (De Astis *et al.*, 2006; Bianchini *et al.*, 2008; Conticelli *et al.*, 2009a); (3) the gradual exhaustion of the K_2O and incompatible element enriched veined mantle—along with a decrease of X_{CO2}—and increasing contribution to melt production of the ambient mantle (Perini *et al.*, 2004).

The geochemical and isotopic variations of the Middle Latin Valley mafic rocks indicate a decrease in the sedimentary component of the source from the kamafugitic magmas to the CA-type magmas. The latter, however, still display a strong crustal signature– albeit with an increase in the contribution from the subducted basalt with respect to the marly sediment (Figs 14 and 15). There is no evidence, however, for a within-plate mantle component (Figs 5 and 12), unlike the Monte Vulture volcano and the late-stage activity of Roccamonfina volcano (e.g. De Astis *et al.*, 2006; Conticelli *et al.*, 2009*a*).

The increased contribution of the subducted basalt component (supercritical fluid) to the mantle source of the Middle Latin Valley mafic magmas is also time-related, consistent with gradual exhaustion of the metasomatic veins and incremental participation of the surrounding mantle in melt production. This scenario is, therefore, the simplest and most feasible model to explain the shift in melt geochemistry from ultrapotassic to sub-alkaline magmas with time.

The two metasomatic agents could either be added sequentially to the mantle wedge or generated contemporaneously during active subduction. In the latter case, the two metasomatic agents should mix in different proportions to form the entire spectrum of mafic magmas; it is therefore unclear why we should observe a time-related compositional change in the mafic parental magmas.

The Apennine chain is the result of the collision between the Eurasian plate and the Adria microplate (Faccenna *et al.*, 2001; Rosenbaum *et al.*, 2008, and references therein). On this basis we might predict a progressive increase in the sedimentary component in the mantle source, which is not consistent with the observed data. A plausible explanation is the occurrence of an older mantle metasomatic event caused by the supercritical fluid component from subducting basaltic oceanic crust, pervasively metasomatizing the mantle wedge with no magma production, followed by, in more recent times, the sedimentary melt component, which overprinted the earlier event, concentrating possibly in veins.

Some of the western Mediterranean ultrapotassic rocks (i.e. lamproites) host spinel-lherzolite xenoliths that provide evidence for lithospheric mantle veining and/or metasomatism (Ancochea & Nixon, 1987; Conticelli & Peccerillo, 1990; Beccaluva *et al.*, 2004; Coltorti *et al.*, 2007). The net-veined mineral assemblage clearly has a lower melting point than the ambient mantle (Foley, 1992*b*).

Kamafugitic melts have equilibrated with a modified mantle mineral assemblage, in which $CaCO_3$ has an important role in producing strongly silica-undersaturated ultrapotassic magmas. Partial melting of the vein mineralogy is capable of forming ultrapotassic magmas characterized by the highest amounts of the recycled crustal component (Figs 14 and 15). Temperature increase along with the exhaustion of the vein can trigger melting of the surrounding mantle, leading to a progressive decrease in alkali and incompatible trace element enrichment

(Foley, 1992b). The required increase of temperature in the mantle source of the Middle Latin Valley magmas is supported by the increase in temperature on the saturation surface of olivine for the various groups of rocks (Boari & Conticelli, 2007), which is progressively higher from kamafugitic to CA-type magmas.

The above scenario is able to produce parental magmas that exhibit a systematic compositional change with time because of the dilution effect without modifying the shape of the mantle-normalized trace element patterns (Fig. 5). Partial melting occurs within the same mantle zone under similar pressure (depth) conditions involving different amounts of the two extreme metasomatizing agents. This simple explanation can also be applied to other Italian potassic and ultrapotassic volcanoes (e.g. Perini *et al.*, 2004; Conticelli *et al.* 2007, 2009*b*).

Upper mantle characteristics of the southern sector of the Italian peninsula

The principal debate about the origin of the correlation between geochemical and Sr–Nd–Pb isotopic variations and the geographical occurrences of Italian ultrapotassic rocks, from RMP-LD to RMP-ND (e.g. Beccaluva *et al.*, 1991; Peccerillo, 2005, for a review), can be confined between two extreme hypoytheses, which are not necessarily in conflict with each other: (1) an increasing influence of asthenospheric mantle inflow through slab tears located in the Southern Italian peninsula (e.g. Peccerillo, 2005, and references therein); (2) variation in the metasomatizing melt component(s) within the mantle source of the magmas (e.g. Avanzinelli *et al.*, 2008, 2009, and references therein).

Seismic tomography data clearly reveal the existence of a slab window close to Monte Vulture volcano (i.e. Lucanian Magmatic Province, Fig. 1), not far from Roccamonfina and the Middle Latin Valley volcanoes (Lucente *et al.*, 1999; Wortel & Spakman, 2000; Rosenbaum *et al.*, 2008). The slab tear is located at the northeastern edge of the Calabrian Arc and it is thought to be a consequence of the arcuate morphology of the oceanic lithospheric slab subducting beneath the Italian peninsula, following southeastward slab retreat (Lucente *et al.*, 1999; Wortel & Spakman, 2000). The geochemical and isotopic characteristics of the Monte Vulture and Neapolitan volcanoes strongly suggest an increasing role of asthenospheric mantle inflow through the slab tear (De Astis *et al.*, 2006). The trace element and radiogenic isotope characteristics of the Monte Vulture volcanic rocks (Lucanian Magmatic Province) indicate a clear within-plate asthenospheric mantle signature mixed with a lithospheric mantle component (e.g. Beccaluva *et al.*, 2002; Downes *et al.*, 2002; authors' unpublished data).

U-series data for the Monte Vulture mafic rocks display a striking ~30% ^{230}Th excess (Avanzinelli *et al.*, 2008). The ^{230}Th excess eliminates any similarity to within-plate carbonatites, which always display extremely high U/Th values and ubiquitous ^{238}U excess (>40%, Pyle *et al.*, 1991, and references therein). Instead, a garnet-bearing mantle source is required to generate the observed ^{230}Th excess, which must be located within the asthenosphere. To produce the observed geochemical characteristics partial melting must have started beneath the lithospheric lid, and therefore beneath the subducted slab, as Monte Vulture is very close to the trench. De Astis *et al.* (2006), on the basis of the isotopic characteristics of the Neapolitan volcanoes, suggested that such asthenospheric mantle inflow reached the Neapolitan area in recent times. This has also been suggested for the final stages of shoshonitic to sub-alkaline activity (post-caldera) of the Roccamonfina volcano (Conticelli *et al.*, 2009*a*).

The Middle Latin Valley magmatic rocks have an almost bimodal distribution of their Sr, Nd and Pb isotope characteristics (Figs 6, 8 and 15). The leucite-bearing rocks overlap the range of the Latian Districts of the Roman Magmatic Province (RMP-LD), whereas the leucite-free rocks partially overlap the field of the Neapolitan District (RMP-ND) volcanic rocks (Figs 6 and 8). These variations are undoubtedly significant but not as extreme as those found in the Roccamonfina volcano (Conticelli *et al.*, 2009*b*). Also, no within-plate asthenospheric component can be clearly detected on the basis of the geochemical and radiogenic isotope composition of the ultrapotassic and sub-alkaline mafic magmas.

The Middle Latin Valley magmatic district appears to be located just north of the boundary dividing two mantle domains (Fig. 1): (1) to the north, magmas are produced by partial melting of a lithospheric mantle source metasomatized by two components (sediment melt and supercritical fluid) derived from subducted Tethyan oceanic crust; (2) to the south, the geochemical characteristics of the metasomatized lithospheric mantle have been further modified via asthenospheric mantle inflow through slab tears.

SUMMARY

The Middle Latin Valley Volcanic field is characterized by the occurrence of small monogenetic volcanoes, active between 600 and 250 ka, which have erupted a large compositional range of mafic magmas. The magmas vary from leucite melilitites (KAM), leucitites, plagioclase leucitites (HKS), shoshonites (SHO), to calc-alkaline type basalts (CA). A decrease in K_2O and other incompatible trace elements is systematically correlated with time. Second-order differentiation trends occur within each group of rocks related to shallow-level fractional crystallization processes in both closed (leucite-free rocks) and open (leucitites and plagioclase-leucitites) systems.

The parental magmas were generated within a zone of modified subcontinental lithospheric mantle, metasomatically enriched by two distinct metasomatic agents that originated from a subducted slab of oceanic lithosphere. Melts from a marly sedimentary component dominate the mantle source of the ultrapotassic magmas, whereas partial melts (supercritical fluids) of the altered basalt of the subducted oceanic crust contribute increasingly to the mantle source of the sub-alkaline magmas. The metasomatic components have been introduced into the mantle via westward dipping subduction of the Adriatic plate beneath the Apennine chain. Mantle source heterogeneity is probably expressed as a network of veins in the lower part of the lithospheric mantle.

Olivine- and leucite-bearing melilitites (kamafugites) are the oldest erupted magmas and represent relatively low-temperature melts (~100%) of the mantle veins at high X_{CO2}. A decrease in X_{CO2} along with the dilution of vein-derived melts with melts from the surrounding mantle is the most likely process to explain the changing composition of the magmas from melilitites to leucitites and plagioclase-leucitites. The same holds true (i.e. an even greater contribution from the ambient mantle) to form the leucite-free rocks. This scenario is consistent with the geochemical and time-related variations of mafic magmas in the Middle Latin Valley.

ACKNOWLEDGEMENTS

The authors wish to thank Riccardo Avanzinelli for his help during fieldwork; Chiara M. Petrone, Giulia Perini and Maurizio Ulivi for sharing their time and expertise during isotope analyses; Gabriele Mengel and Klaus Simon (GZ—Göttingen) for their expertise in ion-chromatography and IPC-MS analysis; Giuliana De Grandis (IGG) for help during mineral separation; Riccardo Avanzinelli, Angelo Peccerillo, Jessy Owen, Keith Bell and Leone Melluso for stirring and focusing discussions. Editorial handling by Marjorie Wilson and thoughtful peer-reviews by Marlina Erlburg, Nick Rogers and an anonymous reviewer greatly helped to improve the original manuscript. Financial support was provided by the Università degli Studi di Firenze with doctoral and post-doctoral fellowships granted to E.B., and 'ex 60%' funds to S.C.; the Italian Ministry of Education and Research (MIUR) through PRIN 2008 (Number 2008040502_002); and by the Consiglio Nazionale delle Ricerche (CNR). The Ar–Ar laboratory was funded by the Programma Nazionale di Ricerca in Antartide (PNRA).

SUPPLEMENTARY DATA

Supplementary data for this paper are available at *Journal of Petrology* online.

REFERENCES

Acocella, V., Faccenna, C. & Funiciello, R. (1996). Elementi strutturali della Media Valle Latina. *Bollettino Società Geologica Italiana* **115**, 501–518.

Altherr, R., Meyer, H.-P., Holl, A., Volker, F., Alibert, C., McCulloch, M. T. & Majer, V. (2004). Geochemical and Sr–Nd–Pb isotopic characteristics of late Cenozoic leucite lamproites from the East European Alpine belt (Macedonia and Yugoslavia). *Contributions to Mineralogy and Petrology* **147**, 58–73.

Altherr, R., Topuz, G., Siebel, W., Şend, C., Meyer, H.-P., Satırc, M. & Lahaye, Y. (2008). Geochemical and Sr–Nd–Pb isotopic characteristics of Paleocene plagioleucitites from the Eastern Pontides (NE Turkey). *Lithos* **105**, 149–161.

Ancochea, E. & Nixon, P. H. (1987). Xenoliths in the Iberian Peninsula. In: Nixon, P. H. (ed.) *Mantle Xenoliths*. New York: John Wiley, pp. 119–125.

Angelucci, A., Brotzu, P., Civitelli, G., Morbidelli, L. & Traversa, G. (1974). Il vulcanismo pleistocenico della Media Valle Latina (Lazio). Caratteristiche petrografiche e geologiche dei principali affioramenti lavici. *Geologica Romana* **13**, 83–123.

Appleton, J. D. (1972). Petrogenesis of the potassium-rich lavas from the Roccamonfina Volcano, Roman region, Italy. *Journal of Petrology* **13**, 425–456.

Arculus, R. J. & Johnson, R. W. (1981). Island-arc magma sources: a geochemical assessment of the roles of slab-derived components and crustal contamination. *Geochemical Journal* **15**, 109–133.

Arima, M. & Edgar, A. D. (1983). High pressure experimental studies on a katungite and their bearing on the genesis of some potassium-rich magmas of the west branch of the African rift. *Journal of Petrology* **24**, 166–187.

Avanzinelli, R., Boari, E., Conticelli, S., Francalanci, L., Guarnieri, L., Perini, G., Petrone, C.M., Tommasini, S. & Ulivi, M. (2005). High precision Sr, Nd, and Pb isotopic analyses and reproducibility using new generation thermal ionisation mass spectrometer: aims and perspective for isotope geology applications. *Periodico di Mineralogia* **75**, 187–207.

Avanzinelli, R., Elliot, T., Tommasini, S. & Conticelli, S. (2008). Constraints on the genesis of the potassium-rich Italian volcanics from U/Th disequilibrium. *Journal of Petrology* **49**, 195–223.

Avanzinelli, R., Lustrino, M., Mattei, M., Melluso, L. & Conticelli, S. (2009). Potassic and ultrapotassic magmatism in the circum-Tyrrhenian region: the role of carbonated pelitic vs pelitic sediment recycling at destructive plate margin. *Lithos* (in press).

Baksi, A. K., Archibald, D. A. & Farrar, E. (1996). Intercalibration of $^{40}Ar/^{39}Ar$ dating standards. *Chemical Geology* **129**, 307–324.

Barberi, F., Gasparini, P., Innocenti, F. & Villari, L. (1973). Volcanism of the Southern Tyrrhenian and its geodynamic implications. *Journal of Geophysical Research* **78**, 269–276.

Barbieri, M., Peccerillo, A., Poli, G. & Tolomeo, L. (1988). Major, trace element and Sr isotopic composition of lavas from Vico volcano (Central Italy) and their evolution in an open system. *Contributions to Mineralogy and Petrology* **99**, 485–497.

Basilone, P. & Civetta, L. (1975). Datazione K/Ar dell'attività vulcanica dei Monti Ernici (Latina). *Rendiconti della Società Italiana di Mineralogia e Petrologia* **31**, 175–179.

Beccaluva, L., Di Girolamo, P. & Serri, G. (1991). Petrogenesis and tectonic setting of the Roman Volcanic Province, Italy. *Lithos* **26**, 191–221.

Beccaluva, L., Coltorti, M., Di Girolamo, P., Melluso, L., Milani, L., Morra, V. & Siena, F. (2002). Petrogenesis and evolution of Mt. Vulture alkaline volcanism (Southern Italy). *Mineralogy and Petrology* **74**, 277–297.

Beccaluva, L., Bianchini, G., Bonadiman, C., Siena, F. & Vaccaro, C. (2004). Coexisting anorogenic and subduction related metasomatism in mantle xenoliths from the Betic Cordillera (Southern Spain). *Lithos* **75**, 67–87.

Becker, H., Jochum, P. K. P. & Carlson, R. W. (2000). Trace element fractionations during dehydration of eclogites from high-pressure terranes and the implications for element fluxes in subduction zones. *Chemical Geology* **163**, 65–99.

Ben Othman, D., White, W. M. & Patchett, J. (1989). The geochemistry of marine sediments, island arc magma genesis, and crust–mantle recycling. *Earth and Planetary Science Letters* **94**, 1–21.

Bianchini, G., Beccaluva, L. & Siena, F. (2008). Post-collisional and intraplate Cenozoic volcanism in the Rifted Apennines/Adriatic domain. *Lithos* **101**, 125–140.

Boari, E. (2005). Petrologia e magmatologia del vulcanismo Plio-Pleistocenico del Lazio meridionale e sue implicazioni geodinamiche (in Italian). Ph.D. thesis, Università degli Studi di Firenze, 143 pp.

Boari, E. & Conticelli, S. (2007). Mineralogy and petrology of Mg-rich calc-alkalic, potassic, and ultrapotassic associated rocks: the Middle Latin Valley monogenetic volcanoes, Roman Magmatic Province, Southern Italy. *Canadian Mineralogist* **45**, 1443–1469.

Boari, E., Avanzinelli, R., Melluso, L., Giordano, G., Mattei, M., De Benedetti, A. A., Morra, V. & Conticelli, S. (2009). Isotope geochemistry (Sr–Nd–Pb) and petrogenesis of leucite-bearing volcanic rocks from 'Colli Albani' volcano, Roman Magmatic Province, Central Italy: inferences on volcano evolution and magma genesis. *Bulletin of Volcanology* (in press).

Brey, G. (1978). Origin of olivine-melilitites: chemical and experimental constraints. *Journal of Volcanology and Geothermal Research* **3**, 61–88.

Brey, G. & Green, D. H. (1975). The role of X_{CO2} in the genesis of olivine melilitites. *Contributions to Mineralogy and Petrology* **49**, 93–103.

Carmichael, I. S. E., Lange, R. A. & Luhr, J. F. (1996). Quaternary minettes and associated volcanic rocks of Mascota, western Mexico: a consequence of plate extension above a subduction modified mantle wedge. *Contributions to Mineralogy and Petrology* **124**, 302–333.

Civetta, L., Innocenti, F., Lirer, L., Manetti, P., Munno, R., Peccerillo, A., Poli, G. & Serri, G. (1979). Serie potassica ed alta in potassio dei Monti Ernici (Lazio Meridionale): considerazioni petrologiche e geochimiche. *Rendiconti della Società Italiana di Mineralogia e Petrologia* **35**, 227–249.

Civetta, L., Innocenti, F., Manetti, P., Peccerillo, A. & Poli, G. (1981). Geochemical characteristics of potassic volcanics from Mt. Ernici (Southern, Latium, Italy). *Contributions to Mineralogy and Petrology* **78**, 37–47.

Coltorti, M., Arai, S., Bonadiman, C., Faccini, B. & Ishimaru, S. (2007). Nature of the metasomatising agents in suprasubduction and intraplate settings as deduced by glass and amphibole geochemistry. *Geochimica et Cosmochimica Acta* **71**, A-184.

Conte, A. M. & Dolfi, D. (2002). Petrological and geochemical characteristics of Plio-Pleistocene Volcanics from Ponza Island (Tyrrhenian Sea, Italy). *Mineralogy and Petrology* **74**, 75–94.

Conticelli, S. (1989). Genesi del magmatismo alcalino-potassico dell'Italia centrale: evidenze petrologiche, geochimiche e petrologico sperimentali. Ph.D. thesis, Università degli Studi di Firenze, 404 pp.

Conticelli, S. (1998). Effects of crustal contamination on ultrapotassic magmas with lamproitic affinity: mineralogical, geochemical and isotope data from the Torre Alfina lavas and xenoliths, central Italy. *Chemical Geology* **149**, 51–81.

Conticelli, S. & Peccerillo, A. (1990). Petrological significance of high-pressure ultramafic xenoliths from ultrapotassic rocks of Central Italy. *Lithos* **24**, 305–322.

Conticelli, S. & Peccerillo, A. (1992). Petrology and geochemistry of potassic and ultrapotassic volcanism in central Italy: petrogenesis and inferences on the evolution of the mantle sources. *Lithos* **28**, 221–240.

Conticelli, S., Francalanci, L. & Santo, A. P. (1991). Petrology of the final stage Latera lavas: mineralogical, geochemical and Sr- isotopic data and their bearing on the genesis of some potassic magmas in Central Italy. *Journal of Volcanology and Geothermal Research* **46**, 187–212.

Conticelli, S., Manetti, P. & Menichetti, S. (1992). Petrology, chemistry, mineralogy and Sr-isotopic features of Pliocenic orendites from South Tuscany: implications on their genesis and evolutions. *European Journal of Mineralogy* **4**, 1359–1375.

Conticelli, S., Francalanci, L., Manetti, P., Cioni, R. & Sbrana, A. (1997). Petrology and geochemistry of the ultrapotassic rocks from the Sabatini Volcanic District, Central Italy: the role of evolutionary processes in the genesis of variably enriched alkaline magmas. *Journal of Volcanology and Geothermal Research* **75**, 107–136.

Conticelli, S., Bortolotti, V., Principi, G., Laurenzi, M.A., Vaggelli, G. & D'Antonio, M. (2001). Petrology, mineralogy and geochemistry of a mafic dyke from Monte Castello, Elba Island, Italy. *Ofioliti* **26**, 249–262.

Conticelli, S., D'Antonio, M., Pinarelli, L. & Civetta, L. (2002). Source contamination and mantle heterogeneity in the genesis of Italian potassic and ultrapotassic volcanic rocks: Sr–Nd–Pb isotope data from Roman Province and Southern Tuscany. *Mineralogy and Petrology* **74**, 189–222.

Conticelli, S., Melluso, L., Perini, G., Avanzinelli, R. & Boari, E. (2004). Petrologic, geochemical, and isotopic characteristics of potassic and ultrapotassic magmatism in Central–Southern Italy: inferences on its genesis and on the nature of mantle sources. *Periodico di Mineralogia* **73**, 153–164.

Conticelli, S., Carlson, R. W., Widom, E. & Serri, G. (2007). Chemical and isotopic composition (Os, Pb, Nd, and Sr) of Neogene to Quaternary calc-alkalic, shoshonitic and ultrapotassic mafic rocks from the Italian Peninsula: inferences on the nature of their mantle sources. In: Beccaluva, l., Biachini, G. & Wilson, M. (eds) *Cenozoic Volcanism in the Mediterranean Area. Geological Society of America, Special Papers* **418**, 171–202.

Conticelli, S., Marchionni, S., Rosa, D., Giordano, G., Boari, E. & Avanzinelli, R. (2009*a*). Shoshonite and sub-alkaline magmas from an ultrapotassic volcano: Sr–Nd–Pb isotope data on the Roccamonfina volcanic rocks, Roman Magmatic Province, Southern Italy. *Contributions to Mineralogy and Petrology* **157**, 41–63, doi:10.1007/s00410-008-0319-8.

Conticelli, S., Guarnieri, L., Farinelli, A., Mattei, M., Avanzinelli, R., Bianchini, G., Boari, E., Tommasini, S., Tiepolo, M., Prelević, D. & Venturelli, G. (2009*b*). Trace elements and Sr–Nd–Pb isotopes of K-rich, shoshonitic, and calc-alkaline magmatism of the Western Mediterranean region: Genesis of ultrapotassic to calc-alkaline magmatic associations in a post-collisional geodynamic setting. *Lithos* doi:10.1016/j.lithos.2008.07.016.

Cox, K. G., Hawkesworth, C. J., O'Nions, R. K. & Appleton, J. D. (1976). Isotopic evidence for the derivation of some Roman Region Volcanics from anomalously enriched mantle. *Contributions to Mineralogy and Petrology* **56**, 173–180.

D'Agostino, N., Cheloni, M., Selvaggi, G., Michelini, A. & Zuliani, F. (2005). Strain accumulation in the Southern Alps (NE Italy) and deformation at the north-eastern boundary of Adria observed by

CGPS measurements. *Geophysical Research Letters* **32**, doi: 10.1029/2005GL024266.

Davies, G. R., Stolz, A. J., Mahotkin, I. L., Nowell, G. M. & Pearson, D. G. (2006). Trace element and Sr–Pb–Nd–Hf isotope evidence for ancient, fluid-dominated enrichment of the source of Aldan Shield lamproites. *Journal of Petrology* **47**, 1119–1146.

De Astis, G., Kempton, P. D., Peccerillo, A. & Wu, T. W. (2006). Trace element and isotopic variations from Mt. Vulture to Campanian volcanoes: constraints for slab detachment and mantle inflow beneath southern Italy. *Contributions to Mineralogy and Petrology* **151**, 331–351.

Deniel, C. & Pin, C. (2001). Single-stage method for the simultaneous isolation of lead and strontium from silicate samples for isotopic measurements. *ıAnalytica Chimica Actaı* **426**, 95–103.

DePaolo, D. J. (1981). Trace elements and isotopic effects of combined wall-rock assimilation and fractional crystallization. *Earth and Planetary Science Letters* **53**, 189–202.

de Vries, J. L. & Jenkins, R. (1971). *Spettrometria a raggi X in pratica*. Biblioteca Tecnica Philips, Milano, 160 pp.

Di Vincenzo, G. & Skála, R. (2009). ^{40}Ar–^{39}Ar laser dating of tektites from the Cheb basin (Czech Republic): evidence for coevality with moldavites and influence of the dating standard on the age of the Ries impact. *Geochimica and Cosmochimica Acta* **73**, 493–513.

Downes, H., Kostoula, T., Jones, A. P., Beard, A. D., Thirlwall, M. F. & Bodinier, J.-L. (2002). Geochemistry and Sr–Nd isotopic compositions of mantle xenoliths from the Monte Vulture carbonatite–melilitite volcano, central southern Italy. *Contributions to Mineralogy and Petrology* **144**, 78–92.

Edgar, A. D. (1987). The genesis of alkaline magmas with emphasis on their source regions: inferences from experimental studies. In Fitton J.G., & Upton B.G.J., eds. Alkaline Igneous Rocks. London: *Geological Society Special Publication*, 29–52.

Edgar, A. D., Green, D. H. & Hibberson, W. O. (1976). Experimental petrology of a highly potassic magma. *Journal of Petrology* **17**, 339–356.

Edgar, A. D., Condliffe, E., Barnett, R. L. & Shirran, R. J. (1980). An experimental study of an olivine ugandite magma and mechanisms for the formations of its K-enriched derivatives. *Journal of Petrology* **21**, 475–497.

Elliott, T., Plank, T., Zindler, A., White, W. & Bourdon, B. (1997). Element transport from slab to volcanic front at the Mariana arc. *Journal of Geophysical Research* **102**, 14991–15019.

Faccenna, C., Becker, T. W., Lucente, F. P., Jolivet, L. & Rossetti, F. (2001). History of subduction and back-arc extension in the Central Mediterranean. *Geophysical Journal International* **145**, 809–820.

Ferrari, L., Conticelli, S., Bulamacchi, L. & Manetti, P. (1996). Volcanological evolution of the Monte Amiata volcanic center, southern Tuscany, central Italy: new geological and petrochemical data. *Acta Vulcanologica* **8**, 41–56.

Foley, S. F. (1992*a*). Petrological characterisation of the source components of potassic magmas: geochemical and experimental constraints. *Lithos* **28**, 187–204.

Foley, S. F. (1992*b*). Vein-plus-wall-rock melting mechanisms in the lithosphere and the origin of potassic alkaline magmas. *Lithos* **28**, 435–453.

Foley, S. F. (1994). Geochemische und experimentelle Untersuchungen zur Genese der kalireichen Magmatite. *Neues Jahrbuch für Mineralogie, Abhandlungen* **167**, 1–55.

Foley, S. F. & Jenner, G. A. (2004). Trace element partitioning in lamproitic magmas—the Gaussberg olivine leucitite. *Lithos* **75**, 19–38.

Foley, S. F., Venturelli, G., Green, D. H. & Toscani, L. (1987). The ultrapotassic rocks: characteristics, classification and constraints for petrogenetic models. *Earth-Science Reviews* **24**, 81–134.

Fornaseri, M. (1985). Geochronology of volcanic rocks from Latium (Italy). *Rendiconti della Società Italiana di Mineralogia e Petrologia* **40**, 73–106.

Francalanci, L. (1989). Trace element partition coefficients for minerals in shoshonitic and calc-alkaline rocks from Stromboli volcano, Aeolian Islands. *Neues Jahrbuch für Mineralogie, Abhandlungen* **162**, 229–247.

Francalanci, L., Peccerillo, A. & Poli, G. (1987). Partition coefficients for minerals in potassium-alkaline rocks: data from Roman province (Central Italy). *Geochemical Journal* **21**, 1–10.

Francalanci, L., Taylor, S. R., McCulloch, M. T. & Woodhead, J. (1993). Geochemical and isotopic variations in calc-alkaline rocks of the Aeolian Arc (Southern Tyrrhenian Sea, Italy): constraints on the magma genesis. *Contributions to Mineralogy and Petrology* **113**, 300–313.

Francalanci, L., Tommasini, S. & Conticelli, S. (2004). The volcanic activity of Stromboli in the 1906–1998 A.D. period: mineralogical, geochemical and isotope data relevant to the understanding of Strombolian activity. *Journal of Volcanology and Geothermal Research* **131**, 179–211.

Francalanci, L., Avanzinelli, R., Tommasini, S. & Heumann, A. (2007). A west–east geochemical and isotopic traverse along the sub-aerial volcanism of the Aeolian arc, Southern Tyrrhenian sea: inferences on mantle source processes. In: Beccaluva, L., Bianchini, G. & Wilson, M. (eds) *Cenozoic Volcanism in the Mediterranean Area. Geological Society of America, Special Papers* **418**, 235–263.

Franzini, M., Leoni, L. & Saitta, M. (1972). A simple method to evaluate the matrix effect in X-ray fluorescence analyses. *X-Ray Spectometry* **1**, 151–154.

Frezzotti, M.-L., de Astis, G., Dallai, L. & Ghezzo, C. (2007). Coexisting calc-alkaline and ultrapotassic magmatism at Monti Ernici, Mid Latina Valley (Latium, central Italy). *European Journal of Mineralogy* **19**, 479–497.

Gambardella, B., Cardellini, C., Chiodini, G., Frondini, F., Marini, L., Ottonello, G. & Vetuschi-Zuccolini, M. (2004). Fluxes of deep CO_2 in the volcanic areas of Central–Southern Italy. *Journal of Volcanology and Geothermal Research* **136**, 31–52.

Gasperini, D., Blichert-Toft, J., Bosh, D., Del Moro, A., Macera, P. & Albarède, F. (2002). Upwelling of deep mantle material through a plate window: evidence from geochemistry of Italian basaltic volcanics. *Journal of Geophysical Research* **107**, 2367–2386.

Hawkesworth, C. J., Kempton, P. D., Rogers, N. W., Ellam, R. M. & van Calsteren, P. W. (1990). Continental mantle lithosphere and shallow level enrichments processes in Earth's mantle. *Earth Planetary Science Letters* **96**, 256–268.

Hawkesworth, C. J., Turner, S. P., Peate, D. W., McDermott, F. & van Calsteren, P. (1997). U–Th isotopes in arc magmas: implications for element transfer from the subducted crust. *Science* **276**, 551–555.

Hoogewerff, J. A., Van Bergen, M. J., Vroon, P. Z., Hertogen, J., Wordel, R., Sneyers, A., Nasution, A., Varekamp, J. C., Moens, H. L. E. & Mouchel, D. (1997). U-series, Sr–Nd–Pb isotope and trace element systematics across an active island arc–continent collision zone: implications for element transfer at the slab–wedge interface. *Geochimica et Cosmochimica Acta* **61**, 1057–1072.

Iacono Marziano, G., Gaillard, F. & Pichavant, M. (2008). Limestone assimilation by basaltic magmas: an experimental re-assessment and application to Italian volcanoes. *Contributions to Mineralogy and Petrology* doi:10.1007/s00410-007-0267-8.

Johnson, M. C. & Plank, T. (1999). Dehydration and melting experiments constrain the fate of subducted sediments. *Geochemistry, Geophysics, Geosystems* **1**, paper no. 1999GC000014.

Jourdan, F. & Renne, P. R. (2007). Age calibration of the Fish Canyon sanidine $^{40}Ar/^{39}Ar$ dating standard using primary K–Ar standards. *Geochimica et Cosmochimica Acta* **71**, 387–402.

Kay, R. W. (1980). Volcanic arc magmas: Implications of a melting–mixing model for element recycling in the crust–upper mantle system. *Journal of Geology* **88**, 497–522.

Kessel, R., Schmidt, M. W., Ulmer, P. & Pettke, T. (2005). Trace element signature of subduction-zone fluids, melts and supercritical liquids at 120–180 km depth. *Nature* **437**, 724–727.

Klimm, K., Blundy, J. D. & Green, T. H. (2008). Trace element partitioning and accessory phase saturation during H_2O-saturated melting of basalt with implications for subduction zone chemical fluxes. *Journal of Petrology* **49**, doi:10.1093/petrology/egm001.

Koppers, A. A. P. (2002). ArArCALC—software for ^{40}Ar–^{39}Ar age calculations. *Computers and Geosciences* **28**, 605–619.

Kuno, H. (1968). Differentiation of basalt magmas. In: Hess, H. H. & Poldervaart, A. A. (eds) *The Poldervaart Treatise on Rocks of Basaltic Compositions, 2.* New York: Interscience, pp. 623–688.

Kushiro, I. (1990). Partial melting of mantle wedge and evolution of island arc crust. *Journal of Geophysical Research* **95**, 15929–15939.

Le Bas, M. J., Le Maitre, R. W., Streckeisen, A. & Zanettin, B. (1986). A chemical classification of volcanic rocks based on the total alkali–silica diagram. *Journal of Petrology* **27**, 745–750.

Lloyd, F. E., Arima, M. & Edgar, A. D. (1985). Partial melting of a phlogopite-clinopyroxenite nodule from south-west Uganda: an experimental study bearing on the origin of a highly potassic continental rift volcanics. *Contributions to Mineralogy and Petrology* **91**, 321–329.

Lucente, F. P., Chiarabba, C., Cimini, G. B. & Giardini, D. (1999). Tomographic constraints on the geodynamic evolution of the Italian Region. *Journal Geophysical Research* **104**, 20307–20327.

Marra, F., Taddeucci, J., Freda, C., Marzocchi, W. & Scarlato, P. (2004). Recurrence of volcanic activity along the Roman Comagmatic Province (Tyrrhenian margin of Italy) and its tectonic significance. *Tectonics* **23**, TC4013, doi:10.1029/2003TC001600.

Melluso, L., Conticelli, S., D'Antonio, M., Mirco, N. & Saccani, E. (2003). Petrology and mineralogy of wollastonite–melilite-bearing pyrometamorphic rocks from Colle Fabbri and Ricetto, Central Apennines, Italy. *American Mineralogist* **88**, 1287–1299.

Melluso, L., Conticelli, S., D'Antonio, M., Mirco, N. & Saccani, E. (2005*a*). Mineralogic and bulk rock composition of Italian wollastonite- and melilite-bearing paralavas and clinker: Further evidence for their pyrometamorphic nature. *American Mineralogist* **90**, 1926–1933.

Melluso, L., Conticelli, S., D'Antonio, M., Mirco, N. & Saccani, E. (2005*b*). Wollastonite-, anorthite-, gehlenite-, and fassaite-bearing rocks: Igneous petrological oddity or paralavas? *American Mineralogist* **90**, 1940–1944.

Minissale, A. (2004). Origin, transport and discharge of CO_2 in Central Italy. *Earth-Science Reviews* **66**, 89–141, doi: 10/1016/j.earscirev.2003.09.001.

Mirnejad, H. & Bell, K. (2006). Origin and source evolution of the Leucite Hills lamproites: evidence from Sr–Nd–Pb–O isotopic compositions. *Journal of Petrology* **47**, 2463–2489.

Molina, J. F. & Poli, S. (2000). Carbonate stability and fuid composition in subducted oceanic crust: an experimental study on H_2O–CO_2-bearing basalts. *Earth and Planetary Science Letters* **176**, 295–310.

Murphy, D. T., Collerson, K. D. & Kamber, B. S. (2002). Lamproites from Gaussberg, Antarctica: possible transition zone melts of Archean subducted sediments. *Journal of Petrology* **43**, 981–1001.

Pappalardo, L., Civetta, L., D'Antonio, M., Deino, A., Di Vito, M., Orsi, G., Carandente, A., de Vita, S., Isaia, R. & Piochi, M. (1999). Chemical and Sr-isotopical evolution of the Phlegraean magmatic system before the Campanian Ignimbrite (37 ka) and the Neapolitan Yellow Tuff (12 ka) eruptions. *Journal of Volcanology and Geothermal Research* **91**, 141–166.

Pasquarè, G., Serri, G. & Vezzoli, L. (1985). Carta geologica dell'area della Media Valle Latina. Scala 1:50 000. Progetto finalizzato geodinamica. Sottoprogetto: sorveglianza dei vulcani e rischio vulcanico. In: *Carte tematiche sul vulcanismo recente*. Milan: Istituto di Geologia, Università di Milano.

Peccerillo, A. (1985). Roman Comagmatic Province (Central Italy): Evidence for subduction related magma genesis. *Geology* **13**, 103–106.

Peccerillo, A. (2005). Plio-Quaternary Volcanism in Italy: Petrology, Geochemistry, Geodynamics. Berlin: Springer, 365 pp.

Peccerillo, A. & Panza, G. F. (1999). Upper mantle domains beneath Central–Southern Italy: petrological, geochemical and geophysical constraints. *Pure and Applied Geophysics* **156**, 421–443.

Peccerillo, A. & Taylor, S. R. (1976). Geochemistry of Eocene calk-alkaline volcanic rocks from the Kastamonu area, northern Turkey. *Contributions to Mineralogy and Petrology* **58**, 63–81.

Perini, G. & Conticelli, S. (2002). Crystallization conditions of leucite-bearing magmas and their implications on the magmatological evolution of ultrapotassic magmas: The Vico Volcano, Central Italy. *Mineralogy and Petrology* **74**, 253–276.

Perini, G., Conticelli, S., Francalanci, L. & Davidson, J. P. (2000). The relationships between potassic and calc-alkaline post-orogenic magmatism at Vico Volcano, Central Italy. *Journal of Volcanology and Geothermal Research* **95**, 247–272.

Perini, G., Tepley, F. J. III, Davidson, J. P. & Conticelli, S. (2003). The origin of K-feldspar megacrysts hosted in alkaline potassic rocks: track for low pressure processes in primitive magmas. *Lithos* **66**, 223–240.

Perini, G., Francalanci, L., Davidson, J. P. & Conticelli, S. (2004). The petrogenesis of Vico volcano, central Italy: an example of low scale mantle heterogeneity. *Journal of Petrology* **45**, 139–182.

Pfänder, J. A., Münker, C., Stracke, A. & Mezger, K. (2007). Nb/Ta and Zr/Hf in Ocean Island Basalts—Implications for crust–mantle differentiation and the fate of Nb. *Earth and Planetary Science Letters* **254**, 158–172.

Plank, T. (2005). Constraints from thorium/lanthanum on sediment recycling at subduction zones and the evolution of the continents. *Journal of Petrology* **46**, 921–944.

Plank, T. & Langmuir, C. H. (1998). The chemical composition of subducting sediments and its consequence for the crust and mantle. *Chemical Geology* **145**, 325–394.

Poli, G., Manetti, P., Peccerillo, A. & Cecchi, A. (1977). Determinazione di alcuni elementi del gruppo delle Terre Rare in rocce silicatiche per attivazione neutronica. *Rendiconti della Società Italiana di Mineralogia e Petrologia* **33**, 755–763.

Pyle, D. M., Dawson, J. B. & Ivanovich, M. (1991). Short-lived decay series disequilibria in the natrocarbonatite lavas of Oldoinyo Lengai, Tanzania: constraints on the timing of magma genesis. *Earth and Planetary Science Letters* **105**, 378–396.

Rogers, N. W., Hawkesworth, C. J., Parker, R. J. & Marsh, J. S. (1985). The geochemistry of potassic lavas from Vulsini, Central Italy, and implications for mantle enrichment processes beneath the Roman region. *Contributions to Mineralogy and Petrology* **90**, 244–257.

Rogers, N. W., De Mulder, R. & Hawkesworth, C. J. (1992). An enriched mantle source for potassic basanites: evidence from Karisimbi volcano, Virunga volcanic province, Rwanda. *Contributions to Mineralogy and Petrology* **111**, 543–556.

Rogers, N. W., James, D., Kelley, S. P. & DeMulder, M. (1998). The generation of potassic lavas from the Eastern Virunga Province, Rwanda. *Journal of Petrology* **39**, 1223–1247.

Rosenbaum, G., Gasparon, M., Lucente, F. P., Peccerillo, A. & Miller, M. S. (2008). Kinematics of slab tear faults during subduction segmentation and implications for Italian magmatism. *Tectonics* **27**, TC2008, doi:10.1029/2007TC002143.

Rudnick, R. L. & Fountain, D. M. (1995). Nature and composition of the continental crust: a lower crustal perspective. *Review of Geophysics* **33**, 267–309.

Ryerson, F. G. & Watson, E. B. (1987). Rutile saturation in magmas: Implications for Ti–Nb–Ta depletion in island arc basalts. *Earth and Planetary Science Letters* **86**, 225–239.

Sani, F., Del Ventisette, C., Montanari, D., Coli, M., Nafissi, P. & Piazzini, A. (2004). Tectonic evolution of the internal sector of the Central Apennines, Italy. *Marine and Petroleum Geology* **20**, 1–20.

Saunders, A. D., Norry, M. J. & Tarney, J. (1991). Fluid influence on the trace element compositions of subduction zones magma. *Philosophical Transactions of the Royal Society of London* **335**, 377–392.

Schmidt, M. W. & Poli, S. (1998). Experimentally based water budgets for dehydrating slabs and consequences for arc magma generation. *Earth and Planetary Science Letters* **163**, 361–379.

Schmidt, M. W., Vielzeuf, D. & Auzanneau, E. (2004). Melting and dissolution of subducting crust at high pressures: the key role of white mica. *Earth and Planetary Science Letters* **228**, 65–84.

Shapiro, L. & Brannock, W. W. (1962). Rapid analysis of silicate, carbonate and phosphate rocks. *Geological Survey Bulletin* **1144**, 1–55.

Spera, F. J. & Bohrson, W. A. (2001). Energy-constrained open-system magmatic processes I: general model and energy-constrained assimilation and fractional crystallization (EC-AFC) formulation. *Journal of Petrology* **42**, 999–1018.

Stoltz, A. J., Jochum, K. P., Spettel, B. & Hofmann, A. W. (1996). Fluid- and melt-related enrichment in the sub-arc mantle: evidence for Nb/Ta variations in island arc basalts. *Geology* **24**, 587–590.

Sun, S.-S. & McDonough, W. F. (1989). Chemical and isotopic systematics of oceanic basalts: implications for mantle composition and processes. In: Saunders, A. D. & Norry, M. J. (eds) *Magmatism in the Ocean Basins. Geological Society, London, Special Publications* **42**, 313–345.

Tatsumi, T. (1989). Migration of fluid phases and genesis of basalt magmas in subduction zones. *Journal of Geophysical Research* **94**, 4697–4707.

Thirlwall, M. F. (1991). Long-term reproducibility of multicollector Sr and Nd isotope ratio analysis. *Chemical Geology* **94**, 85–104.

Thomsen, T. B. & Schmidt, M. W. (2008). Melting of carbonated pelites at 2·5–5·0 GPa, silicate–carbonatite liquid immiscibility, and potassium–carbon metasomatism of the mantle. *Earth and Planetary Science Letters* **267**, 17–31.

Tommasini, S., Heumann, A., Avanzinelli, R. & Francalanci, L. (2007). The fate of high-angle dipping slabs in the subduction factory: an integrated trace element and radiogenic isotope (U, Th, Sr, Nd, Pb) study of Stromboli volcano, Aeolian Arc, Italy. *Journal of Petrology* **48**, 2407–2430, doi:10.1093/petrology/egm066.

Turner, S. P., Platt, J. P., George, R. M. M., Kelley, S. P., Pearson, D. G. & Nowell, G. M. (1999). Magmatism associated with orogenic collapse of the Betic–Alboran domain, SE Spain. *Journal of Petrology* **40**, 1011–1036.

van Bergen, M. J., Vroon, P. Z., Varekamp, J. C. & Poorter, R. P. E. (1992). The origin of the potassic rock suite from Batu Tara Volcano (East Sunda Arc, Indonesia). *Lithos* **28**, 261–282.

Wendlandt, R. F. & Eggler, D. H. (1980*a*). The origin of potassic magmas: 1. Melting relations in the systems $KAlSiO_4$–Mg_2SiO_4–SiO_2 and $KAlSiO_4$–MgO–SiO_2–CO_2 to 30 kb. *American Journal of Sciences* **280**, 385–420.

Wendlandt, R. F. & Eggler, D. H. (1980*b*). The origin of potassic magmas: 2. Stability of phlogopite in natural spinel lherzolite and in the system $KAlSiO_4$–MgO–SiO_2–H_2O–CO_2 at high pressure and high temperature. *American Journal of Sciences* **280**, 421–458.

White, W. M. & Dupré, B. (1986). Sediment subduction and magma genesis in the Lesser Antilles: Isotopic and trace element constraints. *Journal of Geophysical Research* **91**, 5927–5941.

Wilson, M., (1989). Igneous Petrogenesis. London: Unwin Hyman, 466 pp.

Workman, R. K. & Hart, S. R. (2005). Major and trace element composition of the depleted MORB mantle (DMM). *Earth and Planetary Science Letters* **231**, 53–72.

Wortel, M. J. R. & Spakman, W. (2000). Subduction and slab detachment in the Mediterranean–Carpathian Region. *Science* **290**, 1910–1917.

Yaxley, G. M. & Green, D. H. (1994). Experimental demonstration of refractory carbonate-bearing eclogite and siliceous melt in the subduction regime. *Earth and Planetary Science Letters* **128**, 313–325.

Elena Boari, Simone Tommasini, Marinella A. Laurenzi, and Sandro Conticelli

Transition from ultrapotassic kamafugitic to sub-alkaline magmas: Sr, Nd, and Pb isotope, trace element and ^{40}Ar-^{39}Ar age data from the Middle Latin Valley volcanic field, Roman Magmatic Province, Central Italy

Appendix 1

^{40}Ar-^{39}Ar analytical tables

Legend: Argon isotopes are in moles.

Steps used to calculate plateau ages are in bold.

Columns headings are as follows: ^{36}Ar(a) = atmospheric ^{36}Ar; ^{38}Ar(Cl) = Cl-derived ^{38}Ar; ^{39}Ar(K) = K-derived ^{39}Ar; ^{40}Ar(r) = radiogenic ^{40}Ar; ^{40}Ar(r)(%) = percentual ratio of radiogenic ^{40}Ar over total ^{40}Ar.

b.d.l. = below detection limit

Total fusion age is calculated summing the isotopic measurements of all steps, and its error includes uncertainty on J value. Errors quoted for individual analyses ages include analytical error only.

ERN-50 g.m. J=0.00019705 ± 0.00000060

Laser power W	^{36}Ar(a)	^{37}Ar(Ca)	^{38}Ar(Cl)	^{39}Ar(K)	^{40}Ar(r)	Age (ka)	± 2 σ	^{39}Ar(K) %	^{40}Ar(r) (%)	K/Ca	± 2 σ
0.2	**9.64E-18**	**8.08E-17**	**2.71E-18**	**1.85E-15**	**2.11E-15**	**405.5**	**89.1**	**2.1**	**42.4**	**12.147**	**5.271**
0.4	**5.32E-17**	**3.55E-16**	**4.33E-17**	**1.94E-14**	**2.09E-14**	**383.4**	**11.8**	**21.9**	**56.7**	**28.935**	**3.061**
0.5	**4.40E-17**	**2.71E-16**	**6.37E-17**	**2.29E-14**	**2.52E-14**	**391.3**	**10.3**	**25.9**	**65.5**	**44.772**	**6.094**
0.6	**3.28E-17**	**2.26E-16**	**4.09E-17**	**1.50E-14**	**1.64E-14**	**389.4**	**15.4**	**17.0**	**62.5**	**35.092**	**5.455**
0.8	**3.37E-17**	**2.96E-16**	**4.89E-17**	**1.28E-14**	**1.43E-14**	**398.9**	**10.9**	**14.5**	**58.6**	**22.847**	**2.852**
0.9	**2.97E-17**	**3.84E-16**	**3.84E-17**	**7.51E-15**	**8.22E-15**	**389.0**	**17.0**	**8.5**	**48.1**	**10.363**	**0.996**
1.1	**1.86E-17**	**4.31E-16**	**2.28E-17**	**2.46E-15**	**2.68E-15**	**388.0**	**108.0**	**2.8**	**32.7**	**3.020**	**0.361**
1.5	**2.40E-17**	**1.02E-15**	**3.16E-17**	**1.92E-15**	**1.91E-15**	**352.7**	**118.1**	**2.2**	**21.1**	**0.996**	**0.056**
2.2	**4.10E-17**	**7.39E-15**	**9.51E-17**	**1.91E-15**	**1.71E-15**	**317.9**	**118.6**	**2.2**	**12.3**	**0.137**	**0.004**
fuse	**9.22E-17**	**6.60E-14**	**6.01E-17**	**2.67E-15**	**2.76E-15**	**368.4**	**163.9**	**3.0**	**9.2**	**0.021**	**0.001**
Total fusion						**387.3**	**9.0**		**46.2**	**0.612**	**0.014**

ERN-34 g.m. J=0.00019591 ± 0.00000078

Laser power W	^{36}Ar(a)	^{37}Ar(Ca)	^{38}Ar(Cl)	^{39}Ar(K)	^{40}Ar(r)	Age (Ma)	± 2 σ	^{39}Ar(K) %	^{40}Ar(r) (%)	K/Ca	± 2 σ
0.2	8.06E-17	1.95E-16	2.35E-17	4.53E-15	5.71E-15	445.3	81.4	4.5	19.3	12.309	2.857
0.3	5.62E-17	5.97E-16	9.32E-17	1.71E-14	1.80E-14	372.3	16.4	17.1	51.8	15.183	1.216
0.4	9.17E-17	1.15E-15	2.97E-16	3.39E-14	3.82E-14	397.6	8.2	33.9	58.2	15.642	0.810
0.5	4.52E-17	6.73E-16	2.50E-16	1.47E-14	1.68E-14	404.0	17.2	14.7	55.4	11.578	0.851
0.6	3.84E-17	7.47E-16	3.36E-16	1.14E-14	1.43E-14	443.6	26.6	11.4	55.5	8.082	0.388
0.75	3.45E-17	8.05E-16	3.80E-16	6.65E-15	8.44E-15	448.5	57.7	6.6	45.1	4.377	0.188
0.9	2.99E-17	9.01E-16	3.48E-16	4.11E-15	5.62E-15	483.7	74.4	4.1	38.8	2.417	0.113
1.1	3.34E-17	1.16E-15	2.14E-16	2.65E-15	3.69E-15	493.2	111.1	2.6	27.1	1.206	0.044
1.5	3.51E-17	3.22E-15	1.28E-16	2.08E-15	2.82E-15	478.2	146.8	2.1	21.3	0.342	0.011
2	5.34E-17	1.80E-14	7.63E-17	1.62E-15	1.67E-15	364.3	153.1	1.6	9.6	0.048	0.001
fusion	9.75E-17	4.81E-14	4.81E-17	1.29E-15	1.47E-15	402.4	332.6	1.3	4.9	0.014	0.000
Total fusion						**412.3**	**11.1**		**39.9**	**0.702**	**0.015**

ERN-40 g.m. J=0.00019678 ± 0.00000060

Laser power W	^{36}Ar(a)	^{37}Ar(Ca)	^{38}Ar(Cl)	^{39}Ar(K)	^{40}Ar(r)	Age (ka)	± 2 σ	^{39}Ar(K) %	^{40}Ar(r) (%)	K/Ca	± 2 σ
0.2	**3.98E-17**	**1.49E-16**	**2.18E-17**	**4.24E-15**	**7.45E-15**	**624.1**	**29.4**	**5.9**	**38.7**	**15.038**	**3.182**
0.27	**7.58E-17**	**2.23E-16**	**5.71E-17**	**1.22E-14**	**2.11E-14**	**613.2**	**14.3**	**16.8**	**48.3**	**28.968**	**3.786**
0.33	**5.38E-17**	**1.68E-16**	**4.52E-17**	**9.48E-15**	**1.61E-14**	**603.2**	**11.7**	**13.1**	**50.2**	**29.846**	**5.218**
0.4	**9.59E-17**	**3.29E-16**	**1.07E-16**	**1.60E-14**	**2.71E-14**	**600.1**	**21.4**	**22.2**	**48.7**	**25.854**	**2.751**
0.47	**5.60E-17**	**2.29E-16**	**7.68E-17**	**8.82E-15**	**1.58E-14**	**636.8**	**24.8**	**12.2**	**48.7**	**20.397**	**3.206**
0.55	**5.52E-17**	**2.45E-16**	**9.32E-17**	**7.41E-15**	**1.27E-14**	**608.2**	**21.9**	**10.2**	**43.7**	**16.013**	**8.754**
0.7	5.11E-17	4.99E-16	1.06E-16	5.43E-15	1.01E-14	663.0	36.9	7.5	40.1	5.761	1.559
0.9	3.97E-17	6.55E-16	9.15E-17	3.08E-15	6.44E-15	743.0	84.9	4.3	35.4	2.491	0.124
1.3	5.35E-17	2.19E-15	8.23E-17	2.37E-15	5.92E-15	886.0	156.8	3.3	27.2	0.575	0.019
1.8	6.44E-17	8.04E-15	4.36E-17	1.32E-15	2.93E-15	790.7	241.4	1.8	13.3	0.087	0.003
2.4	8.34E-17	1.92E-14	2.69E-17	1.11E-15	1.61E-15	517.5	328.8	1.5	6.1	0.031	0.001
fuse	9.01E-17	2.76E-14	2.13E-17	9.39E-16	1.92E-15	726.8	406.4	1.3	6.7	0.018	0.001
Total fusion						**633.4**	**13.7**		**36.5**	**0.645**	**0.013**

ERN-56 leu J=0.00019509 ± 0.00000059

Laser power W	^{36}Ar(a)	^{37}Ar(Ca)	^{38}Ar(Cl)	^{39}Ar(K)	^{40}Ar(r)	Age (ka)	± 2 σ	^{39}Ar(K) %	^{40}Ar(r) (%)	K/Ca	± 2 σ
0.4	1.44E-17	2.97E-17	b.d.l.	1.94E-14	3.35E-14	614.8	8.5	8.0	88.2	347	984
0.6	**3.97E-17**	**6.67E-17**	**9.67E-19**	**7.83E-14**	**1.32E-13**	**600.0**	**3.1**	**32.1**	**91.3**	**623**	**784**
0.7	**4.61E-17**	**5.36E-17**	**1.48E-17**	**6.35E-14**	**1.07E-13**	**597.6**	**3.9**	**26.1**	**88.2**	**628**	**986**
0.8	**4.10E-17**	**2.50E-17**	**1.69E-18**	**4.20E-14**	**7.09E-14**	**600.5**	**4.0**	**17.2**	**84.9**	**891**	**2995**
0.9	**3.76E-17**	**3.81E-17**	b.d.l.	**2.49E-14**	**4.19E-14**	**598.9**	**6.0**	**10.2**	**78.6**	**346**	**763**
1.1	**1.87E-17**	**4.07E-17**	**1.61E-18**	**7.83E-15**	**1.34E-14**	**608.1**	**16.8**	**3.2**	**70.4**	**102**	**40**
2	**2.22E-17**	**1.50E-16**	**2.72E-19**	**4.77E-15**	**8.07E-15**	**602.6**	**20.5**	**2.0**	**55.0**	**17**	**2**
3	8.37E-18	7.19E-17	1.41E-18	2.14E-15	4.00E-15	666.1	37.6	0.9	61.6	16	3
6	5.71E-18	9.10E-17	1.29E-18	9.36E-16	1.93E-15	733.2	99.0	0.4	53.2	5	1
Total fusion						**601.9**	**4.1**		**85.6**	**228**	**77**

ERN-23 g.m. J=0.00019662 ± 0.00000060

Laser power W	^{36}Ar(a)	^{37}Ar(Ca)	^{38}Ar(Cl)	^{39}Ar(K)	^{40}Ar(r)	Age (ka)	± 2 σ	^{39}Ar(K) %	^{40}Ar(r) (%)	K/Ca	± 2 σ
0.2	**1.92E-17**	**2.17E-16**	**6.26E-18**	**6.10E-16**	**7.21E-16**	**419.4**	**308.1**	**0.9**	**11.3**	**1.488**	**0.275**
0.3	**3.88E-17**	**7.48E-16**	**1.27E-17**	**3.96E-15**	**4.28E-15**	**383.9**	**43.0**	**6.0**	**27.1**	**2.805**	**0.173**
0.4	**4.99E-17**	**1.42E-15**	**3.52E-17**	**9.66E-15**	**1.03E-14**	**379.0**	**16.5**	**14.6**	**41.0**	**3.610**	**0.167**
0.5	**4.10E-17**	**1.51E-15**	**6.16E-17**	**1.07E-14**	**1.14E-14**	**377.1**	**14.8**	**16.2**	**48.2**	**3.744**	**0.195**
0.6	**4.06E-17**	**2.01E-15**	**1.02E-16**	**1.10E-14**	**1.19E-14**	**381.7**	**24.0**	**16.7**	**49.5**	**2.913**	**0.131**
0.7	**3.06E-17**	**1.63E-15**	**1.01E-16**	**7.17E-15**	**7.51E-15**	**371.5**	**28.0**	**10.8**	**45.1**	**2.335**	**0.091**
0.85	**3.22E-17**	**1.94E-15**	**1.26E-16**	**6.13E-15**	**6.31E-15**	**364.8**	**23.6**	**9.3**	**39.7**	**1.678**	**0.068**
1.1	**4.05E-17**	**2.89E-15**	**1.73E-16**	**6.09E-15**	**6.12E-15**	**356.2**	**27.5**	**9.2**	**33.7**	**1.119**	**0.044**
1.5	**4.02E-17**	**3.90E-15**	**1.25E-16**	**4.62E-15**	**5.15E-15**	**394.8**	**35.7**	**7.0**	**30.2**	**0.628**	**0.025**
2.2	**6.61E-17**	**1.06E-14**	**7.75E-17**	**3.64E-15**	**4.02E-15**	**391.4**	**67.8**	**5.5**	**17.0**	**0.181**	**0.007**
3	**6.20E-17**	**2.90E-14**	**3.11E-17**	**1.67E-15**	**2.22E-15**	**469.9**	**159.5**	**2.5**	**10.8**	**0.031**	**0.001**
fuse	**5.25E-17**	**1.82E-14**	**1.60E-17**	**8.11E-16**	**8.04E-16**	**351.7**	**230.1**	**1.2**	**4.9**	**0.024**	**0.001**
Total fusion						**379.3**	**10.6**		**31.8**	**0.473**	**0.010**

ERN-86 leu J=0.00019771 ± 0.00000060

Laser power W	^{36}Ar(a)	^{37}Ar(Ca)	^{38}Ar(Cl)	^{39}Ar(K)	^{40}Ar(r)	Age (Ma)	± 2 σ	^{39}Ar(K) %	^{40}Ar(r) (%)	K/Ca	± 2 σ
0.2	**5.95E-18**	**3.52E-17**	**1.02E-18**	**7.10E-16**	**2.55E-16**	**127.9**	**211.4**	**0.4**	**12.6**	**10.7**	**11.4**
0.35	**7.57E-17**	**1.04E-16**	**6.33E-17**	**2.30E-14**	**1.64E-14**	**254.0**	**7.2**	**13.6**	**42.0**	**117.6**	**41.9**
0.5	**1.25E-16**	**7.06E-17**	**1.93E-16**	**5.11E-14**	**3.62E-14**	**252.5**	**7.7**	**30.2**	**49.2**	**383.3**	**232.7**
0.6	**1.41E-16**	**1.14E-16**	**2.20E-16**	**4.87E-14**	**3.43E-14**	**250.6**	**5.8**	**28.8**	**44.8**	**225.8**	**91.8**
0.7	7.92E-17	1.79E-16	1.80E-16	2.28E-14	1.71E-14	267.7	10.3	13.4	41.9	67.3	15.0
0.85	4.97E-17	2.66E-16	1.62E-16	1.15E-14	8.38E-15	260.8	20.3	6.8	36.2	22.8	3.5
1	2.64E-17	2.14E-16	1.34E-16	5.05E-15	3.81E-15	269.1	24.0	3.0	32.7	12.5	2.3
2	2.75E-17	3.32E-16	2.55E-16	4.08E-15	3.87E-15	338.7	30.5	2.4	32.1	6.5	0.8
6	2.75E-17	2.32E-16	4.17E-16	2.41E-15	3.06E-15	452.2	57.9	1.4	27.3	5.5	1.0
Total fusion						**259.7**	**4.2**		**42.8**	**58**	**4.6**

ERN-60 g.m. J=0.00019753 ± 0.00000060

Laser power W	^{36}Ar(a)	^{37}Ar(Ca)	^{38}Ar(Cl)	^{39}Ar(K)	^{40}Ar(r)	Age (ka)	± 2 σ	^{39}Ar(K) %	^{40}Ar(r) (%)	K/Ca	± 2 σ
0.2	1.44E-17	5.75E-17	4.40E-18	2.21E-15	2.09E-15	336.4	51.6	2.2	32.8	20.395	5.031
0.3	**3.82E-17**	**1.65E-16**	**1.86E-17**	**1.35E-14**	**1.52E-14**	**402.1**	**15.9**	**13.1**	**57.1**	**43.455**	**4.648**
0.37	**3.75E-17**	**1.65E-16**	**3.45E-17**	**2.23E-14**	**2.58E-14**	**411.9**	**8.0**	**21.7**	**69.5**	**71.677**	**8.538**
0.44	**3.48E-17**	**1.80E-16**	**3.35E-17**	**1.92E-14**	**2.22E-14**	**411.4**	**10.0**	**18.7**	**67.8**	**56.410**	**5.703**
0.5	**2.33E-17**	**1.39E-16**	**2.56E-17**	**1.18E-14**	**1.39E-14**	**418.9**	**14.9**	**11.5**	**66.4**	**44.823**	**4.554**
0.6	**2.63E-17**	**2.08E-16**	**2.57E-17**	**1.16E-14**	**1.35E-14**	**414.8**	**16.5**	**11.3**	**63.1**	**29.562**	**2.459**
0.75	**2.58E-17**	**3.84E-16**	**3.21E-17**	**8.47E-15**	**1.02E-14**	**428.5**	**18.7**	**8.3**	**56.9**	**11.691**	**0.615**
0.9	**1.83E-17**	**3.96E-16**	**1.59E-17**	**3.50E-15**	**4.07E-15**	**413.5**	**37.3**	**3.4**	**42.7**	**4.695**	**0.524**
1.5	**4.03E-17**	**2.90E-15**	**5.56E-17**	**3.63E-15**	**4.03E-15**	**396.1**	**68.8**	**3.5**	**25.3**	**0.662**	**0.023**
2.2	**8.56E-17**	**2.23E-14**	**8.70E-17**	**3.15E-15**	**3.94E-15**	**445.2**	**60.6**	**3.1**	**13.5**	**0.075**	**0.002**
fuse	**9.65E-17**	**4.38E-14**	**3.86E-17**	**3.32E-15**	**3.24E-15**	**347.9**	**113.4**	**3.2**	**10.2**	**0.040**	**0.001**
Total fusion						**409.8**	**7.2**		**47.5**	**0.770**	**0.018**

Age monitor of the previous samples: FCT biotite, 28.26 Ma (Di Vincenzo & Skála, 2009)
The correction factors for reactor induced interfering reactions were: ^{39}Ar/^{37}Ar (Ca) = 0.00075 ± 0.00006; ^{36}Ar/^{37}Ar (Ca) = 0.00024 ± 0.00002; ^{40}Ar/^{39}Ar (K) = 0.0112 ± 0.0022.

ERN-20 g.m. J=0.0001826 ± 0.00000086

Laser power W	^{36}Ar(a)	^{37}Ar(Ca)	^{38}Ar(Cl)	^{39}Ar(K)	^{40}Ar(r)	Age (Ma)	± 2 σ	^{39}Ar(K) %	^{40}Ar(r) (%)	K/Ca	± 2 σ
0.25	**2.34E-17**	**8.31E-16**	**3.01E-17**	**4.22E-15**	**4.26E-15**	**331.9**	**40.1**	**8.9**	**37.9**	**2.693**	**0.168**
0.35	**3.46E-17**	**1.45E-15**	**1.02E-16**	**9.93E-15**	**1.04E-14**	**345.1**	**11.7**	**20.8**	**50.2**	**3.634**	**0.219**
0.45	**3.11E-17**	**1.46E-15**	**1.50E-16**	**8.73E-15**	**9.24E-15**	**348.8**	**13.1**	**18.3**	**49.9**	**3.160**	**0.190**
0.55	**3.23E-17**	**1.82E-15**	**2.47E-16**	**7.51E-15**	**8.27E-15**	**362.6**	**22.3**	**15.7**	**46.2**	**2.184**	**0.132**
0.7	3.09E-17	1.92E-15	3.44E-16	5.09E-15	5.02E-15	324.7	19.2	10.7	35.4	1.404	0.087
0.9	2.66E-17	2.28E-15	4.37E-16	3.79E-15	4.33E-15	377.0	28.9	7.9	35.5	0.880	0.053
1.3	3.07E-17	3.47E-15	5.50E-16	3.39E-15	3.45E-15	335.2	25.3	7.1	27.5	0.518	0.031
1.9	4.08E-17	8.02E-15	4.90E-16	2.55E-15	2.51E-15	324.5	43.0	5.3	17.2	0.169	0.010
4	2.94E-17	1.95E-14	2.10E-16	1.14E-15	1.27E-15	366.9	115.6	2.4	12.7	0.031	0.002
fusion	3.39E-17	2.21E-14	1.30E-16	1.34E-15	1.22E-15	299.1	120.6	2.8	10.8	0.032	0.002
Total fusion						**345.1**	**8.9**		**35.0**	**0.402**	**0.022**

ERN-91 g.m. J=0.0001848 ± 0.00000083

Laser power W	^{36}Ar(a)	^{37}Ar(Ca)	^{38}Ar(Cl)	^{39}Ar(K)	^{40}Ar(r)	Age (Ma)	± 2 σ	^{39}Ar(K) %	^{40}Ar(r) (%)	K/Ca	± 2 σ
0.25	**1.12E-16**	**6.42E-16**	**7.43E-17**	**5.42E-15**	**5.92E-15**	**364.4**	**37.1**	**11.3**	**15.1**	**4.469**	**0.275**
0.35	**1.85E-16**	**9.61E-16**	**1.63E-16**	**9.96E-15**	**1.06E-14**	**355.3**	**17.8**	**20.7**	**16.2**	**5.491**	**0.328**
0.45	**1.77E-16**	**1.16E-15**	**2.29E-16**	**9.43E-15**	**1.03E-14**	**365.0**	**28.3**	**19.6**	**16.5**	**4.315**	**0.268**
0.55	**1.53E-16**	**1.44E-15**	**3.38E-16**	**7.99E-15**	**8.76E-15**	**365.3**	**28.0**	**16.6**	**16.2**	**2.933**	**0.179**
0.65	**9.57E-17**	**1.20E-15**	**3.74E-16**	**4.75E-15**	**4.98E-15**	**349.5**	**35.9**	**9.9**	**15.0**	**2.103**	**0.130**
0.9	**7.04E-17**	**1.81E-15**	**5.69E-16**	**3.34E-15**	**4.00E-15**	**399.5**	**57.4**	**6.9**	**16.1**	**0.979**	**0.059**
1.3	**5.96E-17**	**3.44E-15**	**7.50E-16**	**2.45E-15**	**2.38E-15**	**323.0**	**74.8**	**5.1**	**11.9**	**0.378**	**0.023**
1.9	**7.19E-17**	**8.91E-15**	**5.43E-16**	**2.13E-15**	**2.19E-15**	**342.5**	**74.5**	**4.4**	**9.3**	**0.127**	**0.008**
4	6.41E-17	2.29E-14	2.43E-16	1.34E-15	8.39E-16	209.0	134.7	2.8	4.2	0.031	0.002
fusion	5.02E-17	1.71E-14	7.98E-17	1.24E-15	1.48E-15	396.4	179.3	2.6	9.0	0.038	0.002
Total fusion						**357.2**	**13.4**		**14.4**	**0.428**	**0.023**

ERN-94 g.m. J=0.0001816 ± 0.00000099

Laser power W	^{36}Ar(a)	^{37}Ar(Ca)	^{38}Ar(Cl)	^{39}Ar(K)	^{40}Ar(r)	Age (Ma)	± 2 σ	^{39}Ar(K) %	^{40}Ar(r) (%)	K/Ca	± 2 σ
0.2	5.17E-18	4.53E-16	9.59E-18	4.23E-17	0.00E+00	0.0	0.0	0.6	0.0	0.050	0.004
0.4	1.37E-17	3.06E-15	7.48E-17	5.89E-16	2.64E-16	146.8	95.8	7.9	6.1	0.102	0.006
0.6	**1.38E-17**	**3.57E-15**	**1.07E-16**	**1.45E-15**	**1.49E-15**	**337.2**	**70.9**	**19.3**	**26.7**	**0.215**	**0.013**
0.8	**1.21E-17**	**2.21E-15**	**7.93E-17**	**1.36E-15**	**1.29E-15**	**310.9**	**49.8**	**18.2**	**26.5**	**0.327**	**0.019**
1	**1.07E-17**	**1.72E-15**	**4.93E-17**	**1.17E-15**	**9.63E-16**	**270.3**	**52.7**	**15.6**	**23.3**	**0.360**	**0.022**
1.3	**1.08E-17**	**2.16E-15**	**2.93E-17**	**9.98E-16**	**9.02E-16**	**296.2**	**55.6**	**13.3**	**21.9**	**0.245**	**0.015**
1.8	1.91E-17	4.38E-15	2.12E-17	9.85E-16	5.76E-16	191.6	83.3	13.2	9.2	0.119	0.007
3	9.46E-18	3.64E-15	7.41E-18	3.28E-16	6.18E-16	616.8	392.1	4.4	18.1	0.048	0.003
fusion	1.77E-17	7.81E-15	7.63E-18	2.15E-16	0.00E+00	0.0	0.0	2.9	0.0	0.015	0.001
fusion bis	2.11E-17	1.29E-14	1.34E-17	3.57E-16	4.28E-17	39.3	482.7	4.8	0.7	0.015	0.001
Total fusion						**268.9**	**37.4**		**13.5**	**0.095**	**0.005**

ERN-100 g.m. J=0.0001810 ± 0.00000099

Laser power W	^{36}Ar(a)	^{37}Ar(Ca)	^{38}Ar(Cl)	^{39}Ar(K)	^{40}Ar(r)	Age (Ma)	± 2 σ	^{39}Ar(K) %	^{40}Ar(r) (%)	K/Ca	± 2 σ
0.3	**1.03E-17**	**5.72E-16**	**3.14E-18**	**5.13E-17**	**5.01E-17**	**318.6**	**2677.0**	**0.6**	**1.6**	**0.048**	**0.009**
0.5	**1.03E-17**	**1.67E-15**	**1.09E-17**	**3.47E-16**	**4.21E-16**	**395.6**	**427.4**	**3.7**	**12.1**	**0.110**	**0.007**
0.7	**8.50E-18**	**1.54E-15**	**1.24E-17**	**7.08E-16**	**7.62E-16**	**351.2**	**196.8**	**7.6**	**23.2**	**0.244**	**0.015**
0.9	**8.31E-18**	**9.32E-16**	**9.21E-18**	**7.58E-16**	**9.31E-16**	**401.1**	**187.5**	**8.2**	**27.4**	**0.431**	**0.027**
1.1	**5.21E-18**	**6.19E-16**	**7.76E-18**	**7.65E-16**	**8.17E-16**	**348.6**	**167.9**	**8.2**	**34.5**	**0.656**	**0.047**
1.5	**1.03E-17**	**1.57E-15**	**6.28E-18**	**1.46E-15**	**1.26E-15**	**281.8**	**51.6**	**15.7**	**29.3**	**0.494**	**0.030**
2.6	**1.62E-17**	**7.15E-15**	**6.03E-18**	**1.62E-15**	**1.36E-15**	**274.0**	**69.2**	**17.4**	**22.1**	**0.120**	**0.007**
fusion	**5.68E-17**	**3.54E-14**	**1.90E-17**	**3.34E-15**	**2.88E-15**	**281.7**	**64.6**	**35.9**	**14.6**	**0.050**	**0.003**
fusion bis	5.41E-18	2.40E-15	1.77E-18	2.56E-16	0.00E+00	0.0	0.0	2.8	0.0	0.056	0.004
Total fusion						**297.6**	**43.3**		**17.9**	**0.095**	**0.005**

ERN-101 Phlog J=0.0001854 ± 0.00000088 Total fusion

	^{36}Ar(a)	^{37}Ar(Ca)	^{38}Ar(Cl)	^{39}Ar(K)	^{40}Ar(r)	Age (Ma)	± 2 σ	^{39}Ar(K) %	^{40}Ar(r) (%)	K/Ca	± 2 σ
1 crystal	**1.35E-16**	**5.34E-17**	**4.32E-18**	**9.53E-15**	**1.13E-14**	**397.0**	**29.2**	**-**	**22.0**	**94.5**	**17.4**
1 crystal	**1.17E-16**	**1.56E-17**	**6.05E-18**	**1.26E-14**	**1.50E-14**	**398.5**	**22.5**	**-**	**30.3**	**429.8**	**335.5**
1 crystal	**2.38E-16**	**2.31E-17**	**7.66E-18**	**1.49E-14**	**1.85E-14**	**414.5**	**15.6**	**-**	**20.8**	**341.7**	**69.7**
1 crystal	2.96E-16	1.44E-17	1.28E-17	7.06E-15	1.55E-14	733.7	45.2	-	15.0	260.0	148.4
3 crystals	7.82E-16	1.24E-17	5.61E-18	6.61E-15	9.31E-15	470.9	91.0	-	3.9	283.3	169.8
5 crystals	6.38E-16	2.71E-17	8.21E-18	1.71E-14	2.67E-14	524.2	34.8	-	12.4	333.6	108.8
1 crystal	**3.05E-16**	**1.60E-17**	**9.73E-18**	**1.96E-14**	**2.32E-14**	**395.7**	**22.6**	**-**	**20.4**	**646.7**	**211.4**

ERN-101 Phlog J=0.0001854 ± 0.00000088 mini-SH

Laser power W	^{36}Ar(a)	^{37}Ar(Ca)	^{38}Ar(Cl)	^{39}Ar(K)	^{40}Ar(r)	Age (Ma)	± 2 σ	^{39}Ar(K) %	^{40}Ar(r) (%)	K/Ca	± 2 σ
#1											
1.4	3.10E-16	b.d.l.	b.d.l.	6.72E-16	1.39E-15	690.7	520.3	6.8	1.5	n.d.	
fusion	3.45E-16	5.53E-17	1.13E-17	9.16E-15	2.12E-14	775.2	54.8	93.2	17.2	87.8	16.0
Total fusion						769.4	62.4		10.5	94.3	23.9
#2											
1.4	9.04E-17	8.90E-17	b.d.l.	7.11E-16	2.44E-15	1148.5	311.2	5.3	8.4	4.2	0.7
fusion	**4.47E-17**	**2.76E-17**	**5.10E-18**	**1.28E-14**	**1.61E-14**	**420.8**	**23.5**	**94.7**	**54.7**	**245.3**	**99.6**
Total fusion						459.1	27.8		31.7	61.3	9.6
#3											
1.4	1.42E-16	6.67E-17	1.94E-19	4.86E-16	9.24E-16	635.5	762.8	3.5	2.2	3.9	0.9
fusion	**1.55E-16**	**4.26E-17**	**5.15E-18**	**1.32E-14**	**1.65E-14**	**417.9**	**89.5**	**96.5**	**26.5**	**164.6**	**83.3**
Total fusion						425.6	90.6		16.6	66.5	16.4
#4											
1.9	2.12E-16	2.11E-17	2.78E-18	6.49E-16	3.13E-15	1611.2	942.9	4.2	4.8	16.3	6.5
fusion	3.46E-16	2.56E-17	2.03E-17	1.49E-14	3.30E-14	739.5	80.4	95.8	24.4	308.9	274.4
Total fusion						775.9	86.7		18.0	176.7	91.9

ERN-102 Phlog J=0.0001860 ± 0.00000059

Laser power W	^{36}Ar(a)	^{37}Ar(Ca)	^{38}Ar(Cl)	^{39}Ar(K)	^{40}Ar(r)	Age (Ma)	± 2 σ	^{39}Ar(K) %	^{40}Ar(r) (%)	K/Ca	± 2 σ
3 crystals											
0.9	5.24E-17	b.d.l.	4.14E-19	1.63E-16	0.00E+00	0	0	1.0	0.0	n.d.	
fusion	**3.28E-16**	**2.74E-17**	**9.23E-18**	**1.58E-14**	**2.00E-14**	**425.6**	**33.8**	**99.0**	**17.1**	**305.0**	**77.2**
Total fusion						421.3	33.5		15.1	308.2	111.8
2 crystals											
1.1	8.12E-17	2.10E-18	6.04E-19	3.18E-16	3.57E-16	377.7	579.9	2.6	1.5	80.0	535.5
fusion	**1.47E-16**	**1.73E-16**	**1.53E-18**	**1.20E-14**	**1.63E-14**	**454.0**	**21.8**	**97.4**	**27.2**	**36.8**	**3.7**
Total fusion						452.0	26.0		19.8	37.3	4.8
1 crystal											
1.1	5.34E-17	9.82E-16	7.56E-19	3.17E-16	1.21E-15	1284.6	596.7	3.8	7.1	0.2	0.0
fusion	**4.83E-17**	**1.90E-16**	**4.82E-18**	**7.95E-15**	**1.04E-14**	**437.9**	**29.7**	**96.2**	**42.0**	**22.2**	**1.7**
Total fusion						470.3	36.6		27.8	3.74	0.2
1 crystal											
1.2	2.47E-16	1.92E-17	1.44E-18	3.20E-16	1.31E-16	137.2	1376.4	3.1	0.2	8.8	3.8
fusion	**3.64E-17**	**5.30E-17**	**5.19E-18**	**1.01E-14**	**1.27E-14**	**420.0**	**34.0**	**96.9**	**53.9**	**101.4**	**21.3**
Total fusion						411.4	53.5		13.3	76.7	14.8
1 crystal											
0.9	2.73E-16	b.d.l.	7.71E-19	6.06E-16	2.67E-15	1476.7	787.8	5.1	3.2	n.d.	
fusion	**1.33E-16**	**1.18E-17**	**4.87E-18**	**1.12E-14**	**1.36E-14**	**406.2**	**52.3**	**94.9**	**25.7**	**503.7**	**1446.1**
Total fusion						461.1	63.9		11.9	530.9	1658.8
1 crystal											
0.9	5.49E-17	4.71E-18	6.04E-19	4.84E-16	6.38E-16	442.6	459.5	2.8	3.8	54.5	151.1
fusion	**8.00E-17**	**2.55E-17**	**9.66E-20**	**1.68E-14**	**1.97E-14**	**392.2**	**42.6**	**97.2**	**45.3**	**350.4**	**271.2**
Total fusion						393.6	43.4		33.8	304.2	238.5
1 crystal											
0.9	1.72E-16	3.59E-16	1.04E-18	4.91E-16	1.26E-15	857.3	475.7	3.1	2.4	0.7	0.1
fusion	**1.48E-16**	**8.17E-17**	**6.41E-18**	**1.54E-14**	**1.93E-14**	**421.7**	**47.7**	**96.9**	**30.6**	**99.7**	**21.1**
Total fusion						435.2	48.5		17.9	19.1	1.5
1 crystal											
0.9	4.14E-17	8.18E-18	4.94E-19	3.12E-16	9.15E-16	984.1	836.2	1.8	7.0	20.2	34.5
fusion	**8.06E-17**	**2.51E-17**	**4.28E-18**	**1.75E-14**	**2.05E-14**	**393.0**	**47.1**	**98.2**	**46.0**	**368.6**	**120.2**
Total fusion						403.4	48.6		37.2	283.0	137.7
1 crystal											
0.8	3.14E-17	b.d.l.	1.67E-18	5.65E-16	6.14E-16	364.5	695.5	3.2	6.2	n.d.	
fusion	**1.02E-16**	**2.23E-17**	**1.62E-19**	**1.73E-14**	**2.23E-14**	**431.9**	**28**	**96.8**	**42.3**	**410.9**	**115.7**
Total fusion						429.8	34.9		36.7	424.4	143.1

Age monitor for the second set of samples: FCT sanidine, 28.03 Ma (Jourdan & Renne, 2007).
The correction factors for reactor induced interfering reactions were: ^{39}Ar/^{37}Ar (Ca) = 0.00075 ± 0.000075; ^{36}Ar/^{37}Ar (Ca) = 0.00024 ± 0.00002; ^{40}Ar/^{39}Ar (K) = 0.00925 ± 0.0009.

Elena Boari, Simone Tommasini, Marinella A. Laurenzi, and Sandro Conticelli

Transition from ultrapotassic kamafugitic to sub-alkaline magmas: Sr, Nd, and Pb isotope, trace element and ^{40}Ar-^{39}Ar age data from the Middle Latin Valley volcanic field, Roman Magmatic Province, Central Italy

Appendix 3

^{40}Ar-^{39}Ar dating.

Age spectra, K/Ca spectra, inverse isochron plots, probability plots of analysed samples.
Age spectrum: cumulative percentage ^{39}Ar release versus age. Error boxes represent ± 2 σ analytical errors. The lines show the steps used to calculate the plateau ages.
K/Ca spectrum: cumulative percentage ^{39}Ar release versus K/Ca ratio. Error boxes represent ± 2 σ analytical errors.
Inverse isochron plot: solid squares represent the points used to calculate the isochron age, while empty squares are the points not used for the calculation. Error bars are ± 2 σ analytical errors.
Probability plot: cumulative probability distribution of single crystal dating (ERN-101 and -102)
The uncertainty on age is ± 2 σ total error.

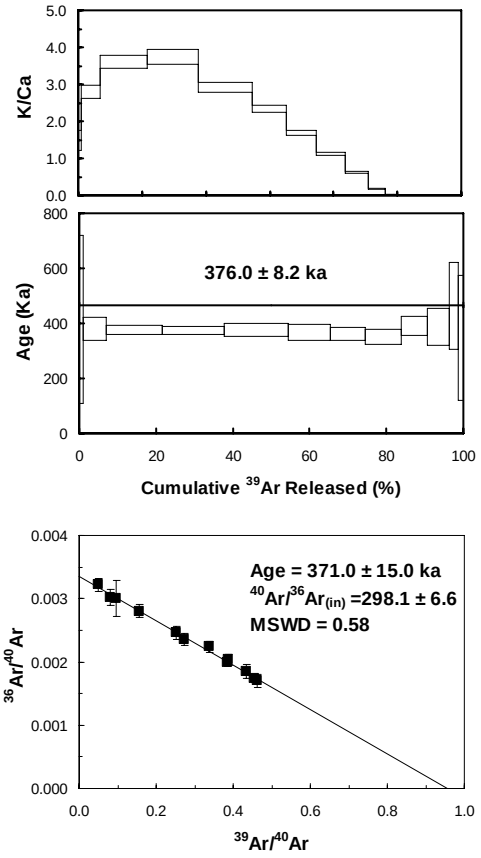

ERN-23 (ground mass)

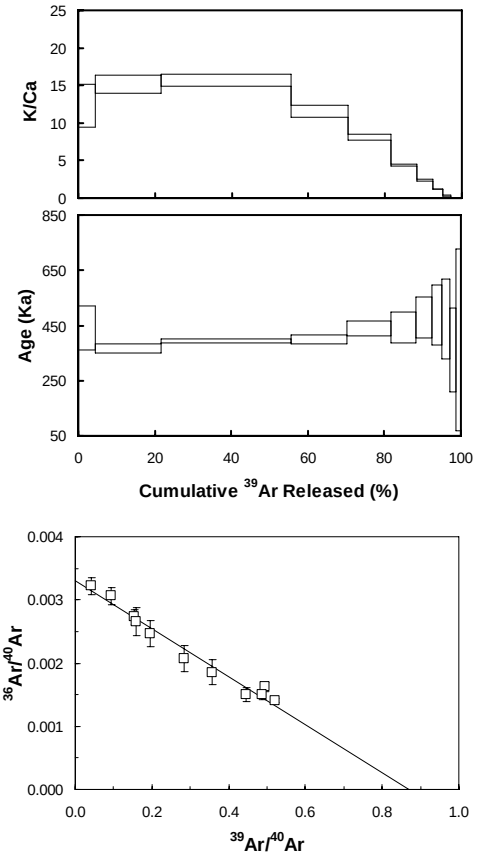

ERN-34 (ground mass)

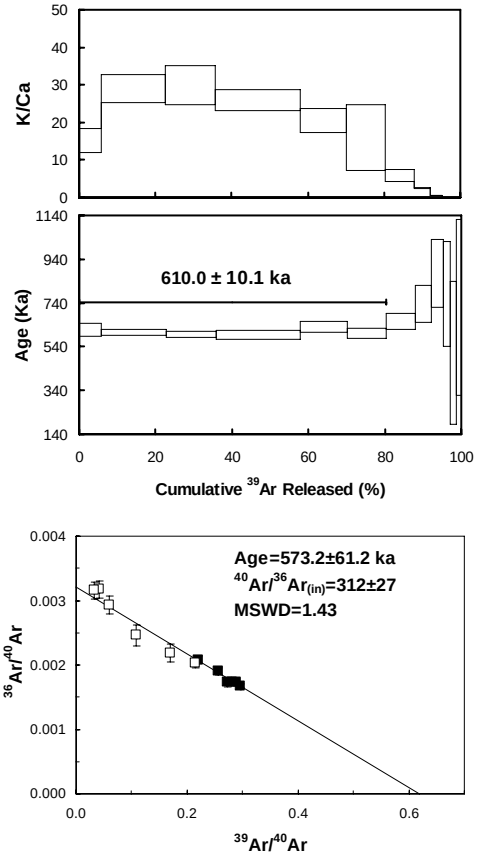

ERN-40 (ground mass)

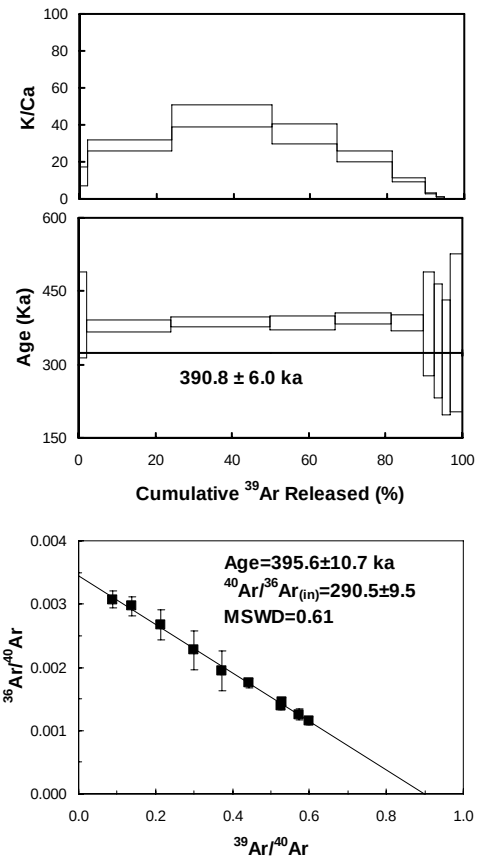

ERN-50 (ground mass)

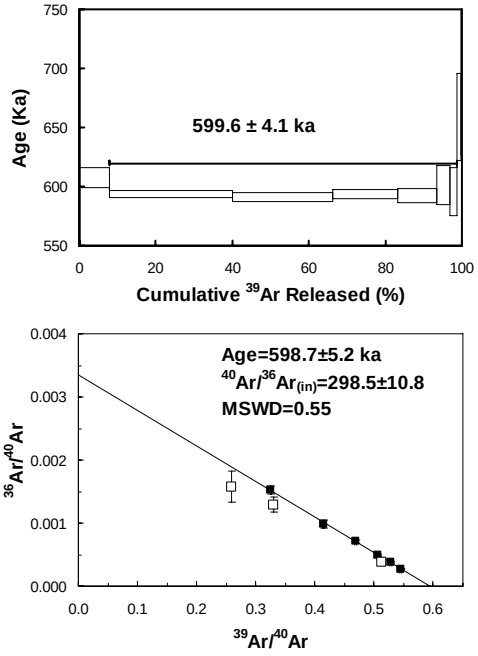

ERN-56 (leucite)

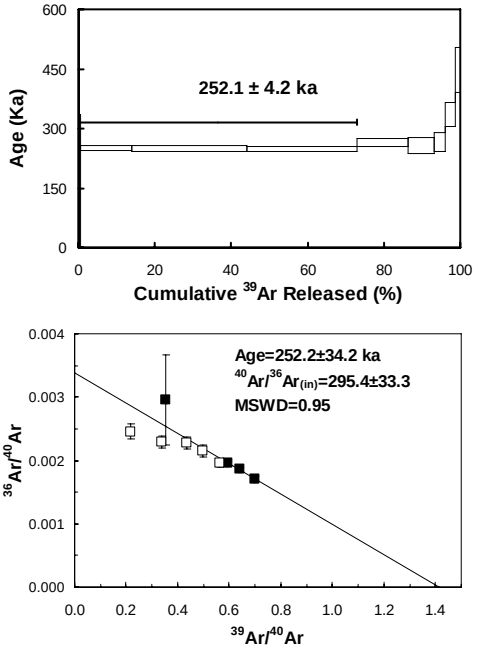

ERN-86 (leucite)

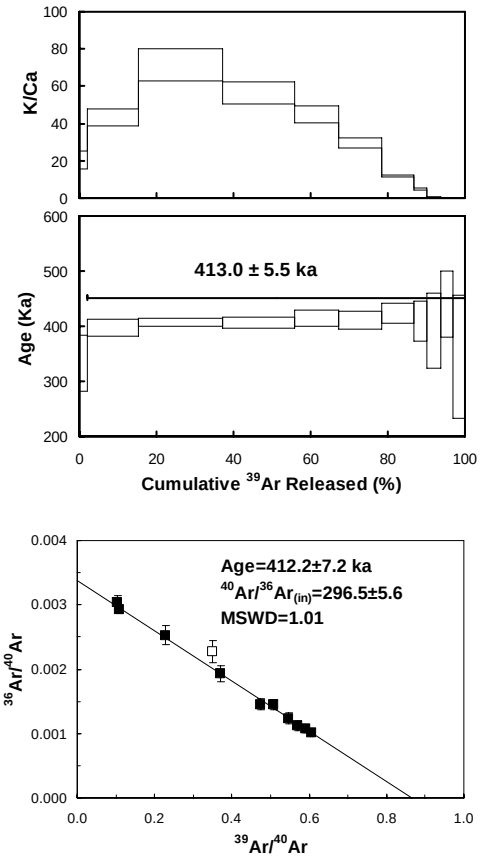

ERN-60 (ground mass)

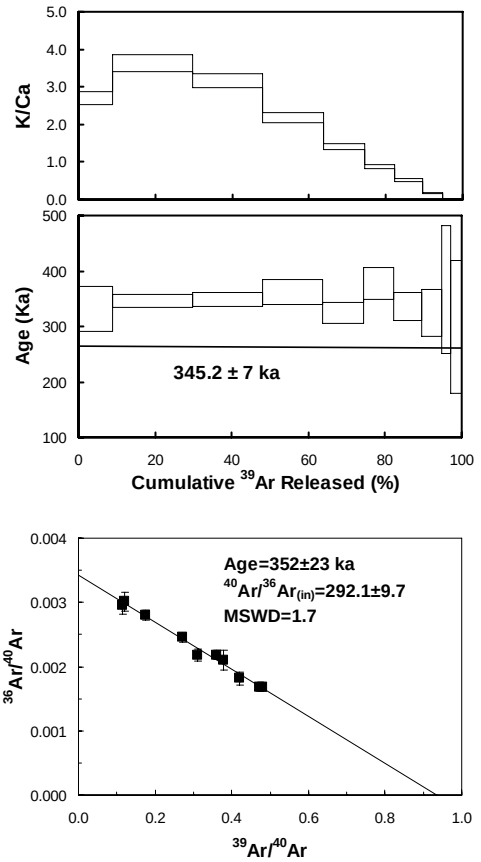

ERN- 20 (ground mass)

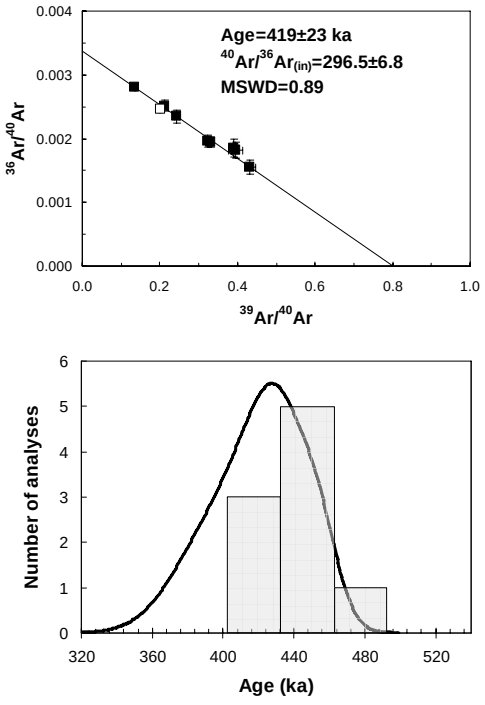

ERN-102 (phlogopite)

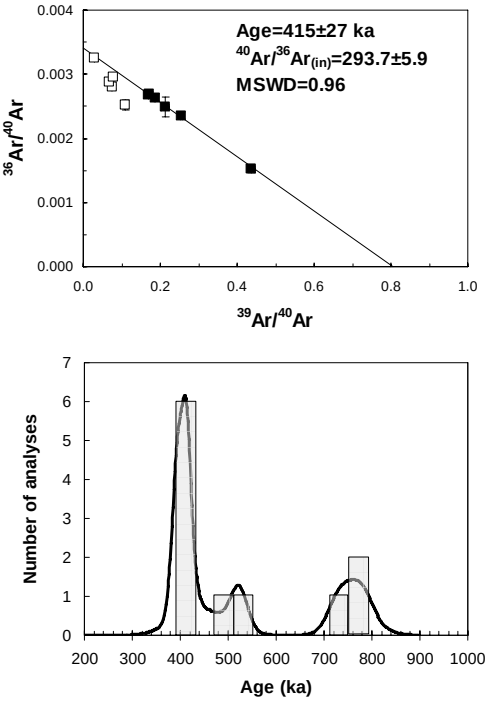

ERN-101 (phlogopite)

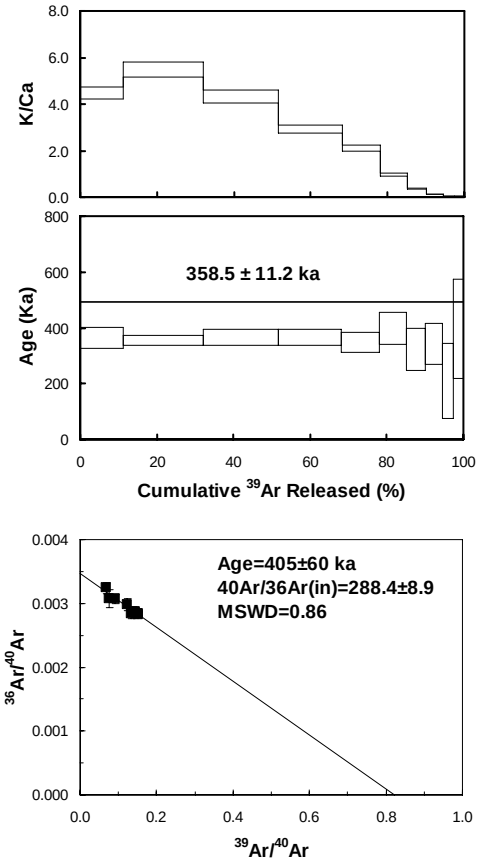

ERN-91 (ground mass)

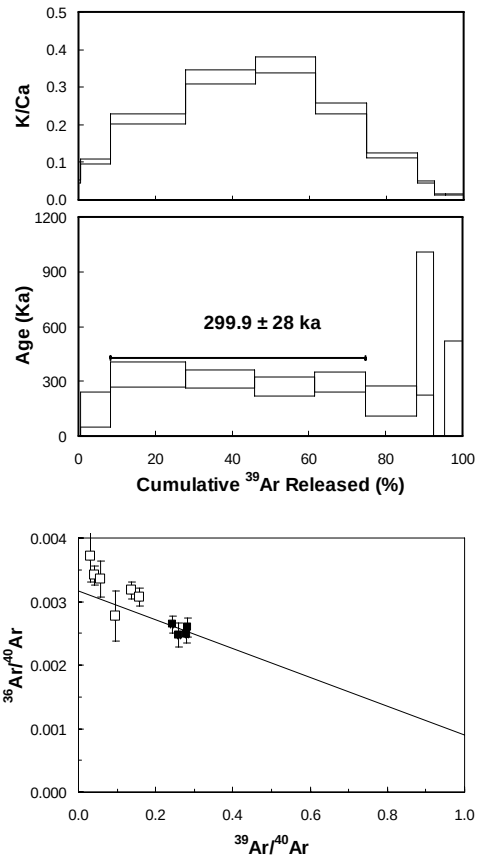

ERN-94 (ground mass)

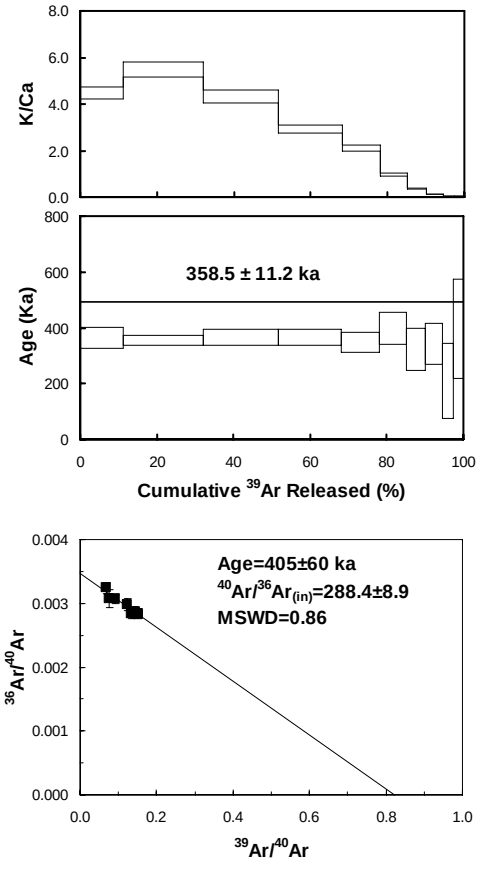

ERN-100 (ground mass)

Appendix II - Chemical data on whole rocks for Middle Latin Valley rocks

Boari & Conticelli (2006)

Locality:	*Colle*	*Colle*	*Colle*	*Colle*	*Colle*	*Colle*	*Santo*	*Santo*	*Morolo*	*Morolo*	*Morolo*	*Tecchiena*	*Tecchiena*
Locality:	*Morrone*	*Castellone*	*Castellone*	*Castellone*	*Castellone*	*Castellone*	*Arcangelo*	*Arcangelo*	*Piglione*	*Piglione*	*Piglione*	*Quarticciolo*	*Convento*
Latitude:	41°33'28"N	41°34'08"N	41°34'02"N	40°33'49"N	40°33'49"N	40°33'49"N	41°33'42"N	41°33'42"N	41°37'31"N	41°37'38"N	41°37'34"N	41°40'33"N	41°41'09"N
Longitude:	13°18'11"E	13°18'01"E	13°18'07"E	12°18'08"E	12°18'08"E	12°18'08"E	13°18'29"E	13°18'29"E	13°12'39"E	13°12'37"E	13°12'38"E	13°19'16"E	13°19'20"E
Group:	limestone	KAM	KAM	KAM	KAM	KAM	HKS	HKS	HKS	HKS	HKS	HKS	HKS
Sample:	**ERN57**	**ERN55**	**ERN56**	**ERN84s**	**ERN84t**	**ERN84**	**ERN86**	**ERN85**	**ERN39**	**ERN41**	**ERN40**	**ERN36**	**ERN33**
Number:	1	2	3	4	5	6	7	8	9	10	11	36	37
Key:	*0*	*1*	*1*	*-*	*-*	*1*	*2*	*2*	*3*	*3*	*3*	*8*	*8*
Note:	*limestone*	*lava*	*lava*	*lava*	*lava*	*lava*	*lava*	*lava*	*lava*	*lava*	*lava*	*scoria*	*lava*
Age Ma:	*0.602000*	*0.602000*	*0.602000*	*0.602000*	*0.602000*	*0.602000*	*0.260000*	*0.260000*	*0.610000*	*0.610000*	*0.610000*	*0.412000*	*0.412000*
SiO2	7.66	45.51	46.03	46.45	46.54	46.54	46.83	47.01	46.98	47.14	46.65	47.35	48.46
TiO2	0.07	1.04	1.06	1.10	1.10	1.10	0.83	0.81	0.84	1.00	0.98	0.85	0.79
Al2O3	2.09	16.27	16.46	16.63	16.64	16.64	18.25	18.05	16.46	17.61	16.85	18.21	18.18
Fe2O3	0.62	2.85	4.59	5.59	5.33	5.33	4.93	5.15	4.72	4.78	4.06	6.41	4.73
FeO	0.13	4.66	3.18	2.79	2.83	2.83	3.24	2.95	2.38	1.96	2.92	1.43	2.24
MnO	0.03	0.14	0.14	0.15	0.15	0.15	0.16	0.16	0.14	0.13	0.13	0.15	0.14
MgO	1.05	4.79	4.61	4.05	4.07	4.07	3.63	3.71	6.51	6.05	6.27	4.45	4.48
CaO	47.59	10.81	10.55	10.17	10.26	10.26	9.64	9.66	11.64	10.25	10.33	10.43	10.03
Na2O	0.55	1.92	2.17	1.55	1.56	1.56	2.17	2.11	2.00	2.15	2.59	2.08	2.39
K2O	0.28	9.29	9.77	9.53	9.53	9.53	9.14	8.99	6.45	7.77	7.99	7.49	7.17
P2O5	0.08	0.91	0.97	0.95	0.92	0.92	0.50	0.52	0.42	0.41	0.42	0.36	0.32
LOI	39.85	1.82	0.47	1.05	1.07	1.07	0.70	0.89	1.47	0.75	0.80	0.79	1.07
Sum	100.00	100.00	100.00	100.00	100.00	100.00	100.00	100.00	100.00	100.00	100.00	100.00	100.00
Mg-V	76.11	58.06	56.82	51.93	52.68	52.68	49.66	50.51	67.22	66.84	66.55	56.33	59.00
CO2	-	-	-	-	-	-	-	-	-	-	-	-	-
Li *	4.3	-	32.4	-	31.8	31.8	26.7	-	-	-	26.2	-	-
Be *	0.22	-	8.25	-	8.41	8.41	9.76	-	-	-	6.94	-	-
B	-	-	-	-	-	-	-	-	-	-	-	-	-
F	-	-	-	-	-	-	-	-	-	-	-	-	-
S	-	-	-	-	-	-	-	-	-	-	-	-	-
Cl	-	-	-	-	-	-	-	-	-	-	-	-	-
Sc *	1.2	-	20.1	-	20.4	20.4	11.0	-	-	-	20.1	-	-
V	15	249	242	254	250	252	277	277	197	190	219	227	233
V *	17	-	223	-	228	228	275	-	-	-	198	-	-
Cr	bdl	14	13	13	13	13	26	18	207	228	205	52	66
Co	1.90	33	28.5	29.0	29.0	29.0	26.7	25	28	25	25.5	27	22
Ni	bdl	34	34.0	32.0	29.8	30.9	27.0	26	101	93	95.0	40	41
Cu	bdl	97	111	89	89	89	77	94	55	23	47	72	49
Cu *	3.10	-	93.6	-	87.8	87.8	71.8	-	-	-	46.8	-	-
Zn	12	73	71	71	71	71	72	68	60	59	61	75	67
Zn *	14.7	-	71.2	-	73.4	73.4	74.2	-	-	-	57.7	-	-
As *	5.04	-	17.50	-	12.30	12.30	8.74	-	-	-	15.70	-	-
Rb	14	417	434	474	463	468	441	431	431	362	335	446	444
Rb *	15	-	491	-	504	504	447	-	-	-	391	-	-
Sr	301	2144	2553	-	1933	1933	2393	2376	1991	2332	2231	2160	2072
Sr *	386	-	2500	-	1870	1870	2260	-	-	-	2140	-	-

	A	B	C	D	E	F	G	H	I	J	K	L	M	N
53	Y	6	44	43	23	45	34	36	33	34	32	33	26	34
54	Y *	4.5	-	43.2	-	42.8	42.8	40.0	-	-	-	33.2	-	-
55	Zr	15	509	516	533	525	529	415	417	350	342	346	284	266
56	Zr *	10	-	547	-	512	512	417	-	-	-	344	-	-
57	Nb	bdl	36	36	35	35	35	21	22	23	26	25	17	16
58	Nb *	1.62	-	35.2	-	35.2	35.2	20.9	-	-	-	24.5	-	-
59	Mo *	1.44	-	1.21	-	1.75	1.75	2.71	-	-	-	1.69	-	-
60	Cd *	0.46	-	0.13	-	0.08	0.08	0.08	-	-	-	0.04	-	-
61	Sn *	0.29	-	6.79	-	4.83	4.83	5.51	-	-	-	5.19	-	-
62	Sb *	0.16	-	1.41	-	1.18	1.18	0.74	-	-	-	1.56	-	-
63	Cs *	0.59	-	53.9	-	60.8	60.8	41.0	-	-	-	38.6	-	-
64	Ba	62	3949	3938	3883	3881	3882	1424	1427	1824	2077	1933	1524	1352
65	Ba *	56	-	4010	-	3930	3930	1470	-	-	-	1980	-	-
66	La	bdl	231	242	223	222	222	129	128	128	138	133	102	100
67	La*	4.30	-	241	-	226	226	129	-	-	-	146	-	-
68	Ce	bdl	457	478	454	460	457	287	302	260	276	267	217	213
69	Ce *	7.14	-	478	-	452	452	279	-	-	-	283	-	-
70	Pr *	0.97	-	52.7	-	50.8	50.8	32.5	-	-	-	30.9	-	-
71	Nd	bdl	181	181	180	183	182	121	123	102	100	100	86	84
72	Nd *	3.84	-	196	-	189	189	125	-	-	-	113.0	-	-
73	Sm *	0.78	-	33.7	-	32.4	32.4	22.6	-	-	-	19.7	-	-
74	Eu *	0.19	-	7.03	-	6.76	6.76	4.63	-	-	-	4.17	-	-
75	Gd *	0.84	-	28.8	-	27.8	27.8	19.6	-	-	-	17.3	-	-
76	Tb *	0.13	-	3.02	-	2.92	2.92	2.23	-	-	-	1.91	-	-
77	Dy *	0.72	-	11.9	-	11.5	11.5	9.66	-	-	-	8.28	-	-
78	Ho *	0.15	-	1.84	-	1.79	1.79	1.62	-	-	-	1.40	-	-
79	Er *	0.42	-	4.81	-	4.62	4.62	4.33	-	-	-	3.79	-	-
80	Tm *	0.06	-	0.50	-	0.49	0.49	0.51	-	-	-	0.45	-	-
81	Yb *	0.36	-	3.01	-	2.91	2.91	3.12	-	-	-	2.71	-	-
82	Lu *	0.06	-	0.42	-	0.42	0.42	0.45	-	-	-	0.40	-	-
83	Hf *	0.34	-	14.9	-	12.3	12.3	10.5	-	-	-	9.17	-	-
84	Ta *	0.10	-	1.07	-	0.84	0.84	0.99	-	-	-	1.46	-	-
85	W *	0.24	-	6.68	-	9.62	9.62	10.2	-	-	-	6.75	-	-
86	Tl *	0.08	-	1.99	-	1.92	1.92	3.04	-	-	-	2.02	-	-
87	Pb	bdl	114	141	150	145	147	84	87	106	75	92	46	72
88	Pb *	0.20	-	133	-	134	134	79.4	-	-	-	81.3	-	-
89	Bi *	0.02	-	0.32	-	0.18	0.18	0.51	-	-	-	0.09	-	-
90	Th *	1.00	-	93.5	-	90.5	90.5	53.5	-	-	-	61.6	-	-
91	U *	2.26	-	7.57	-	6.07	6.07	11.2	-	-	-	13.1	-	-
92	87/86Sr)m	0.708841	-	0.711176	-	-	0.711156	0.710071	-	-	-	0.710238	-	-
93	2 sigma	± 0.000007	-	± 0.000006	-	-	± 0.000007	± 0.000007	-	-	-	± 0.000007	-	-
94	87/86Sr)i	0.708840	-	0.711171	-	-	0.711149	0.710069	-	-	-	0.710233	-	-
95	143/144)m	0.512151	-	0.512120	-	-	0.512119	0.512127	-	-	-	0.512132	-	-
96	2 sigma	± 0.000004	-	± 0.000005	-	-	± 0.000004	± 0.000006	-	-	-	± 0.000005	-	-
97	143/144)i	0.512151	-	0.512120	-	-	0.512119	0.512127	-	-	-	0.512132	-	-
98	206/204Pb	-	-	18.7258	-	-	18.7362	18.7796	-	-	-	18.7705	-	-
99	207/204Pb	-	-	15.6704	-	-	15.6823	15.6811	-	-	-	15.6802	-	-
100	208/204Pb	-	-	38.9686	-	-	39.0089	39.0168	-	-	-	39.0095	-	-
101														
102	* performed by ICP-MS at Goettingen													

	O	P	Q	R	S	T	U	V	W	X	Y	Z	AA	AB
1														
2														
3														
4	*Tecchiena*	*Tecchiena*	*Tecchiena*	*Tecchiena*	*Tecchiena*	*Tecchiena*	*Frosinone*	*Frosinone*	*Celleta*	*Celleta*	*Celleta*	*Celleta*	*Celleta*	*Celleta*
5	*Convento*	*Convento*		*F.S.Pietro*	*Convento*	*Campone*	*SelvaMuli*	*SelvaMuli*	*C. Folgara*	*Fornelli*	*C.Schiappa*	*C. Folgara*	*Fornelli*	*C. Folgara*
6	41°41'09"N	41°41'09"N	41°41'49"N	41°39'54"N	41°41'09"N	41°39'58"N	41°37'43"N	41°37'43"N	41°34'17"N	41°34'47"N	41°34'00"N	41°34'17"N	41°34'47"N	41°34'17"N
7	13°19'20"E	13°19'20"E	13°20'16"E	13°19'01"E	13°19'20"N	13°19'32"E	13°17'39"E	13°17'39"E	13°17'34"E	13°16'59"E	13°17'23"E	13°17'33"E	13°16'59"E	13°17'34"E
8	HKS	HKS	HKS	HKS	HKS	HKS	HKS	HKS	HKS	HKS	HKS	HKS	HKS	HKS
9	**ERN34**	**ERN28**	**ERN26**	**ERN38**	**ERN27**	**ERN37**	**ERN30**	**ERN29**	**ERN61**	**ERN64**	**ERN58**	**ERN62**	**ERN65**	**ERN60**
10	38	39	40	41	42	43	34	35	12	13	14	15	16	17
11	*8*	*8*	*8*	*8*	*8*	*8*	*7*	*7*	*4*	*4*	*4*	*4*	*4*	*4*
12	*lava*	*lava*	*lava*	*lava*	*lava*	*lava*	*bomb*	*bomb*	*lava*	*lava*	*lava*	*lava*	*lava*	*lava*
13	*0.412000*	*0.412000*	*0.412000*	*0.412000*	*0.412000*	*0.412000*	*0.412000*	*0.412000*	*0.413000*	*0.413000*	*0.413000*	*0.413000*	*0.413000*	*0.413000*
14														
15	48.47	49.20	49.21	49.30	49.36	49.69	46.63	46.84	46.70	46.77	46.78	46.80	46.83	46.89
16	0.82	0.80	0.80	0.81	0.79	0.71	1.02	1.04	0.82	0.82	0.84	0.84	0.83	0.84
17	18.06	18.64	18.56	18.41	18.62	18.97	18.93	18.04	17.88	18.49	17.47	17.87	17.40	17.46
18	4.37	3.48	3.48	3.88	4.05	3.56	7.71	7.89	4.79	5.17	4.31	4.76	4.31	4.85
19	2.86	3.34	3.30	2.87	2.76	2.79	1.11	1.02	2.65	2.22	3.05	2.78	3.13	2.65
20	0.14	0.14	0.14	0.14	0.14	0.14	0.16	0.16	0.14	0.15	0.14	0.15	0.14	0.15
21	4.46	3.89	3.87	4.35	4.08	3.91	4.58	5.02	5.32	5.10	5.49	5.27	5.30	5.19
22	10.08	9.26	9.09	9.41	8.96	8.82	10.67	11.03	10.90	10.33	11.26	10.98	11.32	11.16
23	2.85	2.57	2.73	2.67	2.91	2.68	1.13	1.48	1.76	1.92	1.97	2.03	2.13	2.07
24	6.90	7.62	7.39	7.35	7.27	7.82	5.74	5.31	7.38	7.42	7.62	6.93	7.67	7.49
25	0.31	0.33	0.31	0.31	0.31	0.30	0.39	0.37	0.38	0.38	0.41	0.39	0.41	0.37
26	0.69	0.73	1.12	0.50	0.75	0.61	1.93	1.80	1.30	1.24	0.67	1.20	0.52	0.88
27	100.00	100.00	100.00	100.00	100.00	100.00	100.00	100.00	100.00	100.00	100.00	100.00	100.00	100.00
28														
29	57.81	55.65	55.67	58.79	57.08	57.65	54.28	56.33	61.47	60.76	62.33	60.90	61.21	60.68
30														
31	-	-	-	-	-	-	-	-	-	-	-	-	-	-
32	-	-	-	-	-	48.0	-	-	-	-	28.8	-	-	33.8
33	40.75	-	-	-	-	6.71	-	20.20	-	-	5.92	-	-	5.81
34	6.14	-	-	-	-	-	-	4.35	-	-	-	-	-	-
35	-	-	-	-	-	-	-	-	-	-	-	-	-	-
36	-	-	-	-	-	-	-	-	-	-	-	-	-	-
37	-	-	-	-	-	-	-	-	-	-	-	-	-	-
38	17.4	-	-	-	-	11.9	-	20.9	-	-	18.7	-	-	18.3
39	227	220	224	230	223	207	235	235	241	237	247	243	243	246
40	211	-	-	-	-	202	-	205	-	-	236	-	-	229
41	71	27	27	52	29	28	31	34	108	65	124	107	109	106
42	23.2	20	19	21	22	20.3	29	28.3	22	25	26.1	24	25	25.6
43	42.0	32	36	41	33	31.0	48	40.2	48	38	47.0	45	47	47.0
44	64	50	85	68	75	51	69	97	67	53	71	49	72	64
45	64.6	-	-	-	-	49.0	-	90.4	-	-	70.7	-	-	70.0
46	69	64	65	67	67	67	71	73	67	67	61	64	64	67
47	64.9	-	-	-	-	68.7	-	66.2	-	-	66.1	-	-	68.1
48	11.60	-	-	-	-	9.84	-	9.55	-	-	13.20	-	-	8.14
49	341	370	454	421	521	593	701	931	338	375	304	323	301	324
50	395	-	-	-	-	560	-	952	-	-	377	-	-	388
51	2036	2059	2003	1966	2088	2243	1927	1984	2268	2229	2208	2209	2306	2284
52	1920	-	-	-	-	2080	-	1860	-	-	2130	-	-	2190

	O	P	Q	R	S	T	U	V	W	X	Y	Z	AA	AB
53	32	33	15	34	36	35	41	40	35	30	35	35	34	33
54	29.8	-	-	-	-	31.7	-	32.0	-	-	35.0	-	-	34.6
55	267	271	287	270	272	276	259	264	281	287	275	272	282	279
56	269	-	-	-	-	293	-	266	-	-	293	-	-	294
57	16	16	18	16	17	17	11	12	15	15	14	13	15	14
58	15.2	-	-	-	-	17.4	-	12.4	-	-	13.7	-	-	14.4
59	3.98	-	-	-	-	4.07	-	1.38	-	-	3.75	-	-	3.67
60	-	-	-	-	-	0.02	-	0.01	-	-	0.02	-	-	0.03
61	3.47	-	-	-	-	3.50	-	3.93	-	-	3.99	-	-	3.87
62	0.93	-	-	-	-	1.07	-	0.66	-	-	0.97	-	-	0.99
63	33.6	-	-	-	-	46.1	-	57.6	-	-	36.1	-	-	36.6
64	1343	1385	1337	1289	1357	1404	1746	1611	1662	1753	1612	1675	1648	1624
65	1320	-	-	-	-	1370	-	1660	-	-	1630	-	-	1660
66	93	94	99	98	102	104	91	92	107	106	103	103	110	106
67	96.4	-	-	-	-	104	-	95.1	-	-	108	-	-	109
68	204	207	220	202	209	218	204	204	234	226	228	243	228	237
69	205	-	-	-	-	219	-	205	-	-	227	-	-	229
70	23.0	-	-	-	-	24.4	-	23.4	-	-	26.5	-	-	26.6
71	79	79	81	80	82	81	85	83	91	90	92	100	92	96
72	86.0	-	-	-	-	90.4	-	91.0	-	-	101	-	-	101
73	15.8	-	-	-	-	16.2	-	17.3	-	-	18.9	-	-	18.8
74	3.38	-	-	-	-	3.49	-	3.86	-	-	4.01	-	-	3.98
75	14.0	-	-	-	-	14.6	-	15.4	-	-	16.6	-	-	16.6
76	1.62	-	-	-	-	1.68	-	1.81	-	-	1.92	-	-	1.90
77	7.23	-	-	-	-	7.55	-	8.15	-	-	8.53	-	-	8.41
78	1.24	-	-	-	-	1.31	-	1.39	-	-	1.44	-	-	1.44
79	3.37	-	-	-	-	3.54	-	3.65	-	-	3.81	-	-	3.80
80	0.41	-	-	-	-	0.45	-	0.44	-	-	0.46	-	-	0.45
81	2.54	-	-	-	-	2.72	-	2.69	-	-	2.79	-	-	2.79
82	0.38	-	-	-	-	0.41	-	0.39	-	-	0.41	-	-	0.41
83	7.08	-	-	-	-	7.49	-	7.59	-	-	7.60	-	-	7.67
84	0.76	-	-	-	-	0.88	-	0.62	-	-	0.59	-	-	0.71
85	5.48	-	-	-	-	7.15	-	4.11	-	-	7.09	-	-	5.38
86	1.87	-	-	-	-	2.42	-	0.70	-	-	1.62	-	-	1.86
87	83	76	73	80	78	84	31	48	82	79	75	85	77	79
88	69.1	-	-	-	-	74.4	-	37.2	-	-	61.6	-	-	68.1
89	0.51	-	-	-	-	0.43	-	0.06	-	-	0.36	-	-	0.17
90	37.5	-	-	-	-	41.7	-	32.3	-	-	41.0	-	-	41.8
91	8.88	-	-	-	-	10.3	-	7.16	-	-	9.91	-	-	10.1
92	0.709421	-	-	-	-	0.709419	-	0.709229	-	-	0.709815	-	-	0.709805
93	± 0.000006	-	-	-	-	± 0.000007	-	± 0.000006	-	-	± 0.000006	-	-	± 0.000008
94	0.709418	-	-	-	-	0.709414	-	0.709221	-	-	0.709812	-	-	0.709802
95	0.512142	-	-	-	-	0.512145	-	0.512150	-	-	0.512121	-	-	0.512121
96	± 0.000005	-	-	-	-	± 0.000005	-	± 0.000004	-	-	± 0.000005	-	-	± 0.000006
97	0.512142	-	-	-	-	0.512145	-	0.512150	-	-	0.512121	-	-	0.512121
98	18.8153	-	-	-	-	18.8461	-	18.7992	-	-	18.8018	-	-	18.8052
99	15.6883	-	-	-	-	15.7255	-	15.6980	-	-	15.6884	-	-	15.6885
100	39.0475	-	-	-	-	39.1753	-	39.0796	-	-	39.0464	-	-	39.0405
101														
102														

	AC	AD	AE	AF	AG	AH	AI	AJ	AK	AL	AM	AN	AO	AP
1														
2														
3														
4	*Celleta*	*Celleta*	*Celleta*	*Giuliano*	*Giuliano*	*Giuliano*	*Giuliano*	*Giuliano*	*Giuliano*	*Giuliano*	*Giuliano*	*Giuliano*	*Giuliano*	*Giuliano*
5	*C.Quatrini*	*C.Schiappa*	*Celleta*	*S.Stefano*	*di Roma*	*di Roma*	*Pietromaggio*	*Valcatora*	*di Roma*	*di Roma*	*Pietromaggio*	*C.LeDanno*	*di Roma*	*di Roma*
6	41°34'59"N	41°33'51"N	41°34'55"N	41°31'00"N	41°32'28"N	41°32'22"N	41°32'20"N	41°31'22"N	41°31'58"N	41°31'58"N	41°32'14"N	-	41°32'27"N	41°31'60"N
7	13°17'24"E	13°17'20"E	13°17'19"E	13°18'35"E	13°16'24"E	13°16'41"E	13°16'24"E	13°17'03"E	13°17'15"E	13°17'15"E	13°16'27"E	-	13°16'30"E	13°16'26"E
8	HKS	HKS	HKS	HKS	HKS	HKS	HKS	HKS	HKS	HKS	HKS	HKS	HKS	HKS
9	**ERN67**	**ERN59**	**ERN66**	**ERN50**	**ERN46**	**ERN44**	**ERN48**	**ERN87**	**ERN52**	**ERN53**	**ERN47**	**ERN24**	**ERN45**	**ERN49**
10	18	19	20	21	22	23	24	25	26	27	28	29	30	31
11	*4*	*4*	*4*	*5*	*6*	*6*	*6*	*6*	*6*	*6*	*6*	*6*	*6*	*6*
12	*lava*	*lava*	*lava*	*lava*	*lava*	*lava*	*lava*	*lava*	*lava*	*lava*	*lava*	*lava*	*lava*	*lava*
13	*0.413000*	*0.413000*	*0.413000*	*0.391000*	*0.391000*	*0.391000*	*0.391000*	*0.391000*	*0.391000*	*0.391000*	*0.391000*	*0.391000*	*0.391000*	*0.391000*
14														
15	47.02	47.04	47.26	46.52	46.52	46.59	46.78	46.78	46.80	46.82	46.83	46.86	46.88	46.89
16	0.80	0.82	0.80	0.84	0.85	0.85	0.85	0.85	0.83	0.86	0.87	0.84	0.86	0.82
17	17.92	17.70	17.79	17.21	16.80	16.45	17.15	16.79	17.81	17.51	17.20	16.88	16.80	17.93
18	3.35	3.81	3.56	4.48	3.63	5.49	4.05	5.20	3.86	4.03	4.24	4.64	4.59	6.48
19	3.90	3.52	3.70	3.42	4.35	2.49	3.67	2.69	3.79	3.77	3.75	3.14	3.34	1.21
20	0.14	0.14	0.14	0.15	0.15	0.16	0.15	0.15	0.15	0.15	0.16	0.15	0.15	0.15
21	5.26	5.29	5.20	6.25	5.82	6.55	6.05	6.19	5.65	5.66	5.60	6.03	5.68	5.94
22	10.42	11.02	10.63	11.11	11.77	11.43	11.39	11.57	10.97	11.27	11.42	11.02	11.55	10.48
23	1.83	1.99	2.11	2.18	1.86	1.92	1.94	2.18	2.15	2.07	2.08	1.89	1.80	1.73
24	7.61	7.44	7.60	6.65	7.02	7.23	6.98	6.55	7.18	7.10	6.83	7.01	7.13	6.34
25	0.38	0.37	0.36	0.36	0.44	0.37	0.39	0.36	0.41	0.40	0.39	0.41	0.41	0.36
26	1.37	0.85	0.85	0.84	0.80	0.47	0.61	0.71	0.42	0.38	0.64	1.14	0.81	1.67
27	100.00	100.00	100.00	100.00	100.00	100.00	100.00	100.00	100.00	100.00	100.00	100.00	100.00	100.00
28														
29	61.36	61.36	61.11	63.64	61.45	64.80	63.32	63.68	61.87	61.49	60.70	63.24	61.35	63.78
30														
31	-	-	-	-	-	-	-	-	-	-	-	-	-	-
32	-	-	34.9	30.1	-	29.5	25.7	-	-	-	-	-	-	-
33	-	-	6.37	6.03	-	6.35	5.69	-	-	-	-	-	-	-
34	-	-	-	-	-	-	-	-	-	-	-	-	-	-
35	-	-	-	-	-	-	-	-	-	-	-	-	-	-
36	-	-	-	-	-	-	-	-	-	-	-	-	-	-
37	-	-	-	-	-	-	-	-	-	-	-	-	-	-
38	-	-	18.4	22.4	-	23.6	21.0	-	-	-	-	-	-	-
39	230	244	234	252	254	251	255	255	250	256	262	260	256	204
40	-	-	230	240	-	-	240	-	-	-	-	-	-	-
41	100	106	98	182	190	175	173	166	120	126	127	176	190	151
42	26	25	25.3	27.7	30	30.0	27.2	31	26	29	29	26	34	28
43	47	48	45.0	73.0	73	71.0	61.0	63	52	51	55	70	73	66
44	60	68	47	80	51	75	59	66	54	45	58	34	74	74
45	-	-	51.8	74.4	-	-	54.8	-	-	-	-	-	-	-
46	67	65	65	64	65	66	59	61	60	62	65	63	65	61
47	-	-	69.4	60.4	-	-	61.7	-	-	-	-	-	-	-
48	-	-	10.80	9.23	-	7.60	7.24	-	-	-	-	-	-	-
49	391	325	374	394	367	393	339	366	335	328	341	400	458	490
50	-	-	429	446	-	456	395	-	-	-	-	-	-	-
51	2244	2237	2327	1893	1806	1896	1990	2007	2062	2017	2075	1926	1873	1942
52	-	-	2260	1790	-	1870	1900	-	-	-	-	-	-	-

	AC	AD	AE	AF	AG	AH	AI	AJ	AK	AL	AM	AN	AO	AP
53	33	28	34	35	35	26	33	35	32	25	32	32	33	36
54	-	-	35.1	32.0	-	33.6	32.6	-	-	-	-	-	-	-
55	275	281	274	283	291	288	268	273	267	271	278	289	289	263
56	-	-	298	280	-	290	271	-	-	-	-	-	-	-
57	15	14	15	13	14	14	14	14	14	13	14	13	14	12
58	-	-	14.8	13.5	-	13.9	12.3	-	-	-	-	-	-	-
59	-	-	4.31	2.27	-	1.73	2.67	-	-	-	-	-	-	-
60	-	-	0.02	-	-	0.02	-	-	-	-	-	-	-	-
61	-	-	3.87	3.65	-	3.70	3.78	-	-	-	-	-	-	-
62	-	-	0.88	0.77	-	0.70	0.64	-	-	-	-	-	-	-
63	-	-	40.6	31.0	-	31.4	28.8	-	-	-	-	-	-	-
64	1712	1638	1714	1172	1103	1226	1231	1234	1367	1301	1292	1161	1173	1254
65	-	-	1720	1150	-	1250	1230	-	-	-	-	-	-	-
66	108	99	103	94	85	90	92	89	93	92	98	96	91	94
67	-	-	111	93.0	-	94.4	93.3	-	-	-	-	-	-	-
68	225	237	235	203	199	207	210	216	201	202	217	203	202	199
69	-	-	231	205	-	206	206	-	-	-	-	-	-	-
70	-	-	26.6	23.7	-	24.2	24.1	-	-	-	-	-	-	-
71	89	94	94	82	84	86	87	90	84	83	92	83	85	81
72	-	-	101	92.2	-	94.5	93.9	-	-	-	-	-	-	-
73	-	-	18.5	17.3	-	17.6	17.8	-	-	-	-	-	-	-
74	-	-	3.98	3.66	-	3.69	3.76	-	-	-	-	-	-	-
75	-	-	16.5	15.2	-	15.5	15.6	-	-	-	-	-	-	-
76	-	-	1.90	1.78	-	1.81	1.84	-	-	-	-	-	-	-
77	-	-	8.39	7.99	-	8.18	8.19	-	-	-	-	-	-	-
78	-	-	1.43	1.37	-	1.39	1.42	-	-	-	-	-	-	-
79	-	-	3.84	3.62	-	3.68	3.72	-	-	-	-	-	-	-
80	-	-	0.46	0.43	-	0.45	0.45	-	-	-	-	-	-	-
81	-	-	2.82	2.65	-	2.68	2.73	-	-	-	-	-	-	-
82	-	-	0.42	0.39	-	0.40	0.41	-	-	-	-	-	-	-
83	-	-	7.60	7.76	-	7.94	7.60	-	-	-	-	-	-	-
84	-	-	0.69	0.61	-	0.58	0.47	-	-	-	-	-	-	-
85	-	-	6.25	5.64	-	4.84	5.35	-	-	-	-	-	-	-
86	-	-	2.34	1.62	-	0.76	1.80	-	-	-	-	-	-	-
87	98	42	69	60	56	46	52	50	55	55	54	56	51	49
88	-	-	58.7	48.2	-	37.9	43.7	-	-	-	-	-	-	-
89	-	-	0.37	0.24	-	0.07	0.17	-	-	-	-	-	-	-
90	-	-	43.1	32.0	-	32.4	30.9	-	-	-	-	-	-	-
91	-	-	10.0	7.45	-	8.31	7.62	-	-	-	-	-	-	-
92	-	-	0.709810	0.709742	-	0.709731	0.709655	-	-	-	-	-	-	-
93	-	-	± 0.000008	± 0.000006	-	± 0.000007	± 0.000006	-	-	-	-	-	-	-
94	-	-	0.709807	0.709738	-	0.709727	0.709652	-	-	-	-	-	-	-
95	-	-	0.512121	0.512139	-	0.512141	0.512147	-	-	-	-	-	-	-
96	-	-	± 0.000004	± 0.000004	-	± 0.000005	± 0.000004	-	-	-	-	-	-	-
97	-	-	0.512121	0.512139	-	0.512141	0.512147	-	-	-	-	-	-	-
98	-	-	18.7923	18.8096	-	18.8122	18.8230	-	-	-	-	-	-	-
99	-	-	15.6782	15.6861	-	15.6862	15.6938	-	-	-	-	-	-	-
100	-	-	38.9981	39.0358	-	39.0417	39.0649	-	-	-	-	-	-	-
101														
102														

	AQ	AR	AS	AT	AU	AV	AW	AX	AY	AZ	BA	BB	BC	BD	BE
1															
2															
3															
4	*Giuliano*	*Giuliano*	*Pofi*	*Pofi*	*Pofi*	*Pofi*	*Pofi*	*Pofi*	*Pofi*	*Pofi*	*Pofi*	*Pofi*	*Giuliano*	*S.Piana*	*S.Piana*
5	*Paese*	*di Roma*	*C. Gori*	*F. Ocaro*	*S.Lucia*	*S.Croce*	*C. Ricci*	*Frantoio*	*C.Cosima*	*C.Berardi*	*Costantini*	*C.le Marte*	*Valcatora*	*C. Egidi*	*C.le Vento*
6	-	41°32'11"N	41°34'08"N	41°33'08"N	41°33'41"N	41°33'54"N	41°33'18"N	41°34'41"N	41°33'58"N	41°34'40"N	41°33'32"N	41°34'01"N	?	41°31'41"N	41°31'45"N
7	-	13°16'44"E	13°26'13"E	13°25'15"E	13°26'02"E	13°24'30"E	13°24'50"E	13°25'35"E	13°26'41"E	13°24'48"E	13°24'48"E	13°25'40"E	?	13°21'46"E	13°21'58"E
8	HKS	HKS	HKS	HKS	HKS	HKS	HKS	HKS	HKS	HKS	HKS	HKS	TRS	SHO	SHO
9	**ERN22**	**ERN54**	**ERN70**	**ERN72**	**ERN69**	**ERN99**	**ERN73**	**ERN75**	**ERN68**	**ERN98**	**ERN74**	**ERN71**	**ERN23**	**ERN92**	**ERN89**
10	32	33	44	45	46	47	48	49	50	51	52	53	54	55	56
11	*6*	*6*	*9*	*9*	*9*	*9*	*9*	*9*	*9*	*9*	*9*	*9*	*10*	-	-
12	*lava*	*lava*	*lava*	*lava*	*lava*	*lava*	*lava*	*lava*	*lava*	*lava*	*lava*	*lava*	*lava*	*lava*	*lava*
13	*0.391000*	*0.391000*	*0.390000*	*0.390000*	*0.390000*	*0.390000*	*0.390000*	*0.390000*	*0.390000*	*0.390000*	*0.390000*	*0.390000*	*0.376000*	*0.359000*	*0.359000*
14															
15	46.91	46.93	47.21	47.39	47.40	47.52	47.52	47.63	47.63	47.67	47.71	47.82	47.97	42.36	45.61
16	0.81	0.83	0.80	0.78	0.82	0.82	0.76	0.78	0.78	0.81	0.80	0.75	0.94	0.75	0.89
17	17.53	16.88	17.31	18.24	17.82	17.21	17.99	17.48	17.76	17.86	17.62	18.67	18.72	26.94	21.92
18	3.34	5.30	3.55	3.94	3.06	7.51	3.56	3.29	3.02	4.13	3.56	3.50	2.08	5.03	4.25
19	4.12	2.52	4.19	3.49	4.41	0.73	3.80	4.14	4.23	3.17	4.09	3.55	5.80	2.71	4.45
20	0.12	0.15	0.16	0.15	0.15	0.15	0.15	0.15	0.15	0.14	0.15	0.14	0.15	0.15	0.16
21	6.01	5.92	5.73	5.40	5.69	5.48	6.04	6.11	5.72	5.78	5.37	5.24	6.21	7.59	7.53
22	10.23	11.32	10.77	10.19	10.76	10.52	9.97	10.55	10.59	10.42	10.33	9.85	11.16	6.93	8.93
23	2.52	2.10	2.00	1.89	2.07	2.09	2.28	2.11	2.03	2.10	2.06	2.18	2.27	1.30	1.65
24	6.99	6.63	6.99	7.20	6.99	7.02	6.70	6.39	7.08	6.75	7.00	7.26	4.05	0.72	0.68
25	0.36	0.35	0.42	0.43	0.39	0.41	0.41	0.42	0.43	0.38	0.39	0.44	0.28	0.47	0.25
26	1.06	1.07	0.88	0.90	0.45	0.54	0.82	0.96	0.59	0.79	0.93	0.60	0.37	5.04	3.67
27	100.00	100.00	100.00	100.00	100.00	100.00	100.00	100.00	100.00	100.00	100.00	100.00	100.00	100.00	100.00
28															
29	63.77	62.89	61.83	61.56	62.39	60.44	64.27	64.24	63.21	63.65	60.56	62.02	62.82	68.64	65.50
30															
31	-	-	-	-	-	-	-	-	-	-	-	-	-	-	-
32	-	-	-	-	-	-	33.6	-	28.8	-	-	-	20.8	-	-
33	-	-	-	-	-	-	6.37	-	6.22	-	-	-	3.37	-	-
34	-	-	-	-	-	-	-	-	-	-	-	-	-	-	-
35	-	-	-	-	-	-	-	-	-	-	-	-	-	-	-
36	-	-	-	-	-	-	-	-	-	-	-	-	-	-	-
37	-	-	-	-	-	-	-	-	-	-	-	-	-	-	-
38	24.0	-	-	-	-	-	19.0	-	20.5	-	-	-	18.7	-	-
39	241	241	238	233	249	248	233	222	233	250	239	231	243	231	263
40	-	-	-	-	-	-	227	-	224	-	-	-	224	-	-
41	132	173	135	127	141	107	118	176	129	139	129	104	117	260	267
42	35	27	24	27	27	27	26	26.0	26	23.0	26	25	29	36.0	37
43	61	68	56	55	54	58	55	64.0	55	53.0	52	47	35	47.0	53
44	-	60	55	64	66	71	75	68	68	54	67	83	35	19	32
45	-	-	-	-	-	-	72.5	-	66.6	-	-	-	44.2	-	-
46	-	64	65	64	64	70	65	61	59	65	69	61	68	58	67
47	-	-	-	-	-	-	65.4	-	63.3	-	-	-	72.1	-	-
48	-	-	-	-	-	-	8.67	-	7.93	-	-	-	4.88	-	-
49	429	382	358	352	340	352	416	327	337	361	335	376	246	120	140
50	-	-	-	-	-	-	476	-	403	-	-	-	246	-	-
51	1611	1980	1860	1828	1773	1805	1849	1756	1797	1841	1838	1841	1220	836	929
52	-	-	-	-	-	-	1800	-	1730	-	-	-	1310	1040	933

	AQ	AR	AS	AT	AU	AV	AW	AX	AY	AZ	BA	BB	BC	BD	BE
53	24	34	34	28	13	24	36	31	33	33	36	35	28	22	17
54	-	-	-	-	-	-	34.4	-	33.6	-	-	-	28.6	21.8	19.8
55	416	280	294	303	301	306	299	280	291	290	301	293	187	142	131
56	-	-	-	-	-	-	298	-	289	-	-	-	193	126	107
57	19	13	13	14	13	14	15	13	13	13	14	13	11	8	8
58	-	-	-	-	-	-	13.9	-	12.9	-	-	-	12.4	-	-
59	-	-	-	-	-	-	2.07	-	1.95	-	-	-	2.73	-	-
60	-	-	-	-	-	-	0.02	-	-	-	-	-	-	-	-
61	-	-	-	-	-	-	3.88	-	3.97	-	-	-	3.38	-	-
62	-	-	-	-	-	-	3.80	-	0.74	-	-	-	0.25	-	-
63	-	-	-	-	-	-	32.3	-	29.8	-	-	-	13.6	-	-
64	1121	1171	884	895	865	852	896	886	889	915	920	919	680	565	746
65	-	-	-	-	-	-	892	-	859	-	-	-	699	-	-
66	99	95	87	93	91	95	95	88	90	89	95	90	61	49	50
67	-	-	-	-	-	-	96.3	-	93.2	-	-	-	58.4	-	-
68	218	195	199	204	196	215	213	201	196	217	212	200	130	81	85
69	-	-	-	-	-	-	213	-	209	-	-	-	131	-	-
70	-	-	-	-	-	-	24.70	-	24.50	-	-	-	15.90	-	-
71	85	80	80	87	81	87	88	79	84	88	87	81	59	41.914161	43
72	-	-	-	-	-	-	95.8	-	94.8	-	-	-	63.5	-	-
73	-	-	-	-	-	-	17.9	-	17.9	-	-	-	12.5	-	-
74	-	-	-	-	-	-	3.67	-	3.71	-	-	-	2.79	-	-
75	-	-	-	-	-	-	15.8	-	15.7	-	-	-	11.2	-	-
76	-	-	-	-	-	-	1.85	-	1.86	-	-	-	1.42	-	-
77	-	-	-	-	-	-	8.40	-	8.43	-	-	-	6.90	-	-
78	-	-	-	-	-	-	1.45	-	1.45	-	-	-	1.26	-	-
79	-	-	-	-	-	-	3.84	-	3.84	-	-	-	3.44	-	-
80	-	-	-	-	-	-	0.47	-	0.47	-	-	-	0.43	-	-
81	-	-	-	-	-	-	2.88	-	2.86	-	-	-	2.70	-	-
82	-	-	-	-	-	-	0.43	-	0.43	-	-	-	0.41	-	-
83	-	-	-	-	-	-	8.1	-	8.2	-	-	-	5.8	-	-
84	-	-	-	-	-	-	0.66	-	0.62	-	-	-	0.82	-	-
85	-	-	-	-	-	-	4.9	-	4.5	-	-	-	2.3	-	-
86	-	-	-	-	-	-	2.32	-	2.21	-	-	-	1.01	-	-
87	-	48	54	44	45	46	50	48	52	37	54	51	31	22.245298	23
88	-	-	-	-	-	-	41.2	-	40.3	-	-	-	18.9	-	-
89	-	-	-	-	-	-	0.2	-	0.2	-	-	-	0.1	-	-
90	-	-	-	-	-	-	32.2	-	30.5	-	-	-	18.0	-	-
91	-	-	-	-	-	-	7.26	-	6.88	-	-	-	4.94	-	-
92	-	-	-	-	-	-	0.709718	-	0.709724	-	-	-	0.708419	-	-
93	-	-	-	-	-	-	± 0.000007	-	± 0.000007	-	-	-	± 0.000007	-	-
94	-	-	-	-	-	-	0.709714	-	0.709720	-	-	-	0.708416	-	-
95	-	-	-	-	-	-	0.512136	-	0.512144	-	-	-	0.512246	-	-
96	-	-	-	-	-	-	± 0.000004	-	± 0.000004	-	-	-	± 0.000004	-	-
97	-	-	-	-	-	-	0.512136	-	0.512144	-	-	-	0.512246	-	-
98	-	-	-	-	-	-	18.8462	-	18.8469	-	-	-	18.8909	-	-
99	-	-	-	-	-	-	15.6964	-	15.7073	-	-	-	15.6821	-	-
100	-	-	-	-	-	-	39.0741	-	39.1149	-	-	-	39.0381	-	-
101															
102															

	BF	BG	BH	BI	BJ	BK	BL	BM	BN	BO	BP	BQ	BR	BS
1														
2														
3														
4	*Spinazzeta*	*Spinazzeta*	*Spinazzeta*	*Spinazzeta*	*S.Piana*	*S.Piana*	*S.Piana*	*La Badia*	*Pofi*	*Spinazzeta*	*F.Valera*	*La Badia*	*La Badia*	*La Badia*
5	*Ferrovia N*	*Ferrovia N*	*Ferrovia S*	*Ferrovia S*	*V.S.Ermete*	*C.Vescovo*	*C.Vescovo*	*C.Piedimonte*	*Pofi*	*Vetta*	*Colle 134*	*C.Piedimonte*	*C.Piedimonte*	*C.Piedimonte*
6	41°33'13"N	41°33'13"N	41°33'07"N	41°33'07"N	41°31'35"N	41°32'02"N	41°32'02"N	41°32'23"N	41°33'50"N	41°33'37"N	41°32'41"N	41°32'35"N	41°32'41"N	41°32'41"N
7	13°21'00"E	13°21'00"E	13°21'08"E	13°21'08"E	13°21'21"E	13°21'28"E	13°21'28"E	13°19'12"E	13°24'50"E	13°21'30"E	13°22'57"E	13°19'19"E	13°19'06"E	13°19'06"E
8	SHO	SHO	SHO	SHO	SHO	SHO	SHO	CA	CA	CA	CA	CA	CA	CA
9	**ERN 20es**	**ERN77**	**ERN21**	**ERN78**	**ERN91**	**ERN97**	**ERN96**	**ERN80**	**ERN100**	**ERN76**	**ERN25**	**ERN83**	**ERN82**	**ERN81**
10	57	58	59	60	61	62	63	64	65	66	67	68	69	70
11	*11*	*11*	-	-	*12*	*12*	*12*	-	-	*13*	-	*14*	*14*	*14*
12	*lava*	*lava*	*lava*	*lava*	*lava*	*lava*	*lava*	*lava*	*scoria*	*lava*	*lava*	*lava*	*lava*	*lava*
13	*0.345000*	*0.345000*	*0.345000*	*0.345000*	*0.359000*	*0.359000*	*0.359000*	*0.269000*	*0.298000*	*0.269000*	*0.269000*	*0.269000*	*0.269000*	*0.269000*
14														
15	48.52	48.66	49.02	49.05	49.57	49.61	49.75	46.25	47.21	48.62	48.51	48.70	49.31	49.91
16	0.75	0.74	0.74	0.74	0.81	0.75	0.78	0.91	0.74	0.76	0.82	0.82	0.84	0.79
17	17.35	17.03	19.06	18.31	17.84	18.13	18.37	18.74	18.46	16.25	18.82	17.36	17.50	18.08
18	2.45	2.40	4.38	4.23	3.50	3.92	4.38	6.94	5.79	3.10	5.16	3.91	2.89	3.45
19	4.92	4.99	2.94	3.20	4.28	3.66	3.30	2.52	3.93	4.72	3.21	4.57	5.71	4.42
20	0.15	0.15	0.14	0.14	0.15	0.15	0.15	0.18	0.15	0.15	0.14	0.16	0.17	0.15
21	8.33	8.47	7.39	7.86	6.55	6.56	6.33	7.52	7.74	9.33	7.74	8.08	7.36	7.21
22	11.59	11.88	10.16	10.38	11.02	10.90	10.68	10.71	10.08	12.14	10.58	12.06	11.60	10.54
23	2.37	2.19	2.55	2.64	2.48	2.44	2.40	1.76	1.79	2.59	2.63	2.98	3.03	3.16
24	3.08	2.76	0.84	0.62	3.39	3.18	3.28	1.03	0.75	0.73	0.21	0.54	0.82	0.63
25	0.26	0.24	0.27	0.26	0.22	0.22	0.22	0.22	0.32	0.21	0.23	0.22	0.18	0.23
26	0.23	0.49	2.82	3.08	0.20	0.49	0.36	3.23	3.05	1.40	2.05	0.89	0.99	0.98
27	100.00	100.00	100.30	100.50	100.00	100.00	100.00	100.00	100.00	100.00	100.10	100.28	100.40	99.55
28														
29	70.93	71.20	69.14	70.07	64.79	65.58	64.58	64.17	63.87	72.17	67.28	67.57	64.89	66.66
30														
31	-	-	-	-	-	-	-	-	-	-	-	-	-	-
32	-	19.9	-	-	25.3	24.8	-	-	-	16.3	-	17.6	-	-
33	-	2.10	-	-	2.27	2.25	-	-	-	1.47	-	1.63	-	-
34	-	-	-	-	-	-	-	-	-	-	-	-	-	-
35	-	-	-	-	-	-	-	-	-	-	-	-	-	-
36	-	-	-	-	-	-	-	-	-	-	-	-	-	-
37	-	-	-	-	-	-	-	-	-	-	-	-	-	-
38	30.1	27.5	-	-	25.7	24.8	-	-	-	33.0	-	32.3	-	-
39	223	217	222	216	228	233	235	259	227	220	232	232	233	228
40	-	209	-	-	226	220	-	-	-	209	-	221	-	-
41	372	408	305	489	167	166	157	267	221	563	403	319	253	212
42	36	32.6	27.0	35	32	31.4	26.0	41	32	35.8	35	34.3	34	36
43	60	69	58.0	33	41	40.0	37.0	50	46	97.0	71	58.0	47	48
44	64	79	32	86	91	93	90	84	28	58	44	66	71	81
45	-	74.7	-	-	84.1	78.2	-	-	-	68.4	-	63.6	-	-
46	58	58	58	55	60	58	58	71	59	56	61	62	65	59
47	-	60.2	-	-	66.3	63.6	-	-	-	58.2	-	60.0	-	-
48	-	3.66	-	-	3.90	3.71	-	-	-	2.96	-	3.63	-	-
49	156	153	183	177	180	185	154	125	-	157	124	125	114	95
50	-	173	-	-	160	190	-	-	-	181	-	130	-	-
51	1120	1058	1168	1065	1076	1082	1062	782	-	1003	957	808	978	897
52	-	*913*	-	-	-	-	-	-	-	1030	1100	-	-	-

	BF	BG	BH	BI	BJ	BK	BL	BM	BN	BO	BP	BQ	BR	BS
53	17	18	24	21	21	23	21	20	-	20	20	19	21	7
54	-	*20.6*	-	-	-	-	-	-	-	21.6	23.1	-	-	-
55	129	124	128	128	132	131	131	117	-	114	115	112	112	113
56	-	*105*	-	-	-	-	-	-	-	116	130	-	-	-
57	9	8	8	7	9	9	9	7	-	6	8	6	8	7
58	-	9.1	-	-	9.5	9.34	-	-	-	6.76	-	6.88	-	-
59	-	2.17	-	-	2.39	2.07	-	-	-	1.43	-	1.87	-	-
60	-	-	-	-	-	-	-	-	-	-	-	-	-	-
61	-	1.90	-	-	2.24	2.27	-	-	-	1.74	-	1.91	-	-
62	-	0.14	-	-	0.28	0.26	-	-	-	0.09	-	0.17	-	-
63	-	9.1	-	-	10.6	10.6	-	-	-	6.99	-	7.40	-	-
64	552	532	612	547	563	545	541	572	-	466	563	459	472	504
65	-	533	-	-	566	556	-	-	-	461	-	454	-	-
66	39	41.0	41	44	42	46	40	41	-	33	35	35	32	38
67	-	39.1	-	-	42.1	42.2	-	-	-	31.0	-	30.8	-	-
68	78	85	86	86	85	87	93	79	-	69	77	68	78	72
69	-	82	-	-	89	90.9	-	-	-	66.5	-	66.8	-	-
70	-	9.81	-	-	10.50	10.7	-	-	-	8.07	-	8.21	-	-
71	33	39.548235	39	37	31	34	36	35	-	30	33	25	31	32
72	-	38.8	-	-	41.2	42.1	-	-	-	32.8	-	33.4	-	-
73	7.3	7.7	-	-	8.2	8.44	-	-	-	6.82	-	7.08	-	-
74	1.5	1.94	-	-	2.02	2.06	-	-	-	1.72	-	1.77	-	-
75	-	7.5	-	-	7.8	7.90	-	-	-	6.45	-	6.69	-	-
76	0.88	0.99	-	-	1.03	1.05	-	-	-	0.88	-	0.91	-	-
77	-	5.13	-	-	5.36	5.42	-	-	-	4.55	-	4.82	-	-
78	-	0.96	-	-	1.00	1.02	-	-	-	0.86	-	0.91	-	-
79	-	2.63	-	-	2.77	2.78	-	-	-	2.34	-	2.47	-	-
80	-	0.35	-	-	0.37	0.37	-	-	-	0.31	-	0.33	-	-
81	2	2.15	-	-	2.27	2.31	-	-	-	1.91	-	2.02	-	-
82	0.27	0.33	-	-	0.35	0.35	-	-	-	0.29	-	0.31	-	-
83	2.9	3.7	-	-	3.79	3.80	-	-	-	3.27	-	3.17	-	-
84	0.53	0.53	-	-	0.62	0.62	-	-	-	0.46	-	0.45	-	-
85	-	1.4	-	-	2.2	1.88	-	-	-	0.95	-	1.74	-	-
86	-	0.55	-	-	0.54	0.52	-	-	-	0.38	-	0.31	-	-
87	23	24.799511	25	17	26	28	29	24	-	22	12	20	25	23
88	-	17.1	-	-	21.2	21.3	-	-	-	12.4	-	13.0	-	-
89	-	0.1	-	-	0.0	0.05	-	-	-	0.14	-	0.08	-	-
90	13.1	13.1	-	-	13.7	13.7	-	-	-	8.51	-	8.72	-	-
91	-	3.49	-	-	4.34	4.51	-	-	-	2.45	-	2.69	-	-
92	0.706967	0.706681	-	-	0.706973	0.706979	-	-	-	0.706534	-	0.706604	-	-
93	± 0.000007	± 0.000006	-	-	± 0.000006	± 0.000006	-	-	-	± 0.000006	-	± 0.000007	-	-
94	0.706965	0.706678	-	-	0.706971	0.706976	-	-	-	0.706532	-	0.706602	-	-
95	0.512347	0.512361	-	-	0.512341	0.512348	-	-	-	0.512373	-	0.512374	-	-
96	± 0.000005	± 0.000004	-	-	± 0.000005	± 0.000005	-	-	-	± 0.000006	-	± 0.000005	-	-
97	0.512347	0.512361	-	-	0.512341	0.512348	-	-	-	0.512373	-	0.512374	-	-
98	18.9486	18.9344	-	-	18.8987	18.9103	-	-	-	18.9396	-	18.9218	-	-
99	15.6999	15.6773	-	-	15.6811	15.6920	-	-	-	15.6745	-	15.6883	-	-
100	39.1106	39.0360	-	-	39.0250	39.0639	-	-	-	39.0304	-	39.0533	-	-
101														
102														

	BT	BU	BV	BW	BX	BY
1						
2						
3						
4	*S.Piana*	*S.Piana*	*S.Piana*			
5	*C. Scolopi*	*C. Scolopi*	*C. Scolopi*			
6	41°32'09"N	41°32'09"N	41°32'09"N			
7	13°21'20"E	13°21'20"E	13°21'20"E			
8	CA	CA	CA			
9	**ERN95**	**ERN94**	**ERN93**			
10	*71*	*72*	*73*			
11	*15*	*15*	*15*			
12	*lava*	*lava*	*lava*			
13	*0.269000*	*0.269000*	*0.269000*		*min*	*max*
14						
15	50.14	50.25	50.51		42.36	50.51
16	0.79	0.77	0.79		0.71	1.10
17	18.06	18.53	18.18		16.27	26.94
18	3.73	3.45	3.36		2.08	7.89
19	4.11	4.19	4.38		0.73	5.80
20	0.15	0.15	0.15		0.12	0.18
21	6.92	7.00	6.81		3.63	9.33
22	10.60	10.39	10.48		6.93	12.14
23	3.53	3.37	3.31		1.13	3.53
24	0.64	0.74	0.68		0.62	9.77
25	0.24	0.24	0.24		0.22	0.97
26	1.09	0.93	1.12		0.20	5.04
27	100.00	100.00	100.00			
28						
29	65.91	66.70	65.76		49.66	72.17
30						
31	-	-	-		0.00	0.00
32	-	19.1	-		19.9	48.0
33	-	1.70	-		2.10	40.75
34	-	-	-		4.35	6.14
35	-	-	-		0	0
36	-	-	-		0	0
37	-	-	-		0	0
38	-	27.6	-		11.0	33.0
39	230	229	227		190	277
40	-	215	-		198	275
41	229	217	209		13	563
42	31	32.8	32		19.0	41.0
43	49	47.0	47		26.0	101.0
44	45	42	59		19	111
45	-	44.5	-		44.2	93.6
46	58	58	56		55	75
47	-	61.5	-		57.7	74.2
48	-	3.00	-		3.66	17.50
49	123	117	123		120	931
50	-	134	-		160	952
51	1019	1007	1044		836	2553
52	-	1080	-		913	2500

	BT	BU	BV	BW	BX	BY
53	21	19	23		13	45
54	-	23.3	-		19.8	43.2
55	119	114	107		124	533
56	-	131	-		105	547
57	8	7	6		7	36
58	-	7.87	-		9.10	35.20
59	-	1.41	-		1.21	4.31
60	-	-	-		0.01	0.13
61	-	2.03	-		1.90	6.79
62	-	0.16	-		0.14	3.80
63	-	8.11	-		9.11	60.80
64	507	537	518		532	3949
65	-	520	-		533	4010
66	36	38	35		39	242
67	-	37.1	-		39.1	241.0
68	75	80	77		78	478
69	-	78.8	-		82.2	478.0
70	-	9.43	-		9.81	52.70
71	33	36	35		31	183
72	-	37.7	-		38.8	196.0
73	-	7.60	-		7.30	33.70
74	-	1.91	-		1.50	7.03
75	-	7.29	-		7.45	28.80
76	-	0.96	-		0.88	3.02
77	-	5.06	-		5.13	11.90
78	-	0.95	-		0.96	1.84
79	-	2.63	-		2.63	4.81
80	-	0.35	-		0.35	0.51
81	-	2.15	-		2.00	3.12
82	-	0.33	-		0.27	0.45
83	-	3.50	-		2.90	14.90
84	-	0.51	-		0.47	1.46
85	-	0.97	-		1.41	10.20
86	-	0.32	-		0.52	3.04
87	21	23	23		17	150
88	-	16.1	-		17.1	134.0
89	-	0.03	-		0.03	0.51
90	-	10.7	-		11.3	93.5
91	-	2.94	-		3.49	13.10
92	-	0.706779	-		0.706681	0.711176
93	-	± 0.000007	-		± 0.000006	± 0.000008
94	-	0.706778	-		#VALUE!	#VALUE!
95	-	0.512360	-		0.512119	0.512374
96	-	± 0.000004	-		± 0.000004	± 0.000006
97	-	0.512360	-		#VALUE!	#VALUE!
98	-	18.9167	-		18.7258	18.9486
99	-	15.6948	-		15.6704	15.7255
100	-	39.0898	-		38.9686	39.1753
101						
102						